A New Method in Fabric Drape Measurement and Analysis of Drape Formation Process

Bidour Al-Gaadi[1], Fatma Göktepe[2], Marianna Halász[1]

[1]Budapest University of Technology and Economics, Faculty of Mechanical Engineering, Department of Polymer Engineering, Hungary
[2]Namik Kemal University, Çorlu Engineering Faculty, Textile Engineering Department, Turkey

Corresponding author: Bidour Al-Gaadi, Budapest University of Technology and Economics, Faculty of Mechanical Engineering, Department of Polymer Engineering, Muegyetem rkp. 3., Budapest, Hungary, H-1111.
E-mail: al-gaadi@pt.bme.hu

Abstract

The paper presents the Sylvie 3D Drape Tester developed for fabric drape measurements and its special auxiliary device that exerts dynamical impact on fabrics during draping. Also, a new draping characteristic, namely the Drape Unevenness Factor, was defined to describe the evenness of the shape of draped textile material numerically. Three special cotton fabrics woven exclusively for this work differing only in twist direction of their weft yarns were used for analysis and effect of twist directions in a woven fabric and influence of the applied dynamical impact on drape test results were analyzed. Based on the test results, the paper also analyses the process of drape formation offering proposals for modification of fabric behavior models to contribute for better fabric simulations.

Keywords

Drapability, dynamically influenced drape, drape unevenness factor, image processing, yarn twist direction, modeling of fabric behavior

INTRODUCTION

Draping – i.e. the 3D deformation of textiles that occurs due to gravity – is a very important characteristic to describe the behavior of textiles. The fabric drapeability directly influences on its behavior in an article of clothing made from it. The research indicates that garment appearance quality is strongly affected by drapeability [1, 2]. The measured fabric properties can be used also for a more exact simulation of the 3D geometry of the fabric.

The most frequently applied measuring device for the determination of draping properties is the Cusick Drape Meter [3]. The equipment projects the contours of the circular draping textile sample placed on the circular sample holder with a parallel light bundle, and the analysis of the shadow image makes it possible to determine the drape coefficient (DC) and number of waves (n). Later, automatic evaluation software based on the photography of the shadow image was prepared as a supplement to this device [4]. The software analyzes the perimeter of the shadow image using Fast Fourier Transformation (FFT). The software determines the variance of the amplitude (the distance between the shadow image contour points and the center of the sample holder) as statistical data and a so-called fitness factor (the ratio of the area below two curves, namely the amplitude graphed as a function of the central angle and the dominant component obtained with FFT) besides the usual characteristics.

As the draping measurement method was improved, some researchers supplemented their devices with a sample holder that rotates the sample at adjustable angular speed and is necessary for the measurement of the draping coefficient. With this new method drapability could be examined under conditions more similar to the real using condition [5-8].

In addition to dynamic drape coefficient, researchers developed some other factors to describe draping as Circularity Factor is an example for these. The circularity factor, which is similar to the drape coefficient, is defined as the ratio of the perimeter and the area of the draping sample describing the extent of fabric draping [9].

A wide range of structural and mechanical properties of fabrics influence draping as well as the external conditions and impacts. The most extensively used system for the determination of the mechanical properties of fabrics is the Kawabata Evaluation System (KES) [10]. Several researchers have been dealt with the determination of the relation between the parameters measured with KES system and drapability as well as application of the obtained relations for modeling of fabric draping. These works reveal that KES parameters influencing

2

draping behavior to the greatest extent are mainly the bending and shearing properties [11, 12].

The behavior of textile materials is a very complex mechanism as the interactions of the individual fibers or yarns result in special properties. Therefore, their mechanical modeling and realistic simulation are both quite complex tasks.

Gräff and Kuzmina [13] deal with the mathematical methods of material behavior simulation. According to their literature review, several attempts have been made in the field of textile modeling since the mid '80s as the elements of continuum mechanics and finite element method were applied in these models and textile material was modeled as a mechanism.

No solution that handles all aspects of the above mentioned complex problem has been found yet. Textiles deform to a great extent and in several different qualities already due to small forces, and this is the main difference compared to other materials that makes their modeling so difficult. Basically, models used in textile modeling can be classified into two groups: Finite element based models and particle system based models.

Jevšnik and Geršak present the use of finite elements method for modeling a fused panel drape. Their results show significant promise for further development of research regarding computer simulation of the behavior of fabrics [14].

The solution worked out by Gräff and Kuzmina [13] is a typical example of modeling based on particle system. A method based on the Second Newtonian Law was applied in which the fabric was modeled with a network of mass points. The material model consists of mass points, flexural, shearing and tensile structural connecting elements. All connecting elements are composed of a spring and damper arranged parallel, where the springs are linear while the dampers are proportional with speed. However, simulation based on this model is always symmetrical and evenly draped. These problems are common in case of all simulation programs. Another problem is that about the results of not providing any explanation or information on larger deviations making very difficult for efficient applications in 3D simulation of textile products.

Therefore, one of the aims of our research is to find out the reasons for having different stable draped shapes and different draping properties varying at a relatively large scale deformation. Our research results also enable us to draw conclusions that help in the improvement of material simulation programs. Furthermore, these programs will be able to characterize the

fitting of reinforcing fabrics – applied also in composites – onto complex spatial shapes [15, 16].

On the other hand, this paper presents a drape tester with a special auxiliary device that exerts dynamical impact on fabrics so that dynamically influenced draping could be measured. Also, a new draping characteristic, named as Drape Unevenness Factor, is defined to express the evenness of the draped textile material objectively. For this aim, three special cotton fabrics were woven exclusively differing only in twist direction of their weft yarns. The effect of twist directions in fabric drape and influence of the applied dynamical impact on drape test results were analyzed offering proposals for the modification of fabric model so that it could contribute to improvement of fabric simulation programs further for a better outcome.

EXPERIMENTAL DETAILS

Material

Three special fabrics used in the experiments were woven in Hungary by Csárda-Tex Ltd. The twist direction of yarns used for these three fabrics, which have the same structural properties and made of 100% cotton, was chosen as different so that the effect of twist on drape behavior could be studied. They were plain woven fabrics as the warp and weft densities as well as the linear density of the warp and weft yarns were the same, hence their area density was also the same (Table 1).

Table 1: Particulars of three special fabric samples

Denote	Material	Type		Density [g/m²]	Type of weave	Yarn count		Yarn density [1/10mm]		Twist direction	
		warp	weft			warp	weft	warp	weft	warp	weft
P	cotton	OE-rotor	OE-rotor	156	plain	30 Tex	30 Tex	26	22	Z	Z
K	cotton	OE-rotor	OE-rotor	156	plain	30 Tex	30 Tex	26	22	Z	S
F	cotton	OE-rotor	OE-rotor	156	plain	30 Tex	30 Tex	26	22	Z	Z+S

The microscopic images of the samples (Figure 1) illustrate the different twist directions of the three fabrics. The warp yarns in all the three fabrics have Z-twist direction, the differences lie only in the twist direction of weft yarns as shown in Table 1.

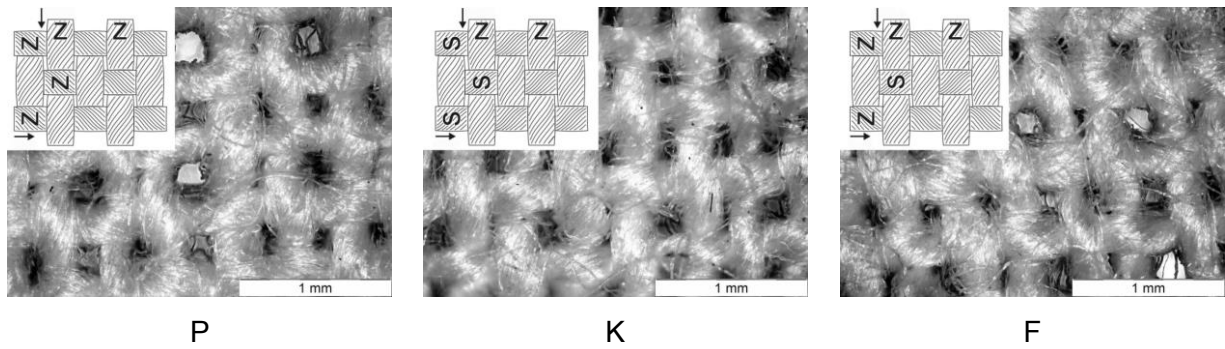Altogether 9 samples of 300 mm diameter, i.e.3 pieces per fabric type were prepared for the tests.

Figure 1: Z and S twist directions of the examined samples

Equipment

The fabrics were tested for their shear and bending properties by using Kawabata Evaluation System (KES) at University of Maribor.

The drapability of experimental samples was measured by the Sylvie 3D Drape tester developed at the Budapest University of Technology and Economics (Figure 2).
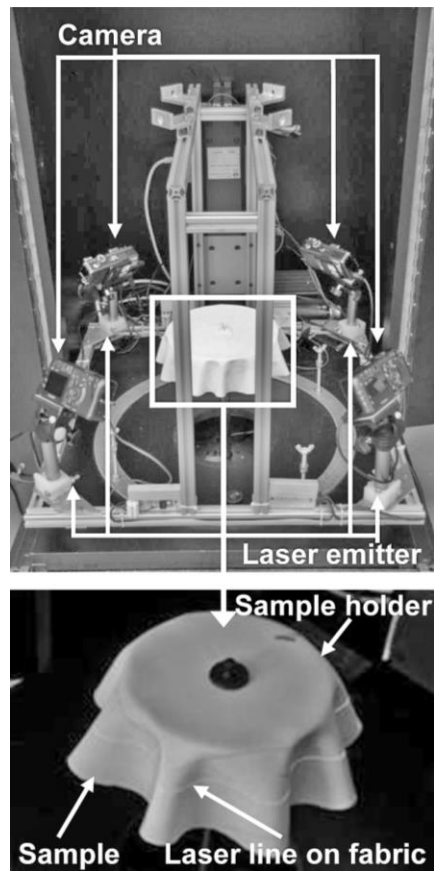

Figure 2: Sylvie 3D Drape Tester

This is a new, computer controlled 3D scanning based equipment. The software reconstructs virtually the measured surface from the measured data, and using that it calculates the ordinary parameters. The equipment can be supplement by rings of different diameters such as 210mm, 240mm and 270 mm, respectively to influence dynamically the evolving nodes.

Measuring Procedure

The table of the Sylvie 3D Drape Tester (Figure 2) at the initial state is in level with the base plate. The diameter of the table is 180 mm. The diameter of the fabric sample is 300 mm [17].

During the tests, the centre of the sample has to be set exactly on the centre of the table, and warp and weft directions have to be parallel with the specified directions. A computer controlled motor lifts the table, assuring that drapability is always studied at the same speed and under the same dynamic effects. During the measurements, four laser emitters project laser lines on the fabric sample in order to determine the cross-section and four cameras record the lines over the laser emitters (Figure 2). The cameras and the laser emitters are mounted on a measuring frame. The frame moves with a determined step distance during scanning the surface of the fabric sample. The computer controlled instrument is constructed in a black box in order to provide darkness during the measurement. After all photographs are taken, the computer downloads those [18].

On the other hand, the software of the device determines the desired draping properties automatically. The draping coefficient is calculated based on the generally accepted definition according to formula (1):

$$DC = \frac{A_r - \pi R_1^2}{\pi R_2^2 - \pi R_1^2} \cdot 100 \quad [\%] \tag{1}$$

where A_r is the area of the planar projection of the draping textile, R_1 is the radius of the sample holding table and R_2 is the radius of the laid fabric (Figure 3).

Then a new parameter, *Drape Unevenness Factor,* was created for the description of the geometric asymmetry and unevenness of drapes of the fabric sample (Figure 4).
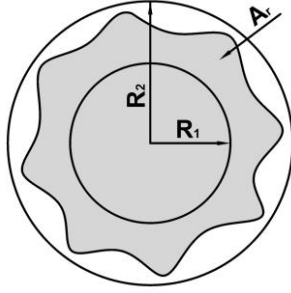
Figure 3: Projection of the plane and the draped fabric sample
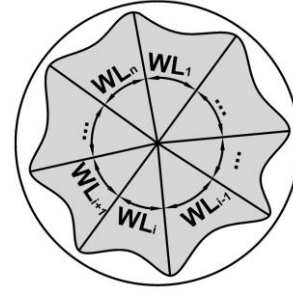

Figure 4: Wave length of the draped fabric sample

The new factor is denoted by DU that is physically the relative deviation of the wavelength of waves formed at the perimeter of the planar projection of the draping fabric (Equation 2).

$$DU = \frac{\sqrt{\dfrac{\sum_{i=1}^{n}(WL_i - \overline{WL})^2}{n-1}}}{\overline{WL}} \tag{2}$$

where WL_i is the central angle between two adjacent maximum amplitudes (i.e. the wave length of single waves), $\overline{WL}$ is the average central angle on one wave (i.e. average wave length, $\overline{WL}$ = 360/n) and n is the number of waves.

The above relation indicates that smaller the value of DU is the more even drape of the examined fabric. Besides factors of DC and DU, the number of waves, the minimum and maximum amplitude and the deviation of amplitudes are also calculated by the software.

Dynamically influenced drapability

The Sylvie 3D Drape Tester was supplemented with exchangeable circular rings that had different inner diameters. The circular ring is placed in the equipment in a way that it pushes the sample through the opening of the ring when the sample holder rises (Figure 5) [19, 20].

The so-called "dynamically influenced draping coefficient" is measured using the rings. The reproducibility of this measurement is outstanding due to the constant speed of rising and same ring parameters. The inner diameters of the applied rings are 210, 240 and 270 mm, respectively (Figure 6), while the diameter of the sample holding table is 180 mm. In order to handle the results of measurements with and without rings uniformly, the static case – i.e. without ring – is considered as if a 300 mm diameter ring was applied. This consideration can be verified easily as a ring with 300 mm diameter would not influence draping, since it would

not even contact the fabric sample which has 300 mm diameter itself before draping, i.e. it is absolutely irrelevant whether there is a ring or not in reality.

The measurement with rings of having different diameters simulates the impacts – that arise during the use of fabrics – at different intensity levels.
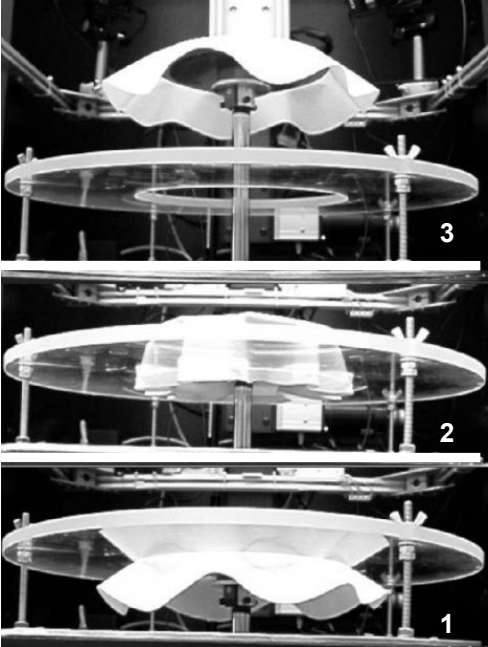

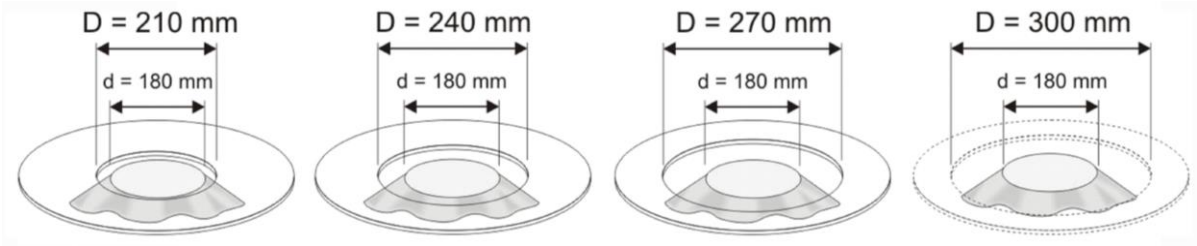**Figure 5:** Ring influenced drape measurement

Figure 6: Rings with different inner diameters

RESULTS AND DISCUSSION

Effect of twist direction on drapeability

The twist direction of the warp and weft yarns in the fabric play an important role in the formation of draping, since it determines the circumstances of the contact of elementary fibers

in the yarns. The results of present extensive experiments reinforce the conclusions of our previously presented test series [21].

The elementary fibers of the two yarns are almost parallel in case of material P (Z-Z twist direction) where two warp and weft yarns cross each other. In case of material K (Z-S twist direction) these elementary fibers lie on each other almost perpendicularly at the crossing point because of the opposite twist direction of the warp and weft yarns.

The crossing of elementary fibers is illustrated in Figure 7 a) and b) simply.
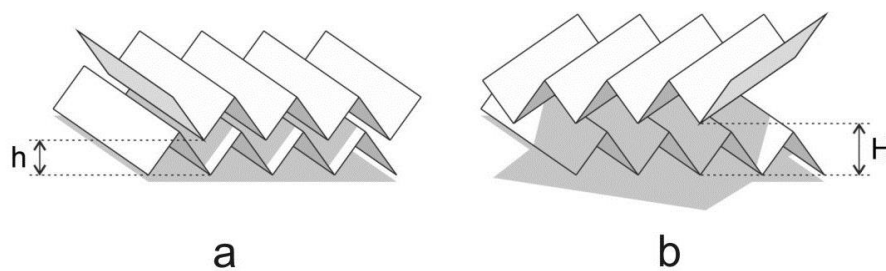

Figure 7: Simple representation of elementary fibers at fabric cross-over points which are parallel or perpendicular direction; a) Z-Z twist yarns; b) Z-S twist yarns

It is clearly shown in this figure that the almost parallel elementary fibers (Z-Z twist direction, figure a) can penetrate among each other – due to the force that compresses the yarn – when crossing, while in case of an almost perpendicular contact (Z-S twist direction, figure b) this is not possible. This phenomenon is also proven by the thicknesses of the fabrics. The thickness of material K is 0.79 mm, while fabric P (Z-Z twist direction) has a thickness of 0.66 mm opposed to the fact that their other structural properties are the same. Hence, the difference can only lie in the different twist directions of weft yarns.

In case of Z-Z twist direction, the almost parallel crossing of elementary fibers result in a larger contact surface, hence larger friction force, while the almost parallel parts of the yarns interconnect in the same way as the teeth of a gear, i.e. connection through shapes. These phenomena together decrease the rotation and slipping of warp and weft yarns and inhibit the formation of shearing and flexural deformation.

Oppositely, in case of Z-S twist direction, the elementary fibers cross almost perpendicularly, hence the contact surface is much smaller, the almost perpendicular 'fibers' of the yarns cannot connect into each other. Therefore, the warp and weft yarns can rotate and slide from each other more easily than in case of Z-Z twist direction.

These phenomena together explain that fabric sample P (Z-Z twist direction) is definitely stiffer, has larger drape coefficient and its number of waves is also higher although only to a small extent. Furthermore, it has higher flexural and shearing modulus and hysteresis (Z-S twist direction) than fabric sample K (Z-S twist direction) (Figures 8, 10 and 11).

The trends of drape unevenness (DU) (Figure 9) show an opposite direction than in case of DC values. The value of DU is much higher in case of fabric sample K (Z-S twist direction) than in case of fabric sample P (Z-Z twist direction), meaning that the draped shape of fabric P is smoother. Hence, we can conclude here that the twist direction of yarns influences the evenness of draping to a great extent.
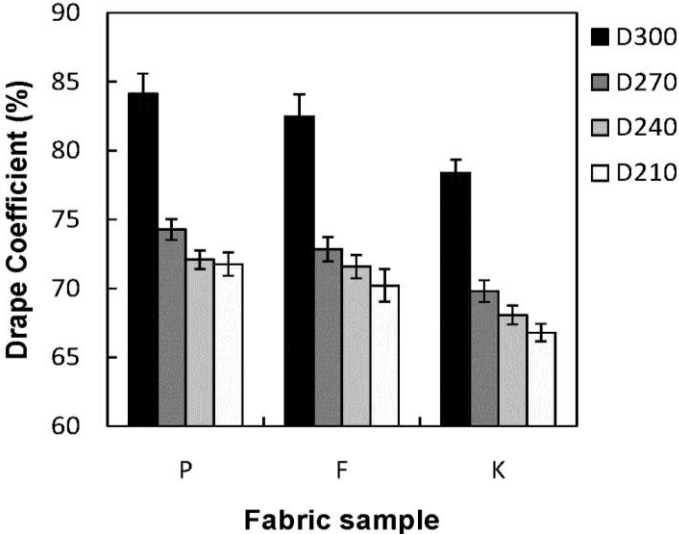

Figure 8: Drape coefficient (DC) measured at different ring diameters as a function of the fabric sample
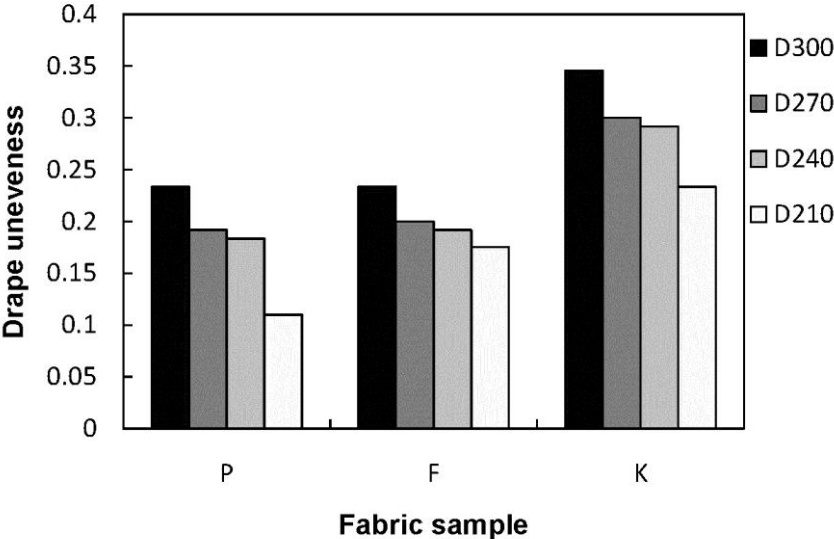

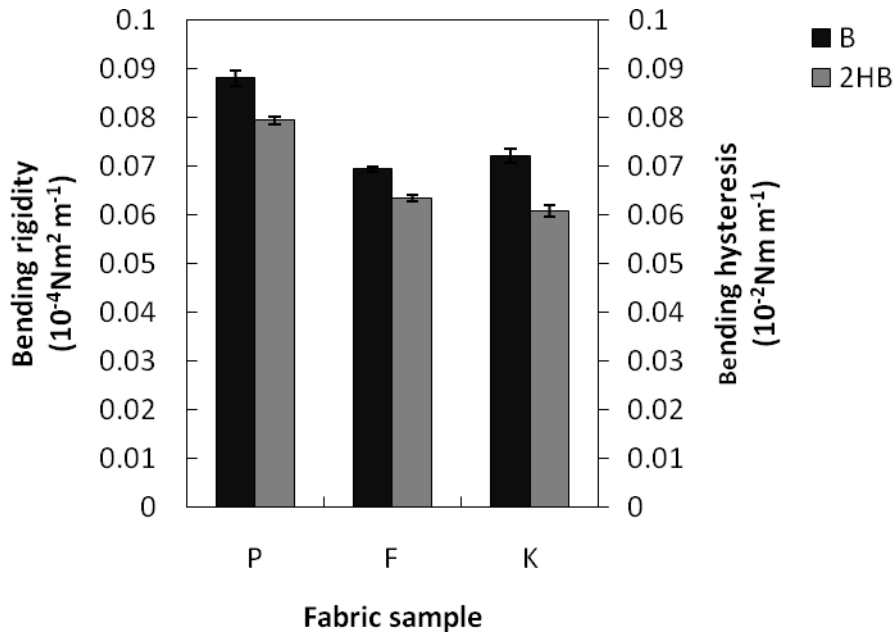**Figure 9:** Drape unevenness (DU) measured at different ring diameters as a function of fabric sample

10

Figure 101: Bending behaviors of fabric samples as a function of fabric type,
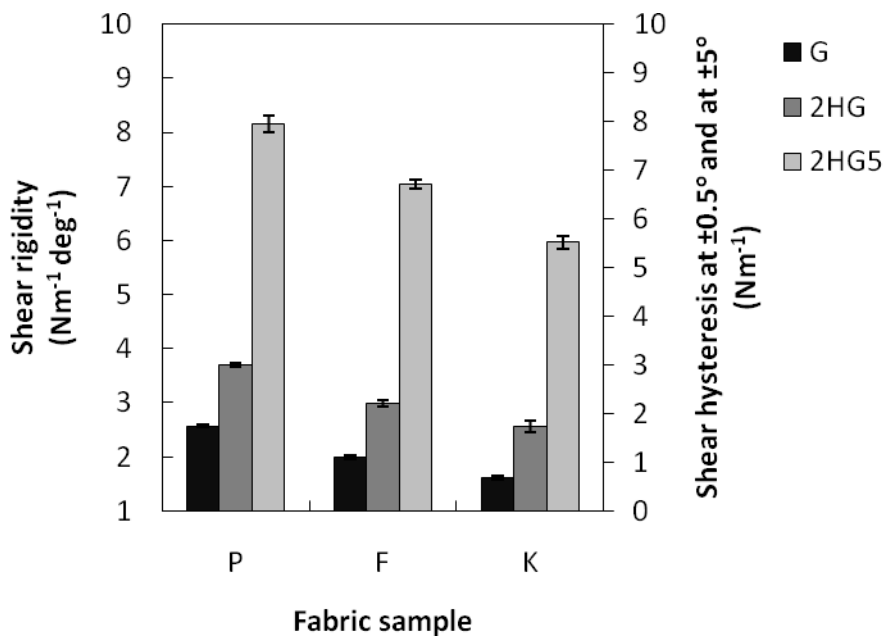B - bending rigidity; 2BH - bending hysteresis

Figure 11: Shear behaviors of fabric samples as a function of fabric type,
G - shear rigidity; 2HG - shear hysteresis at ±0.5°; 2HG5 - shear hysteresis at ±5°

The properties of the third fabric sample denoted by F (Z-Z/S) are between the values of the fabrics of K and P. This is logical since the structure of this fabric is almost exactly in the middle between the other two fabric samples. This also proves the conclusions drawn above.

Applied dynamic impact on drape measurements

During the tests, the drape measurement of every single sample was carried out 10 times per one ring size on both front and back face of fabrics according to DIN 54306 standard, keeping always identical – 12 minutes – relaxation time interval between the measurements. In evaluation of results, the average and deviation of drape coefficient (DC), drape unevenness (DU) and the number of waves (n) were determined and significance of difference between DC values was analyzed using bi-lateral student's t-test and F-test at 0.05 significance level.

The dynamic impact on drape test results was analyzed as a function of differing ring diameters, i.e. 210mm, 240mm, 270mm and 300mm, respectively. The effect of ring diameter on the drape coefficient is significant (Figure 12), while the number of waves is only slightly affected. If the ring size decreases, hence the dynamic influencing effect is larger, the value and deviation of drape coefficient (DC) decrease, the number of waves slightly increases (n) and drape unevenness (DU) decreases (Figure 13).
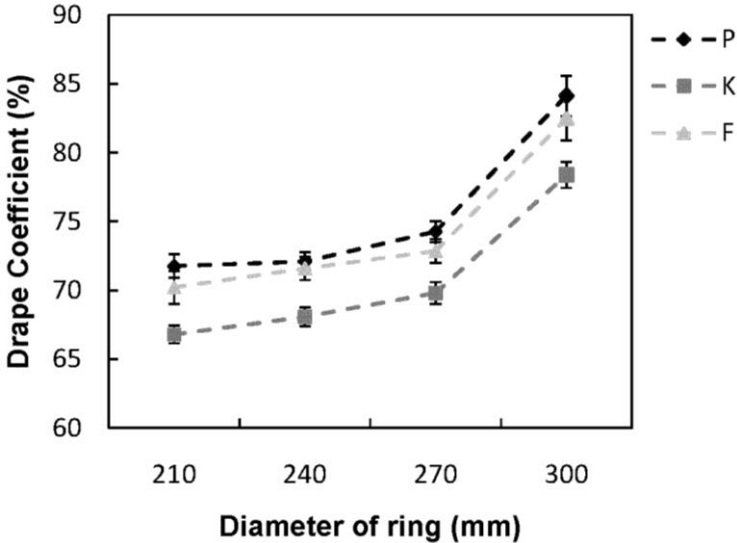

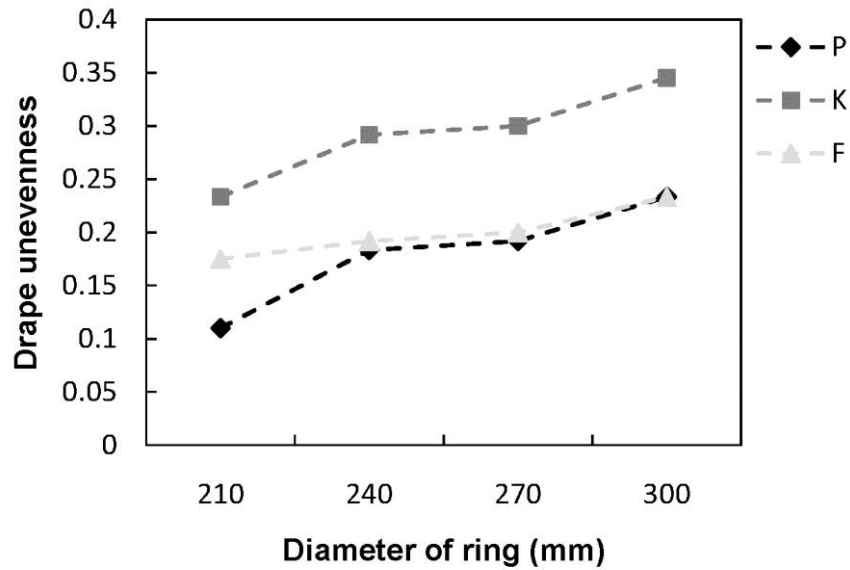**Figure 12:** Drape coefficient as a function of the ring diameter

Figure 13: Drape unevenness as a function of ring diameter

Figure 14 shows the results obtained from the measurements with the different rings. The main tendencies of the measurements are well visible, i.e. in case of using rings the average radius of the drape image contour, i.e. DC decreases, and the draped shape becomes more even.

D210   D240   D270   D300
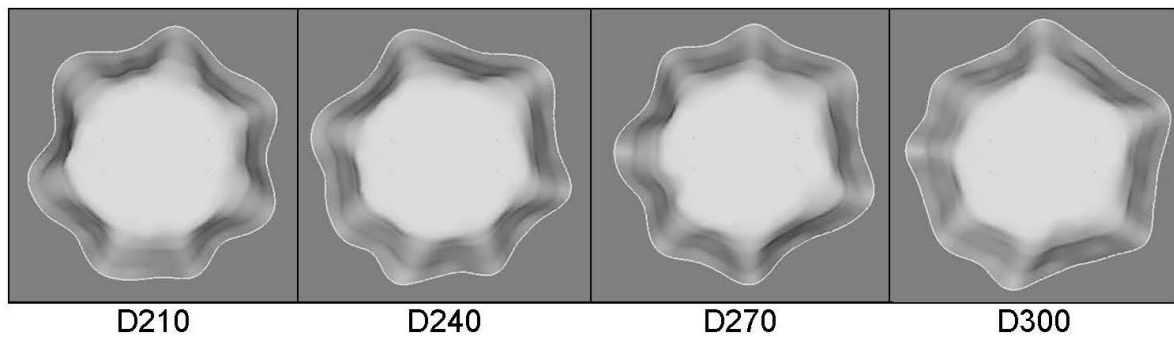
Figure 142: 3D shapes of fabric sample P influenced with 210, 240, 270 and 300 mm inner diameter rings

On the other hand, Student's t-test was applied for samples P and F, since the difference of the mean values is not obvious due to the overlapping deviation fields (Figure 8). According to the results, the DC of these two fabric types are significantly different in case of 300 mm, 270 mm and 210 mm ring diameter at a confidence level of 95%. However, the drape coefficient values measured with the 240 mm and 270 mm diameter rings are very close to each other when we consider the deviations in Figure 8, hence Student's t-test was also

13

carried out in that case. The test proved that the difference of the mean values is significant at a confidence level of 95%.

The test results also prove that dynamic effects on the fabric during drape formation influence draping characteristics although the dynamic effect is not present yet at the time of data recording. This is the reason why the deviation is definitely larger in case of manual testing, compare to the results obtained using a motor driven sample holding table that provides always identical and even lifting speed with no dynamic effects.

In case of measurements with rings, the drapes of the fabrics that passes through the ring (Figure 5) are compressed, and after leaving the ring, they can get their shape back in an elastic way, but that shape is not exactly the same as it was before reaching the ring, and drape properties of the fabric can change. The fabric passes the ring quickly, hence this phenomenon cannot happen due to stress-relaxation as residual deformation cannot be caused this way. Since different results are experienced after dynamic effect ends as in the case without dynamic effects, other factors should play a role in fabric behavior as well as the actual and delayed elastic deformation. The change in the drape properties due to the effect of the ring can be explained with sticking-sliding friction among the yarns of the fabric that explains the hysteresis experienced in bending (Figure 10) and shearing (Figure 11) tests as well. The fact that the draped shape will become more even due to the ring refers to the presence of sticking-sliding friction as well because the ring has a balancing effect on different extent deformations at the different locations of the fabric due to the non-identical sticking-sliding friction forces. Hence, our results also prove that the deviation of sticking-sliding friction force has a significant impact on the formation of the asymmetric draped shape.

Analysis of drape formation process and a proposal for improvement of fabric behavior modeling

The ultimate aim of our investigations is to use our results as a contribution to a material simulation that estimates real case as much as possible. Proposals can be made for the modification of the fabric mechanical model based on the behavior of the examined materials at different ring diameters, KES measurements and the effect of twist direction on the drape coefficient.

Particle system based models take into consideration only viscous friction as an inner damping effect besides the spring that models elastic behavior. However, our measurements prove clearly that sticking and sliding Coulomb friction is also present as a kind of inner resistance. Considering all the previously mentioned facts, the behavior of materials experienced during the application of rings can be explained easily.

The modification proposal is presented through a simplified viscoelastic model of the draping textile (Figure 15). The simplified model is a one-mass oscillating system of the force balance which is described by Equation (3).

$$m \cdot \ddot{x} + k \cdot \dot{x} + s \cdot x + sign(\dot{x}) \cdot F_\mu = F_g \qquad (3)$$

where x: displacement vector, $\dot{x}$: velocity vector, $\ddot{x}$: acceleration vector, m: mass, s: spring stiffness, k: damping factor of the viscous damping element, F_μ: sticking and slipping friction force, F_g: inciter forces.
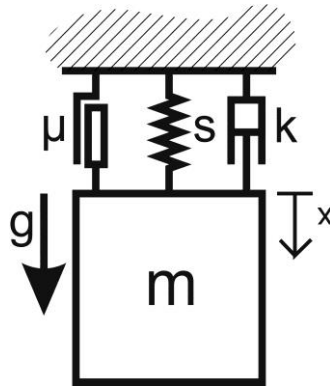

Figure 15: Simplified viscoelastic model of fabric behavior

According to the model in Figure 15, the deflection of the draping fabric – represented by mass "m" – is caused by gravity. The elastic and friction forces in the fabric that work against the deflection caused by gravity – movement of mass "m" – are represented by the stick and slip friction, viscous damping and the spring. The effect of the ring can be taken into consideration with inciter force F_g. The question is where the deflecting fabric – mass "m" – stops, i.e. how much the drape coefficient will be.

Figure 16 demonstrates the process of drape formation with the section of the fabric placed on the sample holding table. The fabric starts from position 1 at the beginning of the measurement and deflects due to gravity. If the fabric is raised at a controlled speed, and its deflection is retarded with an external force meanwhile (e.g. in case of the Sylvie Drape

15

Tester the base plate from which the sample holding table lifts up the fabric at a constant speed brakes the fabric during rising), the slowly forming drapes stop at the upper part of the uncertainty zone. This is the way how the largest drape coefficient of the examined material can be measured. If the fabric is dropped freely from position 1, the fabric enters the uncertainty zone and stops somewhere within (position 2), or passes through it, carries out dampening free oscillating movements, but finally stops within the uncertainty zone.
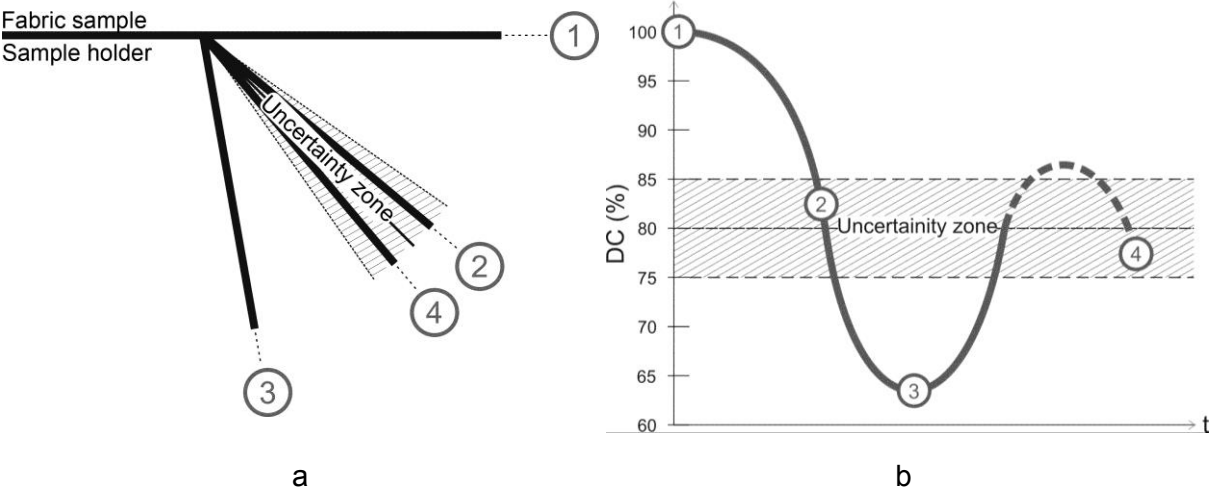

Figure 16: Process of drape formation

a) Section of the draping fabric; b) Change of the drape coefficient as a function of time

If a ring is applied in the measurements, the ring overcomes the resistance of the fabric and hence forces the already formed drapes under the uncertainty zone into position 3 – the extent of the force depends on the diameter of the ring. The fabric, which alternates back after, is not affected by the ring anymore and reaches the uncertainty zone where it stops or passes through it, carries out dampening free oscillating movements, but finally stops within the uncertainty zone (position 4).

The size of the uncertainty zone and the position where the fabric stops depend on the mechanical parameters of the fabric, i.e. the ratio of the specific weight, spring stiffness, viscous damping factor and the stick-and-slip friction coefficient. If the stick friction coefficient is high compared to the other values, the uncertainty zone is wide, and the fabric is likely to stop without oscillation. If the stick friction coefficient is low compared to the other values, the uncertainty zone is less wide, and it is possible that the fabric reaches its equilibrium state after carrying out dampening free oscillating movements.

Hence our proposal for modification is to take into consideration of an element that models the stick-and-slip friction in addition to the spring and viscous damper in particle system based models. Such a modification might make the solution of this already complex system even more complex, however the result of the simulation would be more realistic. On the other hand, further work is needed here which would worth to investigate in detail supported by more experimental data.

Effect of bending and shearing properties on drapeability

Apart from drape measurements, all three specific fabric samples were tested with the KES system. Figures 10 and 11 summarize the results of bending and shearing tests that are the most important ones considering draping behavior.

The results of bending and shearing tests are in line with the results of drape measurements as fabrics with higher shearing and bending stiffness have also higher drape coefficients.

CONCLUSION

Draping properties provide important information for the 3D modeling of fabrics. The most common properties are drape coefficient, DC and number of nodes, n. A new factor, drape unevenness (DU) that helps us to get a better picture of draping was created in our work.

Also in this work, a new method and a new device were described for measurement of draping properties, and with the help of this device the drape properties of the fabric are determined after dynamic influence. The special device is a ring that can exert different intensity dynamic forces on the fabric during drape formation depending on the actual size of the ring. This method makes it possible to measure the drape properties in a more reproducible way that approaches the real usage conditions better than in case of measurements without a ring.

A large number of measurements were carried out on three identical fabrics that differed only in the twist direction of its constituent yarns using Sylvie 3D Drape Tester. The main aims of the measurements were to determine the relation between the drape properties and yarn twist directions and to study the effect of rings.

The analysis of drape properties of fabrics, which composed of yarns with different twist directions, proved that although fabrics in which warp and weft yarns have Z-Z twist direction are thinner, they are mechanically more rigid, their drape coefficient values are higher and

17

have more waves. If the warp and weft yarns of the fabric have Z-S twist direction respectively, the fabric is thicker but mechanically less rigid while their drape coefficients are lower and have less waves.

The analysis of the drape measurements, which was carried out at different dynamic impact, revealed that the stronger dynamic effect, i.e. smaller ring inner diameter, leads to smaller drape coefficient. Dynamic impact reduces the deviation of the drape coefficient as well, and hence makes measurements more reproducible and exact. The method increases the number of waves and makes the drape geometry more even.

Based on the test results obtained in this work, a simplified fabric behavior model was developed as well. Our results were supported by introduction and behavior analysis of the simplified model – one-mass oscillating system – of the fabric. But the analysis of the drape formation process indicates that stick-and-slip Coulomb friction has to be considered as well among the inner forces. With the help of such a modification in the model, we believe that the behavior of the fabric at different ring diameters and the simulation program would provide results closer to real material behavior. However, further work is needed here providing a detailed analysis with more experimental data.

The test results showing the effect of the twist direction of the warp and weft yarns and the dynamically influenced drape testing can contribute to the fabric behavior simulations so that the theoretical models can be improved further for more realistic representations.

Acknowledgements

LITERATURE CITED

[1] Geršak, J. Investigation of the impact of fabric mechanical properties on garment appearance. *Tekstil* 2003; 52: 368-378.

[2]   Geršak, J. Study of relationship between fabric elastic potential and garment appearance quality. *Int J Cloth Sci Technol* 2004; 16: 238-251.

[3]   Cusick GE. The dependence of fabric drape on bending and shear stiffness. *Journal of the Textile Institute* 1965; 56: 596-606.

[4]   DA Design & Measurement [Internet]. Korea: D&M Technology Co. Ltd.; c1997-2008 [updated 2010 Aug 26; cited 2010 Sept 20]. Available from: http://www.dnmco.com/.

[5]   Matsudaira M, Minzhang Y. Features of conventional static and new dynamic drape coefficients of woven silk fabrics. *Textile Research Journal* 2003; 73: 250-255.

[6]   Matsudaira M, Minzhang Y, Kinari T, Shintaku S. Changes in the static and dynamic drape coefficients of polyester fabrics through the finishing stages. *Textile Research Journal* 2003; 73: 59-63.

[7]   Shyr TW, Wang PN. A comparison of the key parameters affecting the dynamic and static drape coefficients of natural-fibre woven fabrics by a newly devised dynamic drape automatic measuring system. *Fibres & Textiles in Eastern Europe* 2007; 15: 81-86.

[8]   Morooka H, Niwa M. Relation between drape coefficients and mechanical properties of fabrics. *Journal of the Textile Machinery Society of Japan* 1976; 22: 67-73.

[9]   Robson D, Long CC. Drape Analysis using Imaging Techniques. *Clothing and Textiles Research Journal* 2000; 18: 1-8.

[10]   Kawabata S. *The standardization and analysis of hand evaluation*. 2nd ed. Osaka: Textile Machinery Society of Japan, 1980, p.75.

[11]   Lam A, Raheja A, Govindaraj M. Neural network models for fabric drape prediction. IEEE Xplore Digital Library [Internet]. 2004 July [cited 2011 Jan 17]; 4: [p. 2925-2929]. Available from: http://ieeexplore.ieee.org/xpls/abs_all.jsp?arnumber=1381128

[12]   Sidabraitė V, Masteikaitė V. Effect of woven fabric anisotropy on drape behaviour. *Materials Science* 2003; 9: 111-115.

[13]   Gräff J, Kuzmina J. Cloth Simulation using Mass and Spring Model. In: Penninger A, Kullmann L, Vörös G, editors. Material science. Mechanical engineering 2004: Proceeding of 4th conference on mechanical engineering; 2004 May 27-28; Budapest, Hungary. Budapest: BUTE; 2004. p. 443-447.

[14]   Jevšnik S, Geršak J. Modelling the Fused Panel for a Numerical Simulation of Drape. *FIBRES & TEXTILES in Eastern Europe* 2004; 12: 47-52.

[15] Rausch J, Zhuang RC, Mäder E. Systematically varied interfaces of continuously reinforced glass fibre/polypropylene composites: Comparative evaluation of relevant interfacial aspects. *eXPRESS Polymer Letters* 2010; 4: 576–588.

[16] Bhattacharyya D, Maitrot P, Fakirov S. Polyamide 6 single polymer composites. *eXPRESS Polymer Letters* 2009; 3: 525–532.

[17] Halász M, Tamás P, Gräff J, Szabó L. Computer Aided Measuring of Textile-mechanical Parameters. *Materials Science Forum* 2008; 589: 311-316.

[18] Tamás P, Geršak J, Halász M., Gróf G. Sylvie 3D Drape Tester - New system for measuring fabric drape. *Tekstil* 2006; 10: 497-502.

[19] Tamas P, Göktepe F, Halasz M, Al-Gaadi B. New Method for Dynamic Drape Measurement of Fabrics. In: Kadoglu H, Kumbasar EPA, Celik P, Arikan CO, Cay A, Damci G, editors. AUTEX 2009: Proceeding of AUTEX 2009 World Textile Conference; 2009 May 26-28; İzmir, Turkey. Izmir: EGE University; 2009. p. 579-584.

[20] Al-Gaadi B, Gersak J, Göktepe F, Halász M, Tamás P, Göktepe Ö. Fabric Drape Examination Using Ring-controlled Equipment. In: Sariisik M, Karabay G, editors. ITTC 2010: Proceeding of 4th International Technical Textiles Congress; 2010 May 16-18; Istanbul, Turkey. Istanbul: Dokuz Eylül University; 2010. p. 7.

[21] Göktepe F, Halasz M, Tamas P, Göktepe Ö, Gersak J, Al-Gaadi B, et al. Twist Direction and Yarn Type Effect on Draping Properties. In: Simoncic B, Hladnik A, Pavko-Cuden A, editors. ISNT 2010: Proceeding of 41th International Symposium on Novelties in Textiles; 2010 May 27-29; Ljubljana, Slovenia. Ljubljana: University of Ljubljana; 2010. p. 171-177.

Influence of Undergarments on the Comfort Level of Scoliosis Brace Wearers

Orsolya Nagy Szabó [1], Jelka Geršak [2], András Koleszár [1] and Marianna Halász [1,*]

[1] Sándor Rejtő Faculty of Light Industry and Environmental Protection Engineering, Institute for Industrial Product Design, Óbuda University, Doberdó út 6., H-1034 Budapest, Hungary; szabo.orsolya@uni-obuda.hu (O.N.S.); koleszar.andras@uni-obuda.hu (A.K.)

[2] Faculty of Mechanical Engineering, Research and Innovation Centre for Design and Clothing Science, University of Maribor, Smetanova ulica 17, SI-2000 Maribor, Slovenia; jelka.gersak@um.si

* Correspondence: halasz.marianna@uni-obuda.hu

Abstract: Bracing has proven to be an effective method for the conventional treatment of scoliosis in young people. A brace, a therapeutic device, covers the upper body and promotes healing by applying pressure to specific areas. However, wearing a scoliosis brace negatively affects the user's thermo-physiological well-being and often leads to discomfort. In this study, we investigated the influence of T-shirts as an undergarment on the thermo-physiological well-being of the brace wearer. For this purpose, we performed a comparative analysis of six T-shirts made from different special knitted fabrics. We carried out wearing tests in a computer-controlled climate chamber according to a predetermined protocol. The test subject wore the orthopedic brace over the different T-shirts at three different temperatures. The results indicate that the knitted fabrics of undergarments and environmental conditions considerably impact the wearer's thermo-physiological comfort. In the tests, the T-shirts made from the selected functional fabrics performed very well. The T-shirt made from the classic cotton fabric containing elastane yarn also performed well and was the most environmentally friendly. Currently, due to its lower price and easier availability, this cotton T-shirt can be recommended for wearing under a scoliosis brace.

Keywords: scoliosis brace; clothing physiology; undergarment; knitted fabrics; textile material testing; climate chamber

1. Introduction

The number of people with scoliosis is increasing year by year [1]. Scoliosis is regarded as a three-dimensional structural deformity of the spine and trunk, which may worsen during growth [1–3]. Scoliosis is most prominent in adolescence (10–16 years) and is more common among girls. Improvement can be achieved with high corrective braces [4–7]. The brace applies external corrective forces to the special points of the trunk to halt the progression of the abnormal spinal curvature, correct it during growth, or to avoid further progression of an already established pathological curve in adulthood [8].

Various braces are available with different approaches and outcomes [4]. Biomechanically, correction may vary according to brace type. Each brace is tolerated differently, which may affect compliance [9,10]. The brace is manufactured according to the patient's measurements and disease type by an orthotist. When making a brace, the orthotist chooses the pressure points of the brace for the healing effect so that when a patient wants to avoid the discomfort they cause, they have to use their own muscle power to bring and hold their body precisely in the correct position. If the patient wears the brace for a sufficient time, usually several years, improvement and even complete recovery are possible [11–14].

The braces usually are made from a special thermoplastic polymer (high- and/or low-density polyethylene, copolymer, or modified polyethylene) and fit around the upper

body. They are worn over undergarments every day. Some are worn overnight; some are worn 23 h a day [15–17].

Although braces for scoliosis today are more comfortable than ever before, they still have a low compliance rate for various physical, physiological, and emotional reasons [18]. Patients who wear orthopedic braces are also faced with specific problems, such as heat, sweat, heaviness, stiffness, and skin discomfort or problems. Therefore, this research investigates the influence of underwear and activity dynamics on thermo-physiological comfort when the orthopedic braces are worn in a warm environment, which corresponds to high summer temperatures between 25 °C and 32 °C.

Several studies have been conducted on creating fashionable undergarments for brace wearers [19–21]. Their functional characteristics can be achieved by designing the cutting lines to avoid the pressure points of the brace and using unique patterns created with body data of 3D optical scanning [22–24]. Still, the design alone is not enough to reduce physiological inconvenience.

Much research has been conducted in the field of thermo-physiology addressing the thermal comfort level of special devices and clothing [25–27], primarily thermal protective clothing, most often firefighter clothing [28–30]. The thermo-physiological comfort of firefighters, workers in some industries, soldiers, or racing car drivers and their safety is an extremely important topic. The problems associated with clothing physiology of young people forced to wear braces for spine treatment is similar, but we did not find any research on this topic.

Much research is devoted to studying functional materials [31], especially those containing microencapsulated phase-change materials (PCMs). Good results have been reported with these materials in thermal protective clothing, even though the PCM capsules have a cooling or heating effect of only approx. 15 min long [26,28–30,32,33]. In addition to materials containing PCM capsules, functional textiles developed specifically for better moisture wicking are also extensively researched, for example, artificial fibers that have a specially shaped cross-section [29,34,35].

Our research aims to reduce the inconvenience of wearing a brace while retaining its essential functions. We set out to improve patients' physiological and mental well-being by creating fashionable undergarments with functional textiles.

A brace, made from a polymeric material, is a thick, continuous, non-porous layer around the upper body; wearing a brace hinders sweat evaporation and heat dissipation, so the user may experience an unpleasant microclimate during physical exertion or when in a warm environment. Therefore, major requirements for the undergarment are its moister absorption attributes, air permeability, and temperature balancing capability.

The undergarment worn under a brace must fit one's body to avoid it from wrinkling or riding up. Wrinkling and riding up are uncomfortable even in normal circumstances, but if they occur under a brace, they can cause pain or produce bruises under the pressure points of the brace. Therefore, it is of primary importance to use elastic materials and create a unique design to make the undergarment act as a 'second skin' without wrinkling, running, or bunching up under the brace. These inconveniences can be avoided with the use of a highly elastic fabric that can ensure that the undergarment fits the body perfectly and can change its shape to adapt to the body and its movements.

Our investigation focused on the selection of fabrics for undergarments. We studied whether the comfort level of wearing undershirts under an orthopedic brace could be affected by the kinds and properties of the fabric of the undergarment. Our aim was to find a fabric with the best thermo-physiological comfort and, if possible, the most environmentally friendly fabric for the undershirts worn under an orthopedic brace [36].

2. Materials

We based the experiments on a special construction of T-shirts as the first layer to be worn under a scoliosis brace in a hot environment. The textiles of T-shirts are different knitted fabrics. The most important criteria for selecting the textiles were appropriate

thermo-physiological properties and highly elastic behavior. Based on these criteria, we selected six textiles, one classic cotton knitted fabric containing elastane yarn (Cotton) and five functional knitted fabrics. For functional knitted fabrics, we chose a high-performance moisture-wicking fabric (MW-C01) and four different types of fabrics containing PCM microcapsules (OU-W02, OU-F03, OU-B04, and OU-C05). We bought the Cotton and the OU-C05 fabrics in a store, and the other four from the manufacturer for our research purpose. We assumed that these fabrics would be suitable for wearing under a brace. Table 1 shows the basic properties of these knitted fabrics.

Table 1. Basic properties of the knitted fabrics.

Kind of Knitted Fabric	Textile Composition	Structure of Fabrics	Thick-ness [mm]	Mass [g/m²]	Yarn Count [Tex]	Course Density [Piece/10 mm]	Wale Density [Piece/10 mm]	PCM Melt Peak [°C] (Nominal Data)	PCM Storage Capacity [J/g] (Nominal Data)
Cotton	97% cotton 3% elastane	Single weft-knitted	0.64	242	19.3	26	16	-	-
MW-C01	100% PES with silver ions, and special filament cross-section	Double pique-knitted	0.73	168	13.0	17	12	Special filament cross-section	
OU-W02	66% cotton 28% viscose with PCM capsules 6% elastane	Single weft-knitted	0.64	198	15.7	28	18	24–27	>2.5
OU-F03	95% cotton 5% elastane coating: silicon with PCM capsules	Single weft-knitted	0.65	146	16.4	22	17	26–30	>6
OU-B04	66% lyocell 28% viscose with PCM capsules 6% elastane	Single weft-knitted	0.66	175	15.6	26	17	24–27	>2.5
OU-C05	59% PES 39% viscose with PCM capsules 2% elastane	Rib weft-knitted	0.68	192	22.4	20	16	no data	no data

We examined the most important physical characteristics of the selected materials in terms of comfort level: water absorption, speed of water-wicking, thickness loss due to abrasion, air permeability, thermal conductivity, and deformability. Table 2 contains these physical characteristics for each fabric, which we determined as the average of 5 tests in each case. The data were measured specifically for the comparison of the tested materials.

Water absorption ability was measured according to the AATCC TM195-2012 [37] standard. During the test, the sample was immersed in water for 20 min and then sandwiched between two sheets of blotting paper to remove excess moisture. We measured the dry and wet weight of samples, and expressed water absorption as a percentage increase in mass (Table 2).

Water-wicking speed was evaluated according to the AATCC TM 197-2013 [38] standard. Wicking refers to spreading water through a given area via capillary action in a material. During the test, the samples were hung vertically, and 10 mm of them were immersed in water. After immersion, the wet area—wicking height—was measured from the water level every 5 min. The results of wicking speed are presented in Table 2.

Table 2. The physical characteristics of selected knitted fabrics.

Kind of Knitted Fabric	Water Absorption m_w [%]	Water-Wicking Speed v_w [mm/min]	Thickness Loss h_{av} [%]	Air Perme-ability $Q \left[\frac{dm^3}{m^2 \cdot s}\right]$	Thermal Conductivity $\lambda \left[\frac{W}{mK}\right]$	Deformation Due to Tensile Force/50 mm	
						0.5 N Wale Direction ε [%]	2.8 N Course Direction ε [%]
Cotton	186	3.6	7.8	14.8	0.0565	5.2	17.7
MW-C01	300	3.5	4.1	210.3	0.0508	2.4	11.6
OU-W02	233	3.8	6.3	28.9	0.0513	5.7	22.3
OU-F03	254	2.7	12.7	51.7	0.0515	8.6	26.4
OU-B04	218	1.3	8.9	99.6	0.0525	9.1	27.6
OU-C05	226	2.6	4.4	141.4	0.0516	3.3	27.5

The thickness loss of knitted fabrics due to abrasion was measured according to the ASTM D4158 [39] standard using the TKI Abrasion Tester. Considering the purpose of use, we chose abrasion with the brace material and the crossing direction movement, which is the most demanding among the movement combinations. Recourse speed was 60 cycles per minute for 30 min with a friction force of 10 N. The results of thickness loss are shown in Table 2.

We measured air permeability according to the ISO 9237:1999 [40] standard using the Metefem FF-12 7236-038 device at a pressure difference of 100 Pa. The results of air permeability tests are presented in Table 2.

We performed the thermal conductivity tests using the KES-F7 Thermo Labo II device for thermal properties (Table 2).

Fabric elasticity is an important parameter, which plays a key role, particularly in the case of tight-fitting garments. Tight-fitting garments of elastic fabric are tailored to a smaller size than the actual size of the wearer's body. Size reduction is usually 5 percent in body length and 15 percent in circumference, but experience has shown that this amount may not be suitable for some fabrics. To specify these values for the selected fabrics, we also performed tensile tests (with a Textenzer tensile tester device) using the Grab testing method on partially gripped specimens according to the ISO 13934-2:2000 [41] standard. Each specimen was 100×150 mm with a gauge length of 100 mm. Based on practical experience, we determined the specific tensile force in both directions where the T-shirt fits the body but is still comfortable for the wearer. These values are 0.5 N/50 mm in the wale (in body length) direction and 2.8 N/50 mm in the course (in circumference) direction. Specific elongation values measured at these specific tensile force values are shown in Table 2.

The Chêneau brace we used is made of a 5 mm thick HDPE (Mass: 0.941 g/cm³) polymer plate. The brace weighs 0.9 to 1.5 kg depending on size. The HDPE polymer plate lacks vapor permeability or moisture-wicking characteristics and is essentially a thermal insulation material. Figure 1 shows a Chêneau brace.

Figure 1. A Chêneau brace, front and back.

3. Methods

These tests aimed to assess the thermo-physiological properties of the undergarment made from selected knitted fabrics, when worn under a brace.

For this purpose, we created a T-shirt prototype pattern (Figure 2).

Figure 2. The T-shirt prototype. Front view (**a**), back view (**b**), front view on the mannequin (**c**), back view on a girl with a decorated brace (**d**).

The special feature of the prototype is that its seam lines avoid the pressure points of the brace, which improves the wearing comfort of the T-shirt.

We could not use brace wearers as test persons due to their young age. Therefore, during the tests, one member of our research team assumed the role of the test person, and she performed the tests in the climate chamber on herself. Salus Orthopaedics Technology Ltd. agreed to make a personalized Chêneau brace for her [15]. Since brace is an expensive orthopedic device, we were only able to use this one test subject. Based on the designed T-shirt prototype, we made a T-shirt from each selected knitted fabric for the test person in her size.

In this study, we carried out wearing tests during which the test person wore the brace over the T-shirts we made. According to a predetermined protocol, we completed the tests in a computer-controlled climate chamber, which provides artificially created ambient conditions, that is, a constant temperature, relative humidity and air velocity. The climate chamber contains a treadmill, a small table, a chair, an alarm and a video camera that transmits the image of the test subject for continually observation (Figure 3).
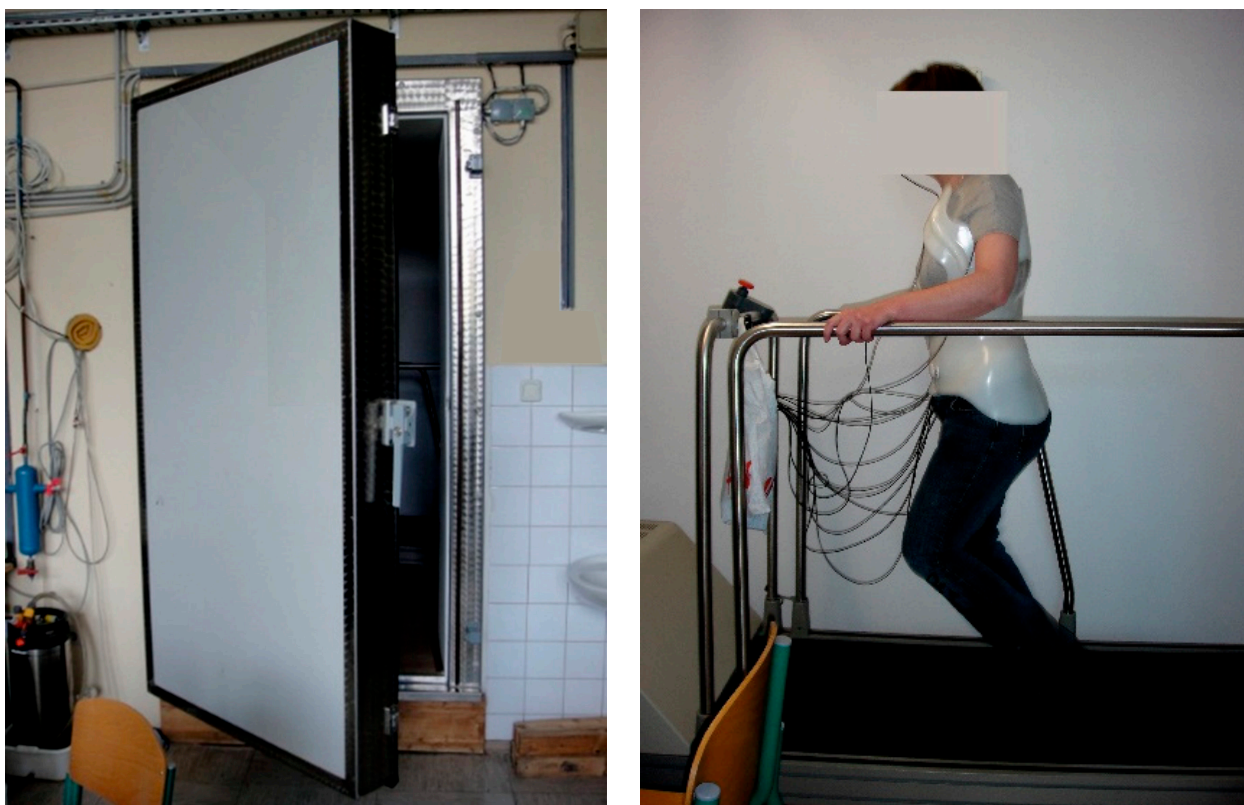
Figure 3. The climate chamber with the treadmill and the test person wearing the brace.

During the tests in the climate chamber, there were three different ambient temperatures (25 °C, 28 °C, and 32 °C), a constant relative humidity of 50%, and an air velocity of 0.5 m/s. At each of the three ambient temperatures, we performed six tests, during which the test subject wore one of the six T-shirts under the brace; therefore, we performed a total of 18 tests.

In this study, we attempted to simulate the activity of a person who wears a brace. In each activity, we gave sufficient time for the test person to adapt to the thermal environment. The total duration of the test was determined based on the preliminary trials and the mental/physical comfort of the brace wearer.

During testing, the test subject wore T-shirts made from the selected knitted fabrics under her personalized Chêneau brace. Each test lasted 75 min based on the pre-determined protocol, which included the following:

- 15 min of preparation and acclimatization without data collection;
- 20 min of rest (seated position);
- 20 min of walking at a speed of 2.5 km/h on the treadmill;
- 15 min of rest (seated position);
- 5 min of walking on the treadmill at a speed of 3.5 km/h.

We examined the thermo-physiological parameters using the MSR (Modular Signal Recorder) measuring device from MSR Electronics GmbH, Seuzach, Switzerland. The MSR device is a modular unit for measuring various physiological parameters, such as skin temperature and humidity at the surface of the skin (microclimate humidity). We measured skin temperature at seven different locations on the body and the humidity on the skin surface at four different locations on the body according to EN ISO 9886: 2004 [42] (Figure 4).
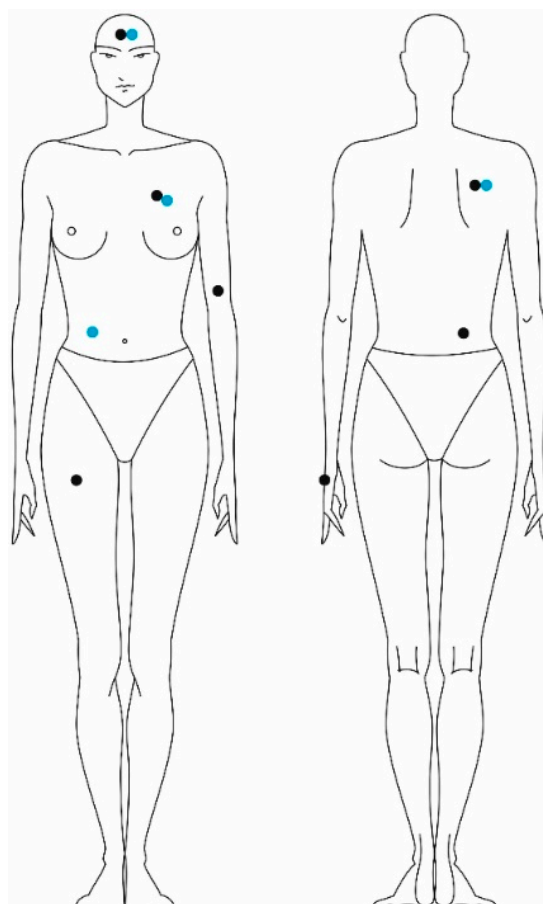
Figure 4. The locations where the skin temperature and relative humidity were measured.

To estimate the sweat rate, the test subject weighed her own mass naked before and after testing. The subject's clothing was also weighed before and after testing. Based on the subject's weight loss and the clothing ensemble's weight gain (through absorption of the subject's sweat during exercise), we determined the loss of the test person's body fluid due to sweating.

4. Results

The results show that the undergarment made from the selected knitted fabrics, and environmental conditions considerably impact the wearer's thermo-physiological comfort.

Skin temperature and relative humidity at the skin surface were also measured in the measuring point on the chest. Figure 5 shows the results in this measuring point at three ambient temperatures.

The analysis of skin temperature shows that with higher ambient temperature, skin temperature increases. The results also show that the undergarment made from Cotton knitted fabric provided similar results to the undergarments made from fabrics containing phase-changing materials. At the beginning of the test, the undergarment with built-in PCM microcapsules slows down the increase in temperature. However, after the PCM melts, it shows no effect on body temperature. At the beginning, the humidity values show some difference, but these minor differences become insignificant after a short time.
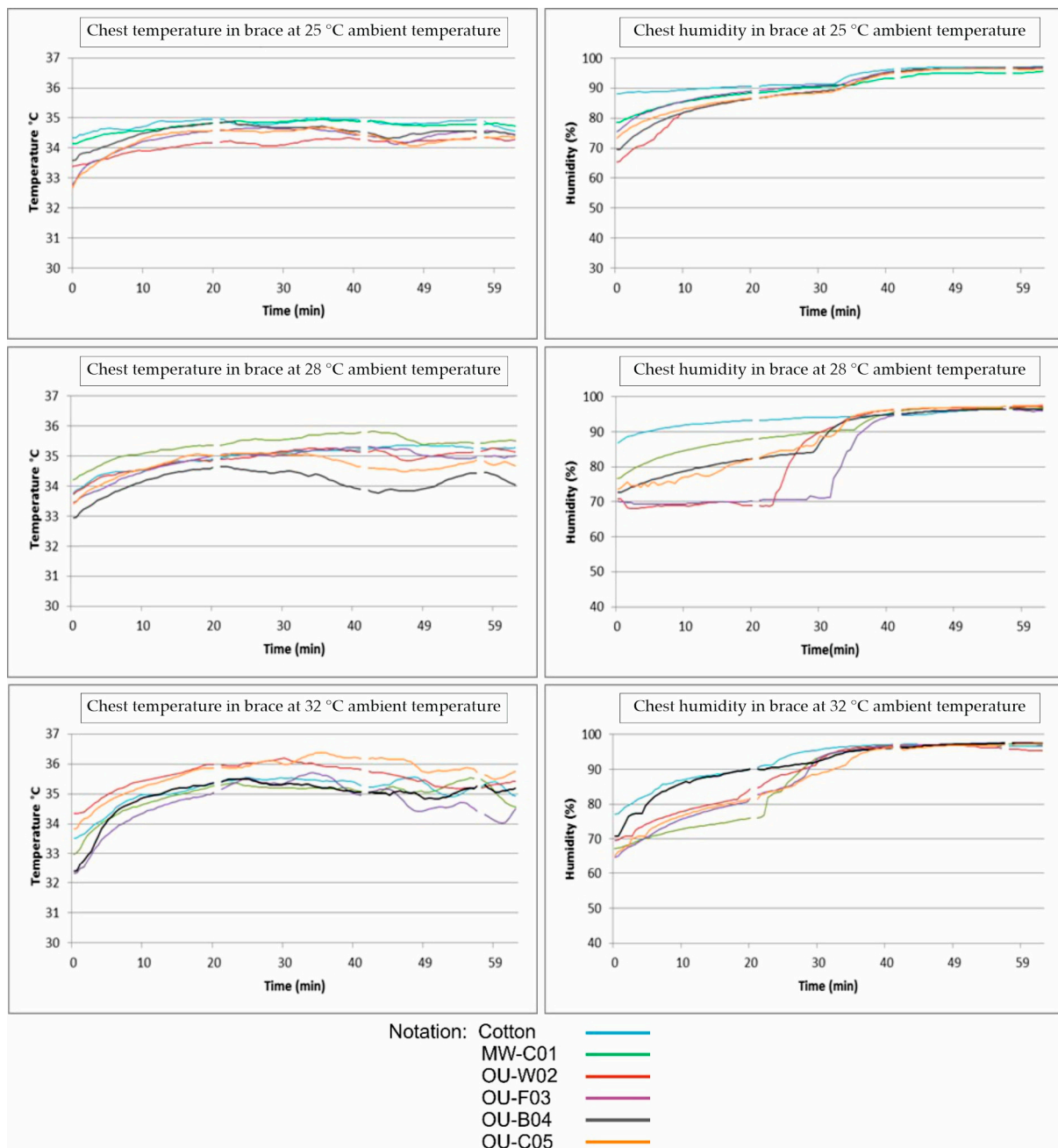
Figure 5. Skin temperature and relative humidity at the skin surface of the test subject as a function of time, at the chest measurement location, at three different ambient temperatures.

In the course of the test, we obtained well-evaluable results by measuring the weight of the test person's body and clothing.

Most heat is dissipated through the skin. The brace prevents this on a large part of the upper body because it prevents the evaporation of sweat, which would cool the body. Therefore, the undergarment must absorb the sweat released by the body which cannot evaporate. We measured the decrease in the body weight of the test person during the time spent in the climate chamber and the increase in weight of the T-shirt after soaking up moisture.

Less moisture picked up by a T-shirt and a lower body weight loss of the test person during a test means that the test person sweated less, so this T-shirt provides a higher

level of comfort. The decrease in body weight is shown in Figure 6, and the weight gain of T-shirts due to moisture absorption is shown in Figure 7.
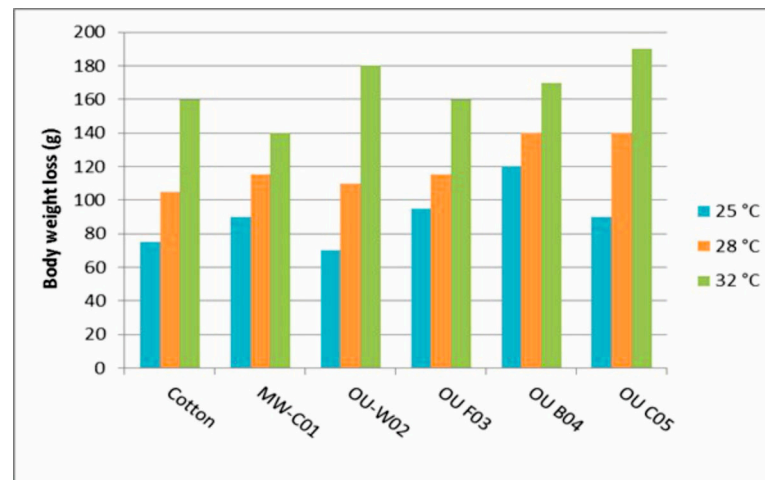

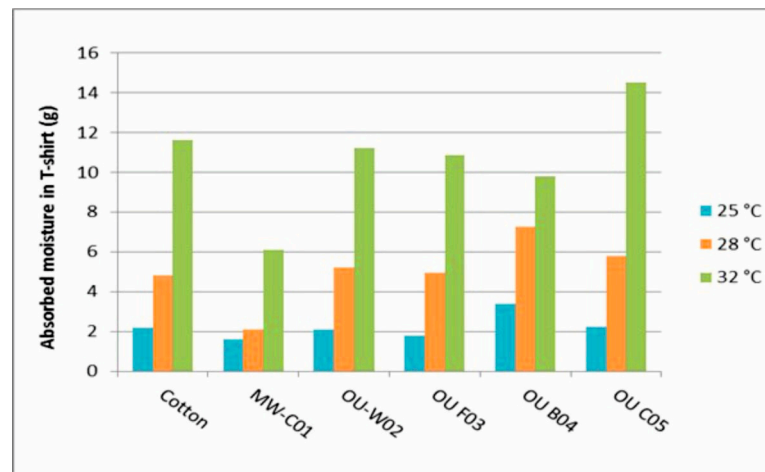**Figure 6.** The effect of different T-shirt fabrics on body weight loss at different temperatures.

Figure 7. The effect of different T-shirt fabrics on the amount of moisture absorbed at different temperatures.

The measurement results show that the body weight decrease depends on the properties of the fabric of the T-shirt. Weight reduction was between 70 and 120 g at the ambient temperature of 25 °C, between 105 and 140 g at 28 °C, and between 160 and 190 g at 32 °C, depending on the fabric of the T-shirt worn. The body weight of the test person mostly decreased the least at all ambient temperatures when she wore the Cotton T-shirt.

Figure 7 shows that the amount of moisture absorbed by the T-shirts depends also on the properties of the knitted fabric. Moisture absorption varied between 1.5 and 3.7 g at the ambient temperature of 25 °C, between 2.0 and 7.5 g at 28 °C, and between 6.0 and 14.5 g at 32 °C, depending on the T-shirt worn. The T-shirt made from high-performance moisture-wicking fabric (MW-CO1) had the lowest amount of absorbed moisture. The T-shirt made from the OU-C05 fabric at 32 °C and the T-shirt made from the OU-B04 fabric at 25 °C and at 28 °C had the highest amount of absorbed moisture.

5. Subjective Assessment

We made T-shirts from the aforementioned selected knitted fabrics, which were worn by 12 people. The test subjects in this examination were girls of age 16 to 18, all wearing braces. The girls voluntarily and willingly agreed to wear the T-shirts for the test. The girls

wore the T-shirts under ordinary conditions in a special four-day long camp organized for the brace wearers. According to the prototype pattern, we made four T-shirts from the selected fabrics for the four days, for every girl specific to their size.

Since only 4 days were available for this wearing test, two fabrics had to be omitted from the test. The T-shirt made from the MW-C01 material was very uncomfortable during the climate chamber tests, so we did not make T-shirts from this material for the girls. The other fabric we omitted was the OU-W02 material because its composition and behavior are similar to those of the OU-B04 material. Therefore, we would presumably get similar results during the wearing test, as in the case of the OU-B04 material.

The girls wore each T-shirt for one day, so the wearing conditions were the same. They rated the T-shirts on the last day of the camp. The testers' feedback was positive; the girls were happy that these T-shirts suited their special needs more than the ones available off the shelf. Some of them have been wearing these T-shirts since then. The girls provided feedback on their experience by filling out a questionnaire. In the questionnaire, we asked the girls about the quality of the material: the feel of the material, the fit to the body, and the comfort of wearing. Tables 3–5 contain their answers to the relevant questions of the questionnaire.

Table 3. Ranking of the T-shirts according to the touch of the fabric. (1 is the best and 4 is the worst).

Kind of Knitted Fabric	Order According to the Girls	Sum	Ranking
Cotton	1, 1, 2, 2, 2, 2, 3, 3, 3, 3, 3	27	2
OU-F03	1, 1, 2, 2, 3, 3, 3, 3, 3, 3, 3	29	3
OU-B04	1, 1, 1, 1, 1, 1, 1, 1, 2, 2, 2, 2	16	1
OU-C05	4, 4, 4, 4, 4, 4, 4, 4, 4, 4, 4, 4	48	4

Table 4. Ranking of the T-shirts according to the comfort of wearing them. (1 is the best and 4 is the worst).

Kind of Knitted Fabric	Order According to the Girls	Sum	Ranking
Cotton	1, 1, 1, 1, 2, 2, 2, 3, 3, 3, 3	24	2
OU-F03	2, 2, 2, 2, 3, 3, 3, 3, 3, 3, 3	32	3
OU-B04	1, 1, 1, 1, 1, 1, 1, 1, 2, 2, 2, 2	16	1
OU-C05	4, 4, 4, 4, 4, 4, 4, 4, 4, 4, 4, 4	48	4

Table 5. Ranking of the T-shirts according to fit. (1 is the best and 4 is the worst).

Kind of Knitted Fabric	Order According to the Girls	Sum	Ranking
Cotton	1, 1, 1, 1, 1, 1, 2, 2, 2, 3, 3	19	1
OU-F03	2, 2, 2, 2, 2, 2, 3, 3, 3, 3, 3	29	3
OU-B04	1, 1, 1, 1, 1, 2, 2, 3, 3, 3, 3, 3	24	2
OU-C05	4, 4, 4, 4, 4, 4, 4, 4, 4, 4, 4, 4	48	4

The girls thought that in wearing comfort and touch of fabric, the OU-B04 material was the best, and the OU-C05 material was the least good. The OU-B04 material is a soft and elastic fabric, which is comfortable to wear, according to the testers. In comfort and touch, Cotton was the second best after OU-B04.

One of the most important criteria of a T-shirt is to fit the body perfectly. In designing undergarments for brace wearers, it is of primary importance that the final product does not wrinkle or run up under the brace and fits the body well.

T-shirts manufactured from Cotton knitted fabrics are close-fitting and follow the body without wrinkles. The T-shirt made from the OU-C05 knitted fabric proved to be too loose, and as a result, wrinkles appeared. Therefore, it did not meet the requirements. With a bigger under-tailoring value, it is possible to improve the fitting of the OU-F03 and OU-B04 fabrics.

During the test wearing, the brace did not damage the T-shirts.

To summarize, the girls preferred the elasticity and the thermo-physiological comfort of the Cotton T-shirt and the thermo-physiological comfort and soft touch of the OU-B04 T-shirt. According to the girls, the OU-F03 knitted fabric proved to be mediocre in every respect, and the OU-C05 knitted fabric was the worst.

6. Discussion

We chose the six tested fabrics because we believed that they might meet the special requirements of undergarment fabrics worn under a brace.

The evaluation of the physical characteristics of the selected fabrics, the tests conducted in the climate chamber, and the subjective assessment of the girls wearing braces provide a complete and detailed picture of the examined fabrics.

Therefore, it is not surprising that the fabrics (except OU-C05) performed well in the tests. The results confirmed our opinion that Cotton, an environmentally friendly, natural, and conventional fabric, can compete with the recently developed functional fabrics.

The significant aspects of the evaluation were the following:

- General thermo-physiological aspects: Good moisture absorption and moisture transmission properties, high air permeability, and advantageous temperature balancing capability.
- Mechanical properties: High elastic elongation and high abrasion resistance.
- Thermo-physiological test results: Lower body weight decrease, and lower perspiration rate of the test person, and suitability of the T-shirts at different temperatures.
- Subjective evaluation by the test persons.
- Availability off the shelf.
- Acceptable price-to-value ratio.
- Being environmentally friendly.

We ranked the fabrics according to different priorities.

Although the MW-C01 fabric was the best regarding moisture absorption and air permeability, and performed well in the climate chamber test as well, it is the worst regarding elastic deformation because it does not contain elastane fibers.

Although the Cotton fabric performed worst in moisture absorption and air permeability, it was good in elastic deformation and was balanced in the climate chamber test.

Among the fabrics containing PCMs, the OU-B04 fabric was the best, while the OU-C05 fabric was the weakest.

Another aspect was the opinions of the girls who performed the wear test. They liked the Cotton and OU-B04 T-shirts best. Due to the small elastic deformation, the MW-C01 fabric probably would not have won the girls' favor.

The last three aspects tip the balance toward the Cotton fabric. This fabric is the cheapest, it is easily available, and it is clearly the most environmentally friendly of the examined fabrics [43]. Since this fabric had a balanced performance in the tests, currently, the Cotton T-shirt can be recommended for wearing under a brace.

The results of our study are of limited validity as the climate chamber tests were performed with the participation of only one test person, and each T-shirt was tested only once at each temperature. Therefore, we have no data for statistical evaluation. Nevertheless, we believe our results are valuable, provide good data for orientation, and they are a good starting point for further more comprehensive investigations.

7. Conclusions

In this study, we researched how undergarment fabrics can influence a brace wearer's thermo-physiological comfort level. We compared six T-shirts made from different special knitted fabrics. In the wearing tests, the test person wore the brace over the undergarment. The tests were performed in a computer-controlled climate chamber at three different temperatures. In addition, we also received subjective assessments from teenage girls

wearing braces, who wore our shirts under their braces for a few days. The results indicate that the knitted fabrics of the undergarments and environmental conditions considerably impact the wearer's thermo-physiological comfort. The recently developed functional, high-performance moisture-wicking fabric and the functional fabrics containing PCMs performed very well in most aspects; therefore, they are suitable for wearing under a brace. However, unfortunately, they are expensive and currently hard to acquire. The T-shirt made from the classic Cotton fabric containing elastane yarn also performed well in the tests. Since this fabric is currently the most environmentally friendly, the cheapest, and the most easily available of all the examined fabrics, it can be recommended for wearing under a brace.

Author Contributions: Conceptualization, M.H. and J.G.; methodology, M.H. and J.G., validation, A.K. and O.N.S.; formal analysis, A.K. and O.N.S.; investigation, M.H. and J.G.; resources, M.H. and J.G.; data curation, A.K. and O.N.S.; writing—original draft preparation, O.N.S. and M.H.; writing—review and editing, J.G.; visualization, A.K. and O.N.S.; project administration, A.K. and O.N.S.; funding acquisition, M.H. and J.G. All authors have read and agreed to the published version of the manuscript.

Institutional Review Board Statement: No permission is required for this research.

Informed Consent Statement: Written informed consent was obtained from all subjects involved in the study to research and publish this paper.

Data Availability Statement: Detailed data can be provided by the corresponding author upon request.

Conflicts of Interest: The authors declare no conflict of interest.

References

1. Von Heideken, J.; Iversen, M.D.; Gerdhem, P. Rapidly increasing incidence in scoliosis surgery over 14 years in a nationwide sample. *Eur. Spine J.* **2018**, *27*, 286–292. [CrossRef]
2. Asher, M.A.; Burton, D.C. Adolescent idiopathic scoliosis: Natural history and long term treatment effects. *Scoliosis* **2006**, *1*, 2. [CrossRef]
3. Hawes, M.C.; O'Brien, J.P. The transformation of spinal curvature into spinal deformity: Pathological processes and implication for treatment. *Scoliosis* **2006**, *1*, 3. [CrossRef]
4. Landauer, F.; Wimmer, C.; Behensky, H. Estimating the final outcome of brace treatment for idiopathic thoracic scoliosis at 6-month follow-up. *Pediatr. Rehabil.* **2003**, *6*, 201–207. [CrossRef]
5. Weiss, H.R.; Moramarco, M. Scoliosis–treatment indications according to current evidence. *OA Musculoskelet. Med.* **2003**, *1*, 2013-03.
6. Weiss, H.R.; Werkmann, M. Rate of surgery in a sample of patients fulfilling the SRS inclusion criteria treated with a Chêneau Brace of actual Standard. *Stud. Health Technol. Inform.* **2012**, *176*, 407–410. [CrossRef]
7. Rigo, M. Radiological and cosmetic improvement 2 years after brace weaning—A case report. *Pediatr. Rehabil.* **2003**, *6*, 195–199. [CrossRef]
8. Grivas, T.B.; Kaspiris, A. European Braces Widely Used for Conservative Scoliosis Treatment. *Stud. Health Technol. Inform.* **2010**, *158*, 157–166. [CrossRef]
9. Wong, M.S.; Cheng, J.C.Y.; Lam, T.P.; Ng, B.K.W.; Sin, S.W.; Lee-Shum, S.L.F.; Chow, D.H.K.; Tam, S.Y.P. The effect of rigid versus flexible spinal orthosis on the clinical efficacy and acceptance of the patients with adolescent idiopathic scoliosis. *Spine* **2008**, *33*, 1360–1365. [CrossRef]
10. Weiss, H.-R.; Moramarco, M. Remodelling of trunk and backshape deformities in patients with scoliosis using standardized asymmetric computer-aided design/computer-aided manufacturing braces. *Hard Tissue* **2013**, *2*, 14. [CrossRef]

11. Nagy Szabó, O. Wear Comfort Improvement of Medical Aids Used for Spine Deformity Treatment. Ph.D. Thesis, University of West Hungary, Sopron, Hungary, 2014. Available online: http://doktori.nyme.hu/484/3/nagyne_szabo_orsolya_angoltezis.pdf (accessed on 29 June 2023).

12. Gaál, Z.; Antal, Á.; Tamás, P. Scoliosis Testing Featuresonthe Basis of Electronically Generated Moire Patterns. In Proceedings of the 8th IEEE International Symposium on Applied Machine Intelligence and Informatics, Herlany, Slovakia, 28–30 January 2010; pp. 335–340.

13. Bogdán, C.; Magony, A.D.; Birkfellner, W.; Antal, Á.; Tunyogi-Csapó, M. Segmentation of Moiré Fringes of Scoliotic Spines Using Filtering and Morphological Operations. *Acta Polytech. Hungarica* **2023**, *20*, 223–241. [CrossRef]

14. Liu, P.-Y.; Yip, J.; Yick, K.L.; Yuen, C.-W.M.; Ng, S.-P.; Tse, C.-Y.; Lawa, D. An Ergonomic Flexible Girdle Design for Preteen and Teenage Girls with Early Scoliosis. *J. Fiber Bioeng. Inform.* **2014**, *7*, 233–246. [CrossRef]

15. Introducing the Brace Maker Ferenc Marlok. Available online: https://www.youtube.com/watch?v=Mlvfol4-Nv (accessed on 2 May 2023). (In Hungarian).

16. Gregor-Svetec, D.; Szentgyörgyvölgyi, R.; Borbély, Á. Tensile and surface properties of foils made from LDPE. In Proceedings of the 5th International Symposium on Novelties in Graphics, University of Ljubljana, Ljubljana, Slovenia, 27–29 May 2010; pp. 689–694.

17. Nagy Szabó, O. Chêneau Brace Air Permeability Test. In Proceedings of the International Joint Conference on Environmental and Light Industry Technologies, Budapest, Hungary, 23–24 November 2017; pp. 195–204.

18. Tomaszewski, R.; Janowska, M. Psychological aspect of scoliosis treatment in children. *Stud. Health Technol. Inform.* **2012**, *176*, 428–432. [CrossRef] [PubMed]

19. Nagy Szabó, O.; Koleszár, A. Garments under brace life quality improve affect experiment of technology and physiology. *Biomech. Hungarica* **2013**, *6*, 67–74. [CrossRef]

20. Nagy Szabó, O.; Koleszár, A. Special underwear for young girls having scolosis problem. In Proceedings of the XXIV Micro CAD International Scientific Conference, Miskolc, Hungary, 18–20 March 2010; pp. 37–43.

21. Csanák, E. The CAL: Cognitive, apperceptive and representative aspects of fashion design—Side note to neuroaesthetic theory. *IOP Conf. Ser. Mater. Sci. Eng.* **2017**, *254*, 172008. [CrossRef]

22. Wenzel, K.; Antal, Á.; Molnár, J.; Tóth, B.; Tamás, P. New Optical Equipment in 3D Surface Measuring. *J. Autom. Mob. Robot. Intell. Syst.* **2009**, *4*, 29–32. Available online: https://www.jamris.org/index.php/JAMRIS/article/view/38/38 (accessed on 29 June 2023).

23. Geršak, J.; Halász, M.; Nagy Szabó, O.; Koleszár, A. 3D body datas integration in functional wear under brace. In Proceedings of the 12th AUTEX World Textile Conference, Zadar, Croatia, 13–15 June 2012; pp. 1023–1028.

24. Nagy Szabó, O.; Koleszár, A.; Halász, M.; Geršak, J. Functional Textiles Under Brace. In Proceedings of the International Joint Conference on Environmental and Light Industry Technologies, Budapest, Hungary, 21–22 November 2011; pp. 441–445.

25. Lang, M.; Müller, A. Climate socket—Focusing on thermal comfort in the prosthetic socket. In Abstract Book of ISPO World Congress, Lyon, France, 22–25 June 2015. p. 331. Available online: https://journals.sagepub.com/doi/pdf/10.1177/0309364615591101 (accessed on 29 June 2023).

26. Gao, C.; Kuklane, K.; Holmér, I. Cooling vests with phase change material packs: The effects of temperature gradient, mass and covering area. *Ergonomics* **2010**, *53*, 716–723. [CrossRef]

27. Arezes, P.M.; Neves, M.M.; Teixeira, S.F.; Lerao, C.P.; Cunha, J.I. Testing thermal comfort of trekking boots: An objective and subjective evaluation. *Appl. Ergon.* **2013**, *44*, 557–565. [CrossRef]

28. Rossi, R.M.; Bolli, W.P. Phase Change Materials for Impruvement of Heat Protection. *Adv. Eng. Mater.* **2005**, *7*, 368–373. [CrossRef]

29. Udayraj; Talukdar, P.; Das, A.; Alagirusamy, R. Heat and mass transfer through thermal protective clothing—A review. *Int. J. Therm. Sci.* **2016**, *106*, 32–56. [CrossRef]

30. Phelps, H.; Sidhu, H. A mathematical model for heat transfer in fire fighting suits containing phase change materials. *Fire Saf. J.* **2015**, *74*, 43–47. [CrossRef]

31. Ornaghi, H.L.; Neves, R.M.; Monticeli, F.M.; Agnol, L.D. Smart Fabric Textiles: Recent Advances and Challenges. *Textiles* **2022**, *2*, 582–605. [CrossRef]

32. Shim, H.; McCullough, E.; Jones, B. Using phase change materials in clothing. *Textile Res. J.* **2001**, *71*, 495–502. [CrossRef]

33. Mondal, S. Phase change materials for smart textiles—An overview. *Appl. Therm. Eng.* **2008**, *28*, 1536–1550. [CrossRef]

34. Das, B.; Das, A.; Kothari, V.K.; Fanguiero, R.; de Araújo, M. Effect of fibre diameter and cross-sectional shape on moisture transmission through fabrics. *Fibres Polym.* **2008**, *9*, 225–231. [CrossRef]

35. Varshneya, R.K.; Kothari, V.K.; Dhamija, S. A study on thermophysiological comfort properties of fabrics in relation to constituent fibre fineness and cross-sectional shapes. *J. Text. Inst.* **2010**, *101*, 495–505. [CrossRef]

36. Firšt Rogale, S.; Rogale, D. Advanced Materials for Clothing and Textile Engineering. *Materials* **2023**, *16*, 3407. [CrossRef]

37. *AATCC TM 195-2012*; Liquid Moisture Management Properties of Textile Fabrics. The American Association of Textile Chemists and Colorists (AATCC): Research Triangle Park, NC, USA, 2012.

38. *AATCC TM 197-2013*; Vertical Wicking of Textiles. The American Association of Textile Chemists and Colorists (AATCC): Research Triangle Park, NC, USA, 2013.

39. *ASTM D4158-01*; Standard Guide for Abrasion Resistance of Textile Fabrics (Uniform Abrasion). ASTM International: West Conshohocken, PA, USA, 2001.

40.   *ISO 9237:1995*; Textiles—Determination of Permeability of Fabrics to Air. ISO: Geneva, Switzerland, 1995.
41.   *ISO 13934-2:2000*; Textiles—Tensile properties of fabrics—Part 2: Determination of maximum force using the grab method. ISO: Geneva, Switzerland, 2014.
42.   *ISO 9886:2004*; Ergonomics—Evaluation of Thermal Strain by Physiological Measurements. ISO: Geneva, Switzerland, 2014.
43.   Muthu, S.S. (Ed.) *Handbook of Life Cycle Assessment (LCA) of Textiles and Clothing*; Woodhead Publishing Series in Textiles: Number 172; Woodhead Publishing: Cambridge, UK, 2015; ISBN 978-0-08-100187-5.
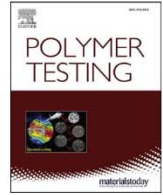
Shear and yarn pull-out grip for testing flexible sheets by universal load machines

Kolos Molnár [a,b], Ábris Dávid Virág [a], Marianna Halász [a,*]

[a] *Department of Polymer Engineering, Faculty of Mechanical Engineering, Budapest University of Technology and Economics, Műegyetem rkp. 3. H-1111, Budapest, Hungary*
[b] *MTA–BME Research Group for Composite Science and Technology, Műegyetem rkp. 3., H-1111, Budapest, Hungary*

ARTICLE INFO

ABSTRACT

The purpose of this research was to develop a novel, multifunctional apparatus that makes possible to carry out two common tests of woven fabrics and flexible sheet-like materials, namely the shear and the yarn-pull out test. We designed an apparatus that can be mounted on a universal load machine and makes possible to test the materials rapidly and precisely.

In this paper we introduce the apparatus and the related simple shear and yarn pull-out test methods, as well as the accuracy and reproducibility of the test results obtained. We carried out cyclic shear and yarn pull-out tests on plain and panama weave materials. We found that the relative deviations of the common shear (*G, 2HG, 2HG5*) and yarn pull-out parameters were around 5–9% in most cases that confirms the repeatability of the test method. With our method, one can carry out these tests without an expensive, dedicated test device.

1. Introduction

At human environmental textiles, at flexible sheets & composites (e. g. canopies), and at composite reinforcements it is necessary to know their various mechanical properties in order to be able to design and create complex structures [1–4].

In the former cases the textile or the flexible sheet has to suit to the shape of the body or adequate draping properties are required for the appropriate optical performance. At composite reinforcements, the textile has to conform the shape of the mold. In all these cases, besides the good handling possibilities, appropriate shear properties, flexibility and the role of the friction between the fiber bundles or yarns have high importance (and moreover these things also influence one another) [5–7].

1.1. The shear-tests of flexible sheets and textiles

The method for investigating the shear properties of textiles and other flexible sheets has to be simple and rapid to fit the current requirements of the industry. There are widely-known methods making available to determine the shear properties, but these are either complicated, or the stress state, generated by the test setup, is not ideal [8,9].

In case of woven textiles maybe the simplest method is when the specimen in bias direction (the weft and warp yarns are located in ±45° directions to the axis of pulling) is tested by a tensile tester [8]. As the endings of the yarns are not constrained in the shear zone, therefore the shear state is suitable, but complex. The problem is with the determination of the exact location of the pure-shearing zone and as the shear deformation is calculated from the strain of the whole sample it is hard to obtain precise results. The method can be further improved by image processing as Domskiené and Strazdiené [10] and Al-Gaadi and Halász [11] demonstrated. This method is more precise but maybe too complex for industrial purposes and besides, it does not make possible to carry out cyclic tests that is a significant disadvantage.

The other widespread method, when the textile or the canopy sample is fixed to a picture frame that has knuckle-joints in the corners. The two opposite corners of the frame are displaced by the load machine thus the square becomes a rhombus the way the specimen is sheared. This method makes possible to make cyclic tests. The method is simple but not precise because the stress state is not ideal near the clamping bars hence the yarns are bent [10–12]. Orawattanasrikul [13] elaborated a special method to avoid the bending of the yarns during tests. The edges of the textile is not clamped, but pinned into needles. These

needles make possible to transfer the shear forces, still makes possible the rotation of the yarns, therefore their bending can be neglected.

The Kawabata's Evaluation System for Fabrics (KES-FB) [14] can also be used for determining the shear properties of flexible sheets and textiles. At this method two parallel 200 mm long sides of a rectangular textile sample are clamped and one of them is moved to shear the specimen (Fig. 1/a) by an F_t [N] force. The initially 50 mm distance of the parallel clamps (X_0) gradually changes ($X(t)$) as a constant transversal pretension is applied during the test. The system is precise and the experiment can be carried out rapidly. The pretension (f_p [N/m]) is generated by a rotating drum and the requisite displacement is calculated from torque measurements that requires additional electronic control devices. As the device only operates in the $\pm 8°$ shear angle range, therefore the bending of the yarns along the two edges can be neglected.

The totally automated, computer controlled KES-FB device does a cyclic shear test. During the test the shear motion changes direction as the shear angle reaches $+8°$ or $-8°$. The schematic of the measurement and a typical specific shear force – shear angle diagram can be seen in Fig. 1. Based on the diagram, the so-called Kawabata parameters can be determined: the hysteresis of shear force at shear angle of 0.5° (2HG [N/m]), the hysteresis of shear force at shear angle of 5° (2HG5 [N/m]), the shear rigidity, calculated from the mean slope of the curve in the region between a shear angle of 0.5° and 5° (G [N/(m°)]), respectively.

1.2. The yarn pull-out tests of woven fabrics

The yarn pull-out test is also a widely researched topic. Various measuring devices were made to do these kinds of tests, but all of them are one of a kind. Currently, the commonly accepted yarn pull-out measurement device is unknown.

The yarn pull-out test can be used to determine the interaction between the yarns of woven fabrics. During the test, the force needed to overcome the mostly frictional connection between the yarn to be pulled out and the crossing yarns is measured. The interaction between the yarns has a fundamental role on the material properties. It influences the shearing, bending, wrinkling, etc. properties, moreover the impact strength and the energy absorbing capacity of woven fabrics, hence it is very important to know this interaction, especially for modelling their mechanical behavior [15,16].

The principle of the yarn pull-out test can be seen in Fig. 2, while Fig. 3 shows a typical result of a single measurement. During the test, the rectangular woven fabric specimen has to be clamped on both sides, then a single yarn is pulled out along the centerline in parallel with the clamps. It is important that the upper end of the yarn is clamped and pulled, the other end of the yarn has to be able to move free. At the first, static stage of the yarn pull-out test (Fig. 3) due to the increasing pull-out force, the yarn being pulled-out straightens out and stretches, which leads to shear deformation on both sides of the yarn. The specimen itself deforms leading to a displacement (d_t). The second, kinetic stage starts when the pull-out force reaches the peak value and overcomes the static friction force among the yarns. At this moment the yarn starts passing through the crossing yarns, leading to the increasing displacement of the yarn (d_y). The pull-out force (F_{po}) is gradually decreasing with periodic waves and tending to zero as the yarn passes through more and more transversal yarns. The magnitude of F_{po} also influences the vertical deformation of the specimen itself (d_t) that also decreases during this stage of the test.

In the case of another, modified test setup the free end of the pulled yarn overhangs the bottom edge of the fabric sample [18,19]. Fig. 4 shows a typical pull-out curve when the overhang was 50 mm. Due to this modification the kinetic phase of the yarn pull-out divides in two more phases. In the first region of the kinetic phase the yarn to be pulled out passes through the same number of crossing yarns, hence the end of the yarn does not reach the bottom edge of the fabric sample. In this phase the mean value of the periodic tensile force after a quick decrease sets at an approximately constant value. When the end of the yarn to be pulled out reaches the bottom edge of the fabric sample, the second region of the kinetic phase starts. This time the pulled yarn passes through fewer and fewer crossing yarns, hence the mean value of the periodic tensile force decreases and tends asymptotically to zero.

Several papers have been published on the yarn pull-out test and its results [11,17–23]. Using the capstan equation some [11,16] tried to determine the coefficient of friction among yarns from the yarn pull-out test results. However, the accuracy of the applied methods has not been proved yet. Knowing the maximal yarn pull-out force and the tensile strength of the yarn, Pan and Yoon [22] determined the critical yarn length. The critical yarn length is similar to the critical fiber length widely used in composite mechanics [24]. The critical yarn length equals the half of the critical fiber length and it means the smallest length of the embedded yarn that breaks due to the load instead of slipping out of the fabric.

1.3. The aim of the research

Yarn pull-out test is not a standardized test, therefore it does not include a standard measuring apparatus. Researchers usually build different clamps for this purpose, but these are typically only U-profile static clamps that are only suitable for yarn pull-out tests. Hence, many times they try to deduce the shear properties of fabrics from yarn pull-out tests [25,26].

To determine the shear properties of woven fabrics, we have previously described some well-known and widely used methods, including the Kawabata shear test. This measurement can be only carried out with
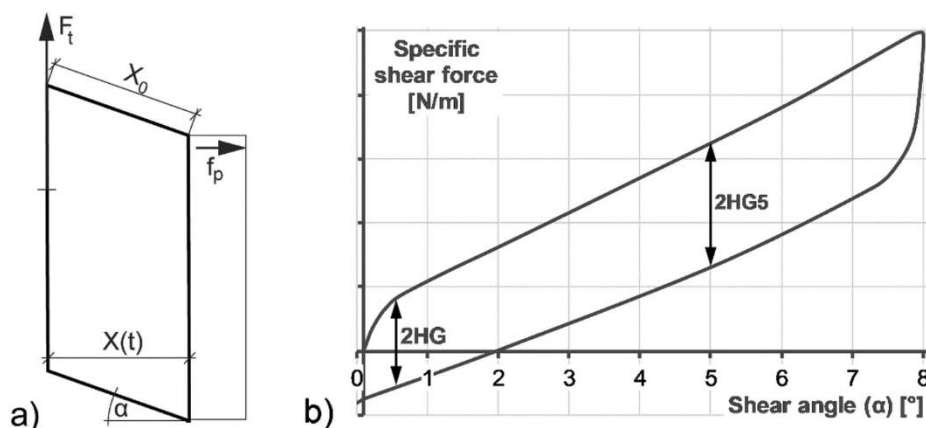

Fig. 1. Schematic of the tensile shear tester device of KES-FB system (a) and a typical specific shear force – shear angle diagram (b).
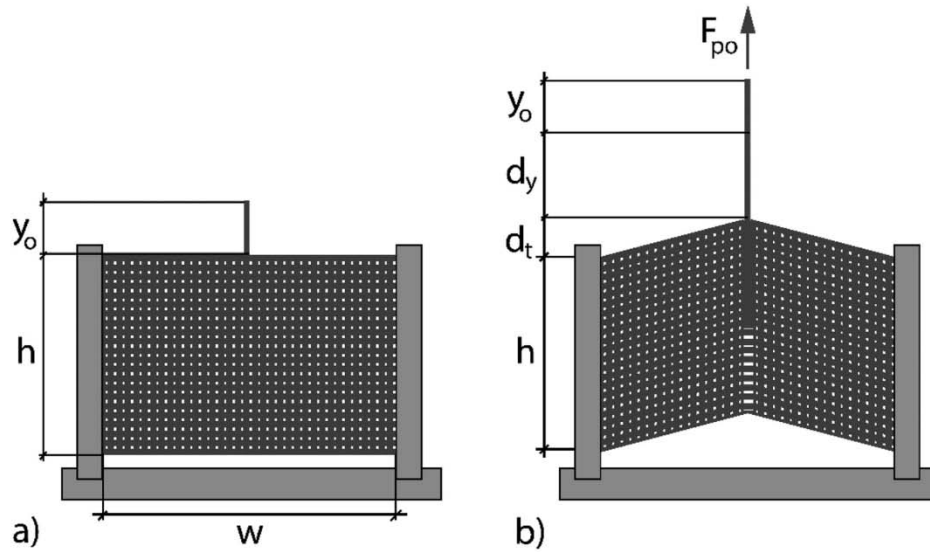
2

Fig. 2. Schematic of the yarn pull-out test a) clamped, unloaded sample, b) sample during test [17] h: height of the sample, w: width of the sample, y_o: yarn overhang, d_y: displacement of the yarn, d_t: displacement of the textile, F_{po}: yarn pull-out force.
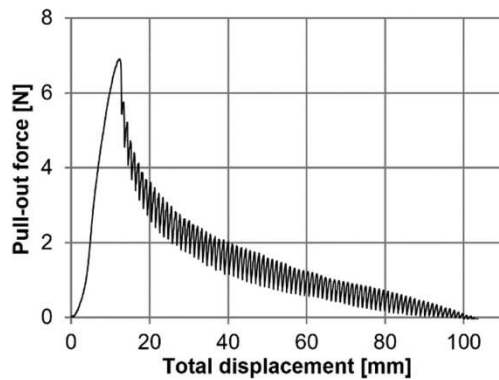

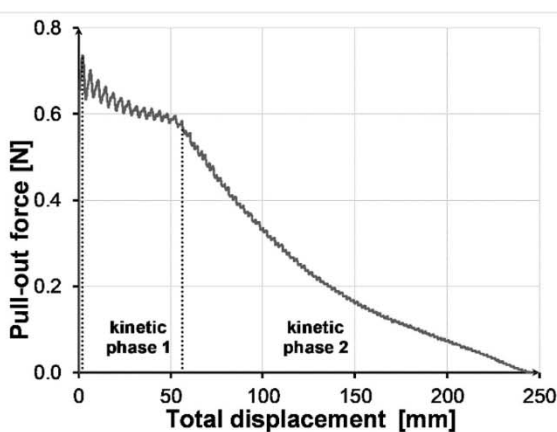**Fig. 3.** A typical yarn pull-out curve.

Fig. 4. Typical yarn pull-out curve in case of a 50 mm overhang.

the KES-FB1-A Tensile and Shear Tester, which is an expensive, stand-alone device for testing the tensile and shear properties of fabrics and from time to time it requires maintenance and calibration.

In our study, the aim was to design and construct an apparatus that makes possible to combine the simplicity of the above-mentioned test methods and the precision of the KES-FB system in order to determine the shear properties of textiles, textile composites and other flexible sheets. A grip that makes possible to maintain transversal pretension of the textile during the tests akin to the KES-FB shearing system was designed. Moreover, the same apparatus can be used for yarn pull-out tests of woven textiles. The pretension is applied by clearly mechanical ways during the tests leading to a simple, easy-to-build, symmetrical construction. There is no need for a complete device dedicated to only shear or yarn pull-out experiments as the grip can be mounted on almost any kind of universal load machine. With the apparatus the tests can be carried out rapidly and the evaluation of the results can be done with the aid of the software of the load machine. In this paper we demonstrate the applicability of this measurements and the accuracy of the results in case of both yarn pull-out and shear tests through some examples of technical materials.

In the current paper we describe the construction of the new apparatus we designed, as well as the shear and yarn-pull out tests we made. Shear tests (with the same principle of the KES-FB system) were made on a glass fabric, a polyester fabric and a canopy material, yarn-pull out test were made on another glass fabric and on a viscose fabric, moreover we introduced new parameters for the yarn-pull out test for the detailed evaluation of the results.

2. Materials and methods

2.1. Materials

For the shear tests we chose materials which are applied in technical fields: two woven fabrics, one was made of glass and the other one was made of polyester (PES) and besides a canopy that was a polyester (PES) fabric reinforced polyvinyl chloride (PVC) one. The structural-geometrical properties of the chosen materials can be seen in Table 1.

For the yarn pull-out tests we chose one glass-based and one viscose-based reinforcing fabric. The structural-geometrical properties of the chosen fabrics can be seen in Table 2.

2.2. Methods

2.2.1. Apparatus design

For all the measurements we used the novel apparatus (the universal grip unit) we designed. The schematic drawing of the apparatus for shear and yarn-pull-out tests can be seen in Fig. 5. The experimental setup is symmetrical. There are two clamps at the vertical edges of the

Table 1
Structural-geometrical properties of the shear-tested materials.

Fabric Type	Material	Weave	Areal density [g/m^2]	Thickness [mm]	Yarn linear density [tex]		Yarn count [1/10 mm]	
					Warp	Weft	Warp	Weft
Glass 1	Glass	Plain	250	1.20	200	300	5	5
PES	Polyester	Panama 2/2	400	0.72	105	105	24	24
Canopy	PVC + PES	Plain	265 + 85	0.31	28	28	15	12

Table 2
Structural-geometrical properties of the yarn pull-out tested materials.

Fabric Type	Material	Weave	Areal density [g/m^2]	Thickness [mm]	Yarn linear density [tex]		Yarn count [1/10 mm]	
					Warp	Weft	Warp	Weft
Glass 2	Glass	Plain	50	0.04	10.9	9.1	25	20
Viscose	Viscose	Plain	200	0.44	67	67	14	14

sample and one in the middle. Only the middle clamp is to be changed for the corresponding test. Yarn pull-out requires a top grip to catch the overhanging yarn at the top, while shearing needs a full-length middle grip (as in Fig. 5). Two parallel edges of a rectangular test sample (Fig. 5: 1) are clamped (Fig. 5: 2A) and the deformation is induced amongst the vertical symmetry line via the middle clamp (Fig. 5: 2B). To achieve a simple but precise construction the pretension is induced by a long helical spring (Fig. 5: 5) having linear characteristics. During the test, the two side clamps can move on a horizontal rail due to the vertical force generated by the load device and the horizontal forces of the pretension spring mechanism. Prior to the test, the spring has to be stretched) by two simple worm gears (Fig. 5: 5) until reaching a desired length related to 20 N tensile (transversal) force. The spring geometry was designed accordingly, and then the spring characteristics was calibrated by a tensile test, hence the length related to the 20 N force was determined. At this displacement a strong (0.24 mm diameter) high performance polyethylene (HPPE) fishing line (Fig. 5: 7) was then fixed to the hooks at the ends of the spring limiting its maximum strain. That way the yarn ensures that the spring can be stretched by the adjustment gears only until reaching the strain related to 20 N.

The mechanical pretension system makes possible to maintain a transversal force during the tests with an accuracy of approximately ±0.5% (at a preload of 20 N and 1 mm displacement of the side clamps) completely avoiding the application of supplementary electronics.

The materialized apparatus mounted on our load machine can be seen in Fig. 6. The whole apparatus can be tilted to a horizontal position around the motherboard after removing two fixing bolts (Fig. 7). In the back side of the apparatus there are two fasteners for fixing the grips on the linear rail. The side clamps (Fig. 6: 3B) can be fixed at any position by a locking lever in order to ensure their appropriate distance. In this

horizontal position of the apparatus the textile test specimen can be fixed to the grips conveniently. Both grips have a rough surface (sanding paper) at one side and soft rubber on the other side therefore avoiding slippage when clenched together by screws. As soon as the specimen is well-fixed, the apparatus can be tilted back to its operating position and fixed by the bolts. Then the locking levers are to be loosened, so the side clamps can again slide free on the rail. The pretension can be applied (Fig. 6: 5–6) by the adjustment gears until reaching the proper strain of the spring. The middle clamping unit is then fixed depending on which test (yarn pull-out or shear) is to be carried out. Fig. 6/a shows the middle clamp for shear test while Fig. 6/b depicts the one for yarn-pull-out test. The middle clamp for the yarn-pull-out test is a common yarn tensile testing clamp.

2.2.2. Shear test method

The shear tests were carried out with the novel apparatus which was mounted on a Zwick Z005 type universal load machine. The force was measured by a sensor having a range of 5 kN and a resolution of 1 mN. The tests were carried out with 20 N pretension force (F_p), i.e. 1 N/cm relative to sample length, induced by the spring. The crosshead speed was 10 mm/min. The shear angle range was ±8° and a whole shear cycle was investigated. Ten samples of each type were investigated in 0°, 90° and 45° directions, relative to the manufacturing direction. For the tests the gripping distance (width) was chosen to be 2 × 50 mm (symmetrical) and the length of the sample was 200 mm. For the measurements we cut specimens from the Glass 1 and PES fabrics and from the canopy. Due to the extra material required for side gripping the test samples size was 150 mm × 200 mm.

The shear properties of some selected textile specimens were tested to demonstrate the applicability of the device for shear tests.

The measurement principle (which is the same as the principle of the KES-FB system) with the novel apparatus can be seen in Fig. 8. On the left, the sample is unloaded prior to the test, while on the right it is loaded.

As the shear modulus is determined at small shear deformations, therefore the pretension induced by the spring can be considered constant from this perspective. According to the construction, during the shear tests the transversal yarns of the specimen have approximately constant length and almost pure shearing takes place. The half-gripping distance (X_0, in Fig. 8/a) is the distance between the middle and the side clamps. This X_0 distance is also identical with the length of the horizontal yarns between the clamps. When the displacement is induced (Fig. 8/b) the length of the initially horizontal yarns remain the same but the clamps come closer to each other ($X(t)$) due to the pretension. As the side clamps can be fixed at any positions it also makes possible to carry out tests with constant gripping distance.

The shear angle $\alpha(t)$ can be calculated from the displacement of the middle clamp as a function of time $\Delta Y(t)$ with equation (1):
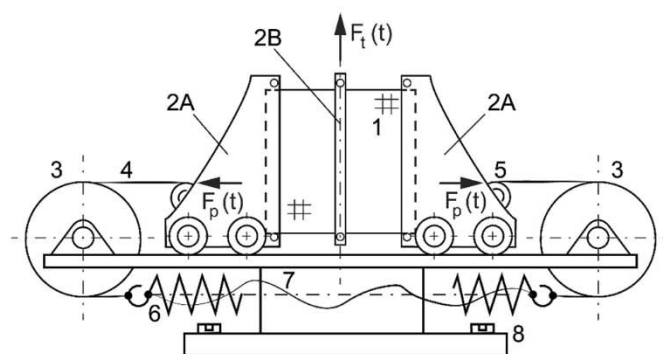

Fig. 5. The schematics of the designed apparatus. 1: specimen, 2A: side clamps, 2B: middle clamp (depicting the one for shear tests), 3: rollers with appropriate bearing, 4: thin rope, 5: gears 6: pretension steel spring, 7: strain limiting yarn, 8: base plate.
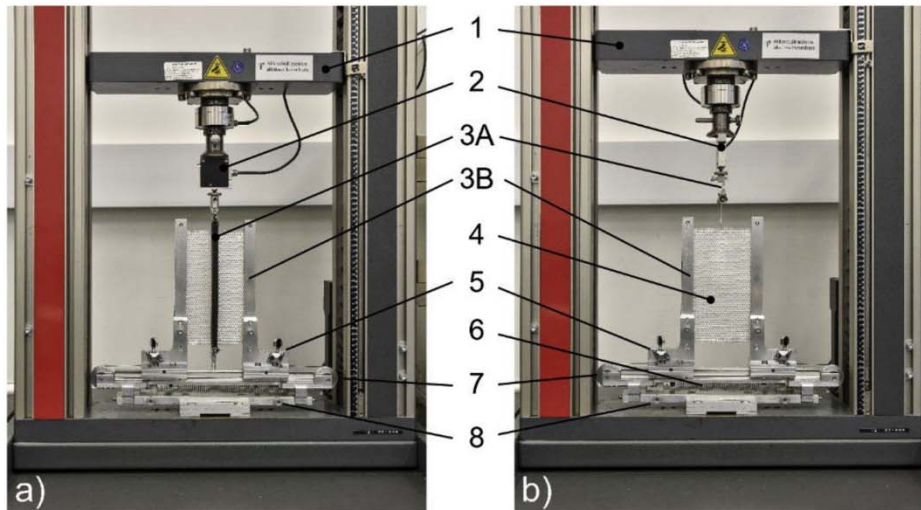
Fig. 6. The apparatus with middle clamp for shear test (a) and yarn pull-out test (b) of woven fabrics. 1: crosshead, 2: force sensor, 3A: middle clamp connected to the crosshead through the force sensor, 3B: side clamps, 4: test specimen, 5: worm gears for adjusting pretension, 6: pretension spring, 7: rollers with bearings, 8: fixing bolts.
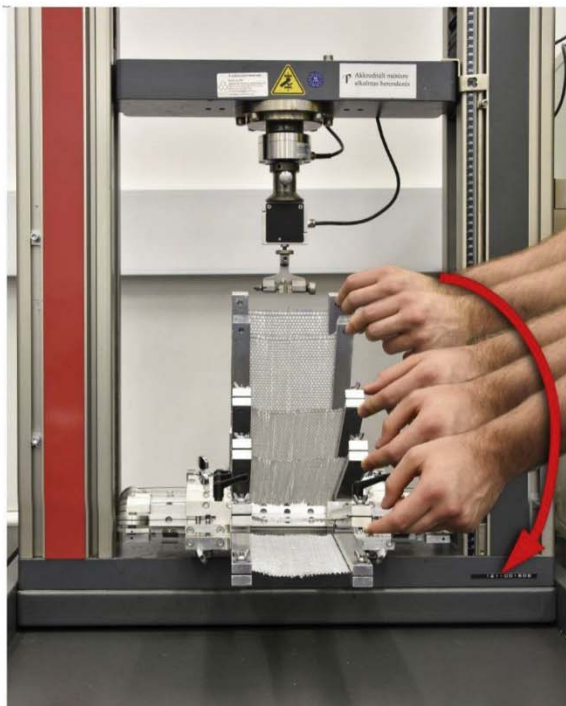

Fig. 7. A montage of tilting the apparatus to horizontal position for changing sample.

$$\alpha(t) = \text{rcsin}(\Delta Y(t)/X_0) \cdot 180/\pi, \; [°] \tag{1}$$

The measurement is carried out cyclically, like at the KES-FB test. The half-gripping distance (X_0) is the same 50 mm as that of the KES-FB. From equation (1) the displacement of the middle clamp can be calculated. If X_0 is 50 mm and the shear angle is 8°, then the measurement cycle has to be done with the maximum displacement of the middle clamp of ± 6.959 mm.

As opposed to the KES equipment, the testing of the samples left and right to the middle clamp are done simultaneously, with opposite shearing directions. The measured shear force is the sum of the forces for the two sides/directions. Therefore, in determining the specific shear
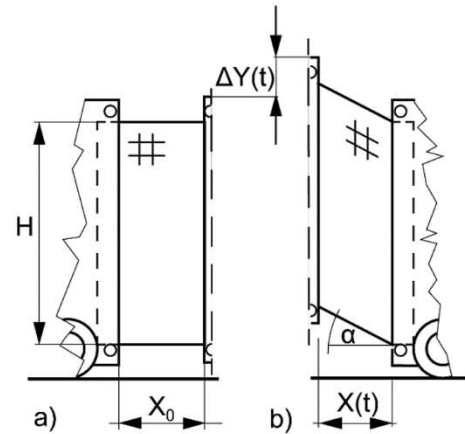

Fig. 8. The principle of the shear test. The sample is unloaded before the shear test (a) and loaded during the shear test (b).

force (N_f [N/m]), half the force measured by the tensile tester (F [N]) has to be taken into account together with the length of the sample that is parallel to the clamps (H [m]) (2):

$$N_f = F/(2H), \; [N/m] \tag{2}$$

The specific shear force – shear angle diagram can be plotted from the results, and the Kawabata-parameters can be determined from the diagram in the usual way.

2.2.3. Yarn pull-out test method and special parameters

The yarn-pull out behavior of fabrics was tested to demonstrate the applicability of the device for yarn pull-out tests. Moreover, we present two special parameters, which can be determined from the yarn pull-out test: the critical adhesion length and the specific resistance against slippage.

The yarn pull-out tests were carried out with the apparatus which was mounted on the same a Zwick Z005 type universal load machine. The force was measured by a sensor having a measuring range of 20 N with a resolution of 1 mN. The tests were carried out with 20 N pretension force, i.e. 1 N/cm (related to sample length), induced by the spring. The tests were carried out with a crosshead speed of 100 mm/min and the warp yarns were pulled out.

For the tests the gripping distance (width) was chosen to be 100 mm and the length of the sample was 200 mm. For the measurements we cut specimens from the Glass 2 and Viscose fabrics. Due to the extra material required for side gripping, the test specimens size was 140 mm × 200 mm. In addition, for the prepared specimens, the yarn to be pulled out overhung the upper and lower edge of the fabric by 30 mm and 100 mm, respectively, due to the type of test. Five samples of each type were investigated.

It is important to see where is the limit where the yarns break instead of slipping out of the textile specimen due to the pull-out force. In order to know the breaking force of the warp yarns that limits the maximum force at the yarn pull-out tests we carried out tensile tests. We made 15 individual measurements for each material (Glass 2 and Viscose), where the gripping length was 50 mm. Every other set up parameter was the same as we used at the yarn pull-out tests. The breaking force (F_S) and the elongation at break (ε_S) were determined.

During the yarn pull-out test, the pull-out force and the displacement of the gripped yarn end are registered by the universal load machine. Various mechanical parameters can be determined from the measurement results that implies the friction between the yarns forming the fabric.

Knowing the breaking force of these yarns, the critical adhesion length can be determined.

From the test results a special parameter, the specific resistance against slippage can be determined. This parameter means the resistance against slippage of the unit length of the yarn that is slipping through the crossing yarns. Therefore, that is the required force per unit length to sustain the slippage of the yarn.

When determining these parameters, we assume that the yarn pull-out force is directly proportional to the length of the yarn embedded into the fabric and we neglect the strains of the yarn and the embedding fabric.

Let the length of the embedding fabric sample be H [mm], the length of the embedded yarn be L [mm], the crimp of the yarn to be pulled-out be B. The crimp can be determined with a simple measurement and it can be calculated according to (3):

$$B = (L - H) / H, \ [-] \tag{3}$$

When determining the critical adhesion length, the peak value of the yarn pull-out force is used ($F_{adh,.max}$ [N]) for the calculation. This force is required to set the yarn in motion. From this, using equation (4) the critical specific adhesion resistance (which is the required force to set the unit length of yarn in motion) ($f_{adh,.max}$ [N]) can be calculated as (4):

$$f_{adh, \ max} = \frac{F_{adh, \ max}}{L} = \frac{F_{adh, \ max}}{H(1 + B)}, \ \left[N \middle/ mm \right] \tag{4}$$

Using the critical specific adhesion resistance and the breaking force of the yarn (F_S [N]), the critical adhesion length (L_{crit} [mm]) can be determined as (5):

$$L_{crit} = \frac{F_s}{f_{adh, \ max}}, \ \left[mm \right] \tag{5}$$

If the measurement is done in such a way that the free end of the yarn to be pulled out overhangs the bottom edge of the fabric sample before the beginning of the test, then the specific resistance against slippage can be determined in two different ways. In this case, the specific resistance against slippage can be determined from the first and the second region of the kinetic phase of the yarn pull-out diagram (Fig. 4). However, the two values may vary significantly depending on the characteristics of the curve.

In the first case, the specific resistance against slippage is determined from the first region of the kinetic phase. In this case, the consolidated mean value of the periodic pull-out force in this region ($F_{slipp, const}$ [N]) is used for the calculation. Such mean force is needed for the yarn to continuously slip out of the H-length fabric. From this force, one kind of

a specific resistance against slippage ($f_{slipp, kin1}$) can be calculated (6):

$$f_{slipp, \ kin1} = \frac{F_{slipp, \ const}}{H(1 + B)}, \ \left[N \middle/ mm \right] \tag{6}$$

In the second case, the specific resistance against slippage is determined from the second region of the kinetic phase. In this phase, the pulled yarn begins to pass through fewer and fewer crossing yarns, hence the mean value of the periodic tensile force decreases and tends asymptotically to zero. Omitting the initial, transitional part of the curve, a linear trend line can be fitted (Fig. 9).

Where the trend line intersects the horizontal axis (Fig. 15, point B), the force decreases to 0 and the pulled yarn leaves the fabric. Point A marks the beginning of the trend line (Fig. 15, A). The displacement from point A to B is the same as the length of the pulled yarn embedded in the fabric at point A (L_A [mm]). The force that can be measured at point A ($F_{slipp, A}$ [N]) is the force that is required to maintain the slip of the L_A-length yarn. From these relationships the other kind of specific resistance against slippage can be calculated ($f_{slipp, kin2}$) (7):

$$f_{slipp, kin2} = \frac{F_{slipp, \ A}}{L_A}, \ \left[N \middle/ mm \right] \tag{7}$$

This kind of specific resistance against slippage can be calculated even if the measurement is done in such a way that the free end of the pulled yarn overhangs the bottom edge of the fabric sample.

The three indicators characterize the mechanical connection of the cross-linked yarns in the fabric. The critical specific adhesion resistance shows the force which is required to set the yarn in motion, the specific resistance against slippage shows the force which is required to sustain the slippage of the yarn. The purpose of use determines which one should be determined.

3. Results and discussion

3.1. Shear test results and discussion

The Kawabata parameters (*2HG*, *2HG5* and *G*) were calculated from the first positive cycle of the tests [10]. The results for the materials can be found in Tables 3–5, respectively.

The specific shear force – shear angle hysteresis diagrams of the tests registered for the 0° direction samples can be seen in Fig. 10/a. Due to the PVC matrix, the canopy was understandably more resistant to the shear force than the Glass 1 or the PES fabric. In the two latter cases the yarns can be easily turn on each other at the interlacing points. The specific shear force – shear angle hysteresis diagrams of the tests made on the 90° direction samples can be seen in Fig. 10/b. The measurement process of the shear tests made on the 45° direction glass fabric samples can be seen in the pictures of Fig. 10/c. In this case the behavior of the three materials was similar, but significantly different from the 0° and
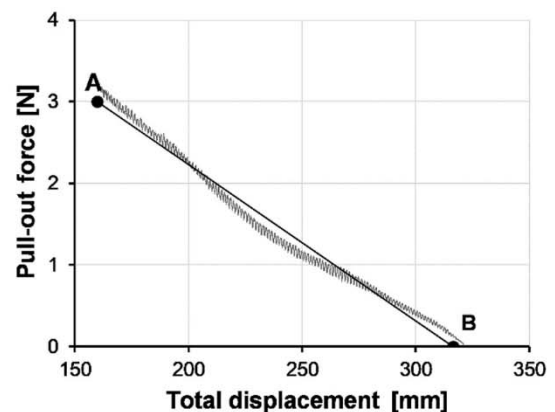

Fig. 9. Linear trend line fitted to the decreasing part of the yarn pull-out curve.

Table 3
Shear properties of the glass fabric.

Glass 1		0°			90°			45°		
		Mean	Standard deviation	Relative standard deviation [%]	Mean	Standard deviation	Relative standard deviation [%]	Mean	Standard deviation	Relative standard deviation [%]
2HG	[N/m]	12.91	1.24	9.6	8.39	0.66	7.9	266.56	55.72	20.9
2HG5	[N/m]	12.1	0.66	5.5	7.58	0.66	8.7	117.34	25.2	21.5
G	[N/m/°]	4.54	0.27	5.9	2.77	0.15	5.4	31.36	6.05	19.3

Table 4
Shear properties of the PES fabric.

PES		0°			90°			45°		
		Mean	Standard deviation	Relative standard deviation [%]	Mean	Standard deviation	Relative standard deviation [%]	Mean	Standard deviation	Relative standard deviation [%]
2HG	[N/m]	5.6	1.15	20.5	17.64	1.94	11.0	170.21	11.18	6.6
2HG5	[N/m]	22.66	1.79	7.9	39.3	3.44	8.8	94.18	4.92	5.2
G	[N/m/°]	6.56	0.4	6.1	8.79	0.77	8.8	40.58	2.56	6.3

Table 5
Shear properties of the PES/PVC canopy.

Canopy		0°			90°			45°		
		Mean	Standard deviation	Relative standard deviation [%]	Mean	Standard deviation	Relative standard deviation [%]	Mean	Standard deviation	Relative standard deviation [%]
2HG	[N/m]	70.07	110.82	158.2	70.84	4.86	6.9	212.46	27.22	12.8
2HG5	[N/m]	3.86	8.08	209.3	109.04	8.42	7.7	117.94	9.27	7.9
G	[N/m/°]	45.33	3.55	7.8	46.32	2.11	4.6	56.25	2.72	4.8

90° direction samples. All three materials were more resistant to shear force and their shear rigidity was much greater than in the cases of parallel direction samples that corresponds to what we experience in everyday use.

The measurement process of the shear tests made on the 0° direction canopy samples can be seen in the pictures of Fig. 11. The series of pictures shows the first quarter of the measurement cycle. Right after starting the measurement wrinkles appeared on the canopy. The glass fabric did not produce such, and on the PES fabric only a few wrinkles formed. That can be originated from the rigid behavior of the composite material, not allowing enough flexibility for the fiber yarns to deform.

The measurement process of the shear tests made on the 90° direction PES fabric samples can be seen in the pictures of Fig. 12. The series of pictures shows the third quarter of the measurement cycle. All the three materials had similar behavior like they have had in the cases of the 0° direction.

The measurement process of the shear tests made on the 45° direction Glass 1 fabric samples can be seen in Fig. 13. The series of pictures shows the first quarter of the measurement cycle. In these cases wrinkles appeared on all the three materials, respectively.

Since we wanted to confirm the proper repeatability of our test method, we compared the standard deviations of the G, 2HG and 2HG5 parameters with those of other methods. In the literature there are different studies with the KES-FB machine, on the picture frame test and the bias extension test. The different materials results in different values for the G, 2HG and 2HG5 parameters, and therefore we focused on the comparison of the deviations. Table 6 summarizes the standard deviations.

From the table we can conclude that the standard deviation of the various test methods depend on the woven fabric tested. The structure of the fabric is highly imperfect due to the stochastic nature of the fiber structures and the weaving itself. At the testing of similar PES fabrics, the different research groups got greatly different results. Even if the weave pattern and the material are similar in the different cases, there can be huge differences in other parameters, e.g. yarn count and area density, hence we can only compare the scattering of the results.

With the KES-FB system the standard deviations of the PES woven fabrics was in between 2 and 53% for the shear rigidity (G). In our test it was around 11–20% for a similar material. The picture frame and the bias extension test produced a 9–11% and 11–15% standard deviations in the shear rigidity. That means that the standard deviations and the reproducibility of the test results are quite similar in the case of the four different methods introduced. That confirms that our simple and rapid method gives the same small deviations as the KES-FB method widely used in the industry and also as the other methods. That also confirms the good repeatability and reliability of the tests.

3.2. Yarn pull-out test results and discussion

The tensile test results of the warp yarns of the chosen fabrics for the yarn pull-out tests can be seen in Table 7. The glass fiber yarns had lower tensile breaking force and also relative elongation at break than those of the viscose yarns. That is because the viscose yarns had much higher linear density (see Table 2). These results are used later for the calculation of the critical adhesion length (L_{crit}).

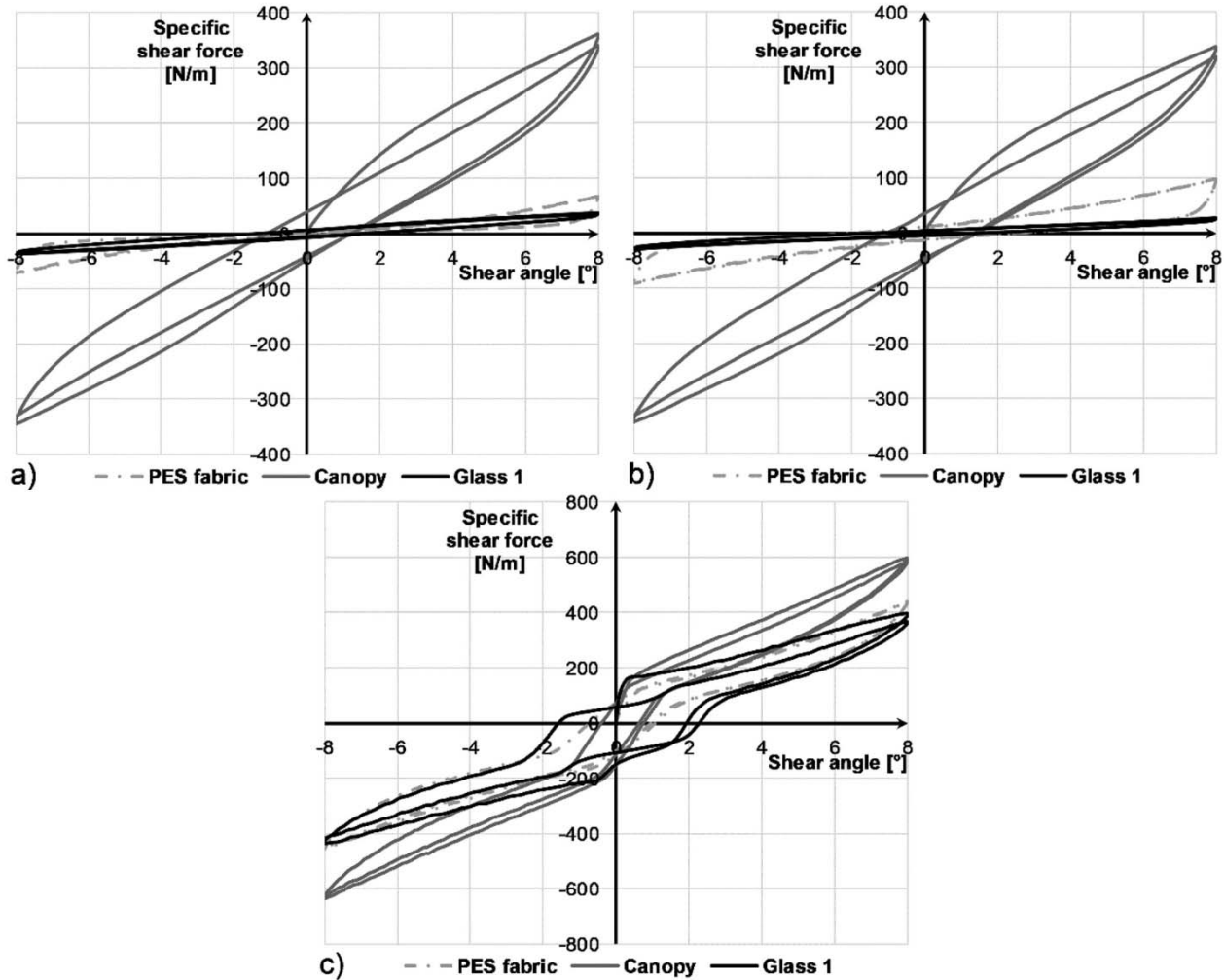Fig. 14 illustrates the process of the yarn pull-out measurements at

Fig. 10. Specific shear force - shear angle diagrams of 0° direction (a), 90° direction (b) and 45° direction samples (c).

Fig. 11. The process of the shear test on the 0° direction canopy samples.

various stages of the test. A typical yarn pull-out curve of the Glass 2 and the Viscose fabric can be seen in Fig. 15.

The force – displacement curves of the two fabrics are similar in characteristics, but the forces acting on the viscose fabric are much greater, than the forces acting on the Glass 2 fabric. Moreover, the shear deformation of the viscose fabric affected by the yarn pull-out was much higher, than that of the glass fabric and in the first region of the kinetic stage the mean value of the force slowly sets a constant value. In case of the viscose fabric, the decreasing part of the curve in the second region of the kinetic stage is almost entirely linear-like, hence in this case a

longer section of the decreasing part can be replaced with a fitted linear trend line, than in the case of the glass fabric. This is the reason why there is much less difference between the two types of resistance against slippage in case of the viscose fabric, than in the case of the Glass 2 fabric.

From the measurement results the critical specific adhesion resistance ($f_{adh,.max}$), the critical adhesion length (L_{crit}) and the specific resistance against slippage from the first ($f_{slipp, kin1}$) and the second ($f_{slipp, kin1}$) regions of the kinetic phase of the yarn pull-out curve were determined. The summary of the yarn pull-out results is shown in Table 8.
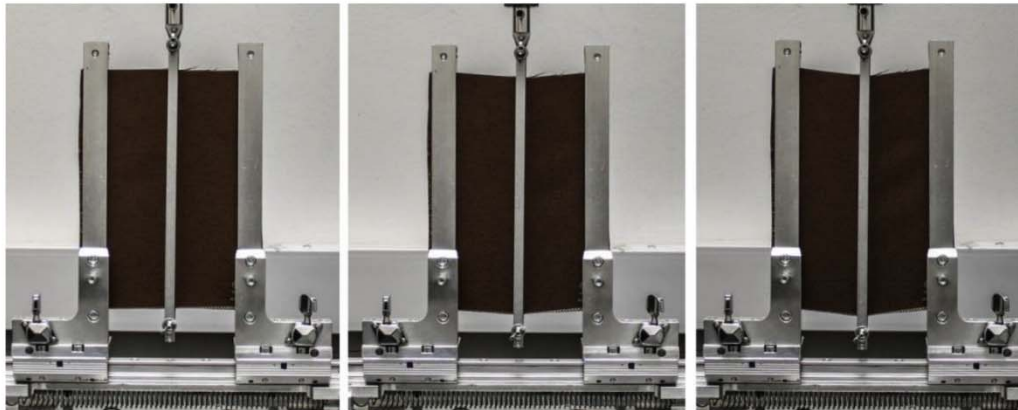
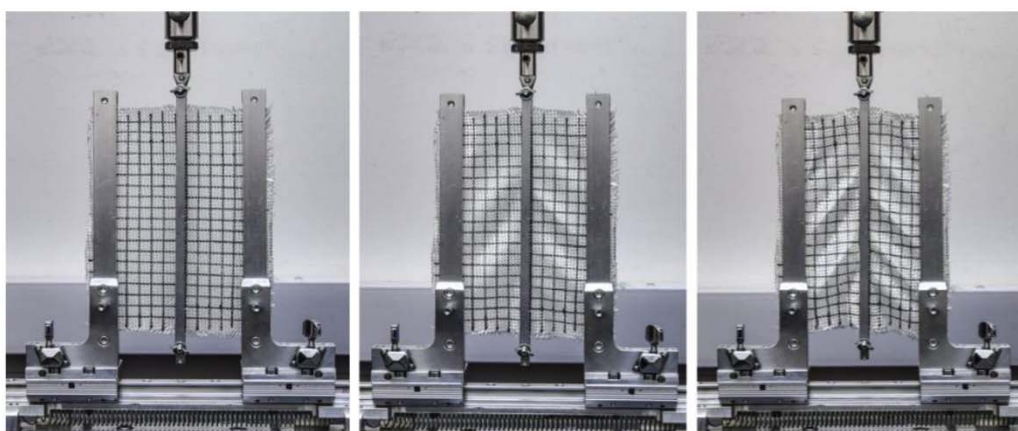**Fig. 12.** The process of the shear test on 90° direction PES fabric samples.

Fig. 13. The process of the shear test on the 45° direction cut glass fabric samples.

Table 6
Comparison of the standard deviations of various shear measurements (all data in %).

Material	Current method		KES-FB						Picture frame		Bias
	Glass	PES	Cotton [27]	Viscose [27]	PES [27]	PES [28]	PES [28]	Cotton [29]	PES [28]	PES [28]	PES [28]
Weave	Plain	Panama 2/2	Plain	Plain	Plain	Plain	Satin	Knitted	Plain	Satin	Plain	Satin
G	5.4–5.9	11.0–20.5	1.8–8.9	1.3–5.3	2.2–7.5	28.3	53.0	3.6	9.2	11.0	17.8	15.0
2HG	7.9–9.6	7.9–8.8	7.9–9.1	8.6–8.8	5.6–8.7	21.4	35.7	5.9	9.0	9.1	13.0	9.0
2HG5	5.5–8.7	6.1–8.8	8.8–9.0	2.9–4.6	4.5–6.0	14.7	24.9	6.8	6.8	6.1	9.0	8.2

The critical adhesion length (L_{crit}) was 1.034 m for the glass material, while it was 0.259 m that fits our experiences. Even though the tensile force of the viscose yarns were greater than that of the glass yarns, the dense structure and friction conditions between the yarns led to smaller critical adhesion length for the viscose material.

In the table it can be seen that the results gave small standard deviation despite the fact that the textile structure itself is imperfect. This can be explained by the sturdy clamping unit that fixes the edges of the specimen firmly and without the fabric slipping. The good repeatability of the tests is confirmed.

4. Conclusions

In this study, we introduce a new, simple method for testing the shear and yarn pull-out of fabrics. The apparatus we designed can be mounted on almost any kind of universal load machine, and it is suitable for various textiles and flexible sheets.

The test arrangement is quite similar to the KES-FB system, but instead of using supplementary electronics, the pretension is generated by a steel spring in order to regulate the stress-state. The simple, clearly mechanical system makes available to have a pretension typically in a ±0.5% range during tests. The results revealed that the device can be used for both yarn pull-out and shear tests properly.

We found that the relative standard deviations of the typical shear (G, 2HG, 2HG5) parameters were in the range of 5–20% for the glass

Table 7
Tensile test parameters of yarns.

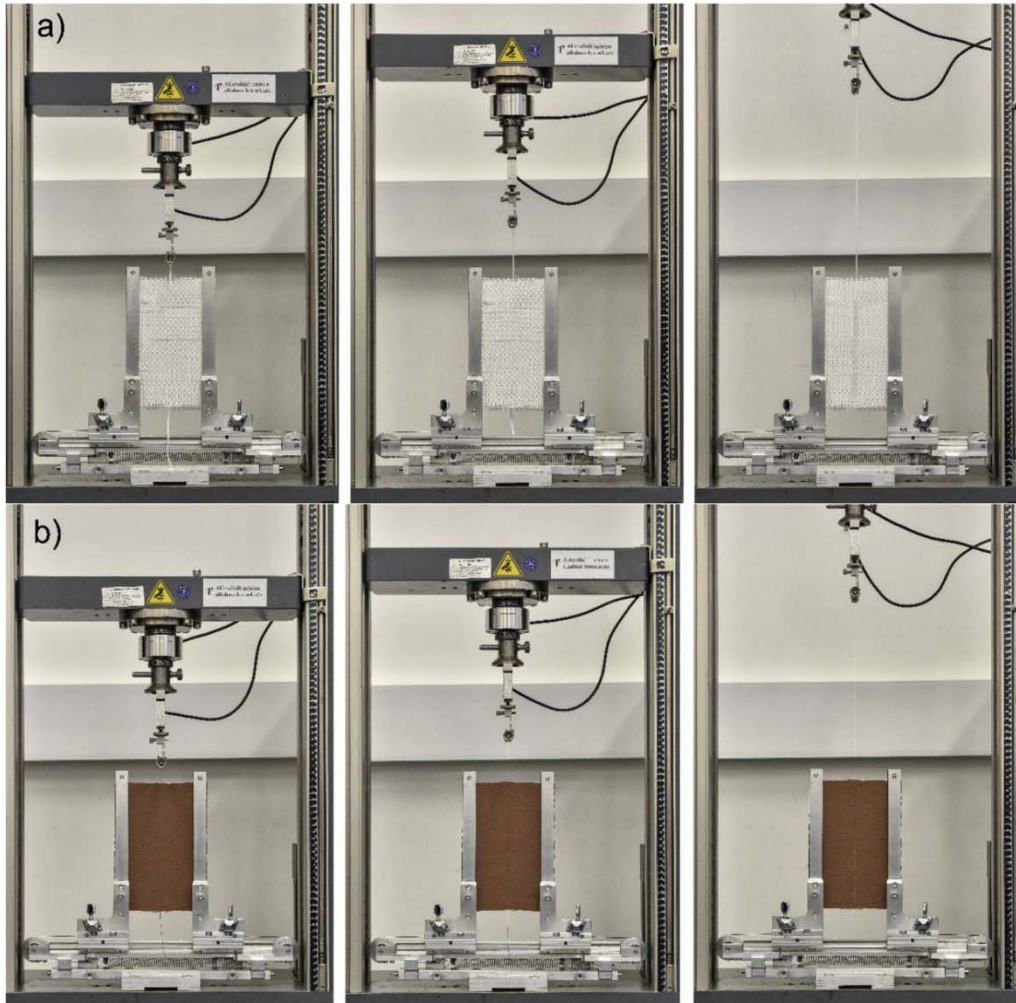| Fabric Type	F_s [N]			ε_s [%]		
	Mean	Standard deviation	Relative standard deviation [%]	Mean	Standard deviation	Relative standard deviation [%]
Glass 2	4.65	0.20	4.3	3.1	0.2	6.5
Viscose	8.19	0.71	8.7	20.0	2.0	10.0

Fig. 14. Glass 2 fabric (a) and Viscose fabric (b) during yarn pull-out test.

fiber and PES fabrics, while the canopy gave greater deviations. The yarn pull-out parameters were tested, and the standard deviation of the parameters was mostly between 5% and 9% for the glass and viscose fabrics tested. The standard deviation of methods gave similar values to that of popular methods presented in the literature.

The main advantages of the device are the excellent repeatability, the cost-effectiveness, the appropriate stress state and the short testing time. For the yarn pull-out test, and the tensile tests the critical adhesion length was determined. The glass fabrics resulted in 1.034 m, and the viscose fabrics resulted in 0.259 m due to the different yarn linear
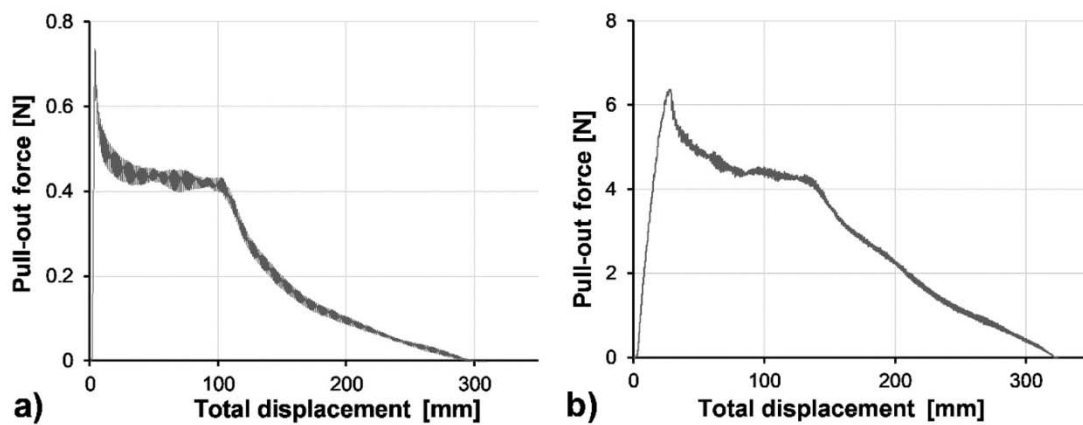

Fig. 15. Typical yarn pull-out curve of the Glass 2 (a) and the Viscose (b) fabric.

Table 8
Results of the yarn pull-out test.

Parameter		Glass 2			Viscose		
		Mean	Standard deviation	Relative standard deviation [%]	Mean	Standard deviation	Relative standard deviation [%]
$F_{adh,\ max}$	[N]	0.899	0.099	11.0	6.321	0.606	9.6
$f_{adh,\ max}$	[N/mm]	0.004497	–	–	0.03161	–	–
L_{crit}	[mm]	1034	–	–	259.1	–	–
$F_{slipp,\ const}$	[N/mm]	0.529	0.062	11.7	4.398	0.503	11.4
$f_{slipp,\ kin1}$	[N/mm]	0.002625	–	–	0.02185	–	–
$f_{slipp,\ kin2}$	[N/mm]	0.001733	0.000307	17.7	0.02094	0.00249	11.9

density and different frictional conditions in between the yarns.

Declaration of competing interests

The authors declare that they have no known competing financial interests or personal relationships that could have appeared to influence the work reported in this paper.

CRediT authorship contribution statement

Kolos Molnár: Validation, Investigation, Resources, Writing - original draft, Writing - review & editing, Visualization. **Ábris Dávid Virág:** Investigation, Writing - original draft, Writing - review & editing. **Marianna Halász:** Conceptualization, Methodology, Writing - original draft, Supervision.

Acknowledgements

Appendix A. Supplementary data

Supplementary data to this article can be found online at https://doi.org/10.1016/j.polymertesting.2020.106345.

References

[1] L. Kovács, G. Romhány, Derivation of ply specific stiffness parameters of fiber reinforced polymer laminates via inverse solution of classical laminate theory, Period. Polytech. Mech. 62 (2) (2018) 158–164, https://doi.org/10.3311/PPme.11846.

[2] M.J. Mochane, T.C. Mokhena, T.H. Mokhothu, A. Mtibe, E.R. Sadiku, S.S. Ray, I.D. Ibrahim, O.O. Daramola, Recent progress on natural fiber hybrid composites for advanced applications: a review, Express Polym. Lett. 13 (2) (2019) 159–198, https://doi.org/10.3144/expresspolymlett.2019.15.

[3] R. Várdai, T. Lummerstorfer, C. Pretschuh, M. Jerabek, M. Gahleitner, B. Pukánszky, K. Renner, Impact modification of PP/wood composites: a new approach using hybrid fibers, Express Polym. Lett. 13 (3) (2019) 223–234, https://doi.org/10.3144/expresspolymlett.2019.19.

[4] S. Hussain, A.R. Dickson, Improving and predicting the mechanical properties of foamed and stretched composite poly(lactic acid) films, Express Polym. Lett. 13 (1) (2019) 18–26, https://doi.org/10.3144/expresspolymlett.2019.3.

[5] T. Yamada, N. Ito, M. Matsuo, Mechanical properties of knitted fabrics under uniaxial and strip biaxial extension as estimated by a linearizing method, Text. Res. J. 73 (11) (2003) 985–997, https://doi.org/10.1177/004051750307301109.

[6] P. Potluri, D.A.P. Ciurezu, R.B. Ramgulam, Measurement of meso-scale shear deformations for modelling textile composites, Compos. Part A-Appl S 37 (2) (2006) 303–314, https://doi.org/10.1016/j.compositesa.2005.03.032.

[7] B. Al-Gaadi, F. Göktepe, M. Halász, A new method in fabric drape measurement and analysis of the drape formation process, Text. Res. J. 82 (5) (2012) 502–512, https://doi.org/10.1177/0040517511420760.

[8] B. Zhu, T.X. Yu, X.M. Tao, Large deformation and slippage mechanism of plain woven composite in bias extension, Compos. Part A-Appl S 38 (8) (2007) 1821–1828, https://doi.org/10.1016/j.compositesa.2007.04.009.

[9] G. Lebrun, M.N. Bureau, J. Denault, Evaluation of bias-extension and picture-frame test methods for the measurement of intraply shear properties of PP/glass commingled fabrics, Compos. Struct. 61 (4) (2003) 341–352, https://doi.org/10.1016/S0263-8223(03)00057-6.

[10] J. Domskienė, E. Strazdienė, Investigation of fabric shear behaviour, Fibres Text. East. Eur. 13 (2) (2005) 26–30.

[11] B. Al-Gaadi, M. Halász, Deformation analysis of composite reinforcing fabrics through yarn- pull-out, drape and shear tests, Fibers Polym. 14 (5) (2013) 804–814, https://doi.org/10.1007/s12221-013-0804-1.

[12] X.Q. Penga, J. Cao, J. Chen, P. Xue, D.S. Lussier, L. Liu, Experimental and numerical analysis on normalization of picture frame tests for composite materials, Compos. Sci. Technol. 64 (1) (2004) 11–21, https://doi.org/10.1016/S0266-3538(03)00202-1.

[13] S. Orawattanasrikul, Experimentelle Analyse der Scherdeformation biaxial verstärkter Mehrlagengestricke, PhD Theses, Technische Universität Dresden, Fakultät Maschinenwesen, Dresden, 2006.

[14] S. Kawabata, The Standardization and Analysis of Hand Evaluation, Textile Machinery Society of Japan, Osaka, 1980.

[15] E.M. Parsons, M.J. King, S. Socrate, Modeling yarn slip in woven fabric at the continuum level: simulations of ballistic impact, J. Mech. Phys. Solids 61 (1) (2013) 265–292, https://doi.org/10.1016/j.jmps.2012.05.005.

[16] A.G. Prodromou, J. Chen, On the relationship between shear angle and wrinkling of textile composite preforms, Compos. Part A-Appl S 28 (5) (1997) 491–503, https://doi.org/10.1016/S1359-835X(96)00150-9.

[17] K. Bilisik, Properties of yarn pull-out in para-aramid fabric structure and analysis by statistical model, Compos. Part A-Appl S 42 (12) (2011) 1930–1942, https://doi.org/10.1016/j.compositesa.2011.08.018.

[18] G. Nilakantan, J.W. Jr Gillespie, Yarn pull-out behavior of plain woven Kevlar fabrics: effect of yarn sizing, pull-out rate, and fabric pre-tension, Compos. Struct. 101 (2013) 215–224, https://doi.org/10.1016/j.compstruct.2013.02.018.

[19] S. Das, S. Jagan, A. Shaw, A. Pal, Determination of inter-yarn friction and its effect on ballistic response of para-aramid woven fabric under low velocity impact, Compos. Struct. 120 (2015) 129–140, https://doi.org/10.1016/j.compstruct.2014.09.063.

[20] Z. Dong, C.T. Sun, Testing and modeling of yarn pull-out in plain woven Kevlar fabrics, Compos. Part A-Appl S 40 (12) (2009) 1863–1869, https://doi.org/10.1016/j.compositesa.2009.04.019.

[21] B. Al-Gaadi, Analysis of 3D Deformation Properties of Woven Composite Reinforcing Structures, PhD Theses, Budapest University of Technology and Economics, Budapest, 2012.

[22] N. Pan, M.-Y. Yoon, Behavior of yarn pull out from woven fabrics: theoretical and experimental, Text. Res. J. 63 (11) (1993) 629–637, https://doi.org/10.1177/004051759306301103.

[23] M. Valizadeh, S. Lomov, S.A.H. Ravandi, M. Salimi, S.Z. Rad, Finite element simulation of a yarn pull out test for plain woven fabrics, Text. Res. J. 80 (10) (2010) 892–903, https://doi.org/10.1177/0040517509346436.

[24] A. Kelly, W.R. Tyson, Tensile properties of fibre-reinforced metals: copper/tungsten and copper/molybdenum, J. Mech. Phys. Solids 13 (6) (1965) 329–338, https://doi.org/10.1016/0022-5096(65)90035-9, in1-in2, 339-350.

[25] K. Bilisik, Experimental determination of fabric shear by yarn pull-out method, Text. Res. J. 82 (10) (2012) 1050–1064, https://doi.org/10.1177/0040517511431318.

[26] R. Bai, W. Li, Z. Lei, Y. Ma, F. Qin, Q. Fang, X. Chen, Y. Chen, Experimental study of yarn friction slip and fabric shear deformation in yarn pull-out test, Compos. Part A-Appl S 107 (4) (2018) 529–535, https://doi.org/10.1016/j.compositesa.2018.02.001.

[27] B. El Abed, S. Msahli, H. Bel Hadj Salah, F. Sakli, Study of woven fabric shear behaviour, J. Text. Inst. 102 (4) (2011) 322–331, https://doi.org/10.1080/00405001003771226.

[28] R.H. Gong, A. Bhatia, Effects of softeners on mechanical properties of cotton fabric, Res. J. Text Appar. 13 (4) (2009) 45–50, https://doi.org/10.1108/RJTA-13-04-2009-B006.

[29] M. Shanbeh, M. Safar Johari, M. Zarrebini, M. Barburski, A. Komisarczyk, Analysis of shear characteristics of woven fabrics and their interaction with fabric integrated structural factors, J. Eng. Fiber Fabr. 14 (1) (2019) 1–13, https://doi.org/10.1108/RJTA-13-04-2009-B006.

Study on the Compression Effect of Clothing on the Physiological Response of the Athlete

Marianna Halász [1,*], **Jelka Geršak** [2], **Péter Bakonyi** [3], **Gabriella Oroszlány** [1], **András Koleszár** [1] and **Orsolya Nagyné Szabó** [1]

1   Institute for Industrial Product Design, Sándor Rejtő Faculty of Light Industry and Environmental Protection Engineering, Óbuda University, Doberdó u. 6, H-1034 Budapest, Hungary; oroszlany.gabriella@uni-obuda.hu (G.O.); koleszar.andras@uni-obuda.hu (A.K.); szabo.orsolya@uni-obuda.hu (O.N.S.)

2   Research and Innovation Centre for Design and Clothing Science, Faculty of Mechanical Engineering, University of Maribor, Smetanova ulica 17, SI-2000 Maribor, Slovenia; jelka.gersak@um.si

3   Department of Polymer Engineering, Faculty of Mechanical Engineering, Budapest University of Technology and Economics, Műegyetem rkp. 3, H-1111 Budapest, Hungary; bakonyi@pt.bme.hu

*   Correspondence: halasz.marianna@uni-obuda.hu

Abstract: The study aimed to analyze whether the high compression of unique, tight-fitting sportswear influences the clothing physiology comfort of the athlete. Three specific sportswear with different compression were tested on four subjects while they were running on a treadmill with increasing intensity. The compression effect of the sportswear on the body of the test persons, the temperature distribution of the subjects, and the intensity of their perspiration during running were determined. The results indicate that the compression effect exerted by the garments significantly influences the clothing physiology comfort of the athlete; a higher compression load leads to more intense sweating and higher skin temperature.

Keywords: clothing physiology; tight-fitting sportswear; running test on a treadmill; thermal comfort; skin temperature; perspiration

1. Introduction

Companies develop advanced high-tech, often high-compression sportswear for professional athletes [1–6]. Researches show that such sportswear can increase the performance of the athlete [7–18]. As a healthy lifestyle involves regular exercise, similar special garments are available for amateur and grassroots sports.

Sportswear has undergone enormous improvement since ancient times. In the ancient Olympic Games, men competed without clothing because they believed the best performance could be achieved this way. Until the 18th century, the manufacturing cost of clothes was so high that only the nobility and wealthy people could afford more clothing, especially for sports. During the Industrial Revolution, however, the textile industry started to develop at a tremendous rate, and so not only rich people could afford a garment or garments intended for sport. Until the 19th century, doing sports was mainly a privilege of men, but this did not bring about considerable changes in sportswear. Women started to play sports in higher numbers in the second half of the 19th century. The demand for women's sportswear started the development of sportswear, continuing intensively to this day [19–22].

The development of sportswear is directly related to the requirements of the sport, the nature and duration of the activities, and the requirements for adequate thermo-physiology comfort of the athlete [23–30]. In addition, scientists are examining the possibility of increasing performance through the compression that the garment exerts on the athlete's body [7–18]. In recent years, fibers for the manufacture of premium sportswear have been

extensively researched and considerably improved. With the advancement of technology and the development of high-performance materials, sportswear now has greatly improved properties. Special emphasis is given to high aerodynamic and absorption properties, air and water permeability, strength, and adhesion. Much has also been performed in the field of design [31]. Sportswear is designed not to restrict the athlete's activity but provide them physical support while exercising [32].

These sportswear fabrics are usually composed of polyester or polyamide fibers and elastomer fibers. The light and strong polyester or polyamide fibers provide the necessary strength and clothing physiology parameters. The elastomer fibers, capable of large, completely elastic deformation, ensure that the garment completely fits the athlete's body during exercise and provides compression on it. The knitted fabric structure also facilitates elastic deformation due to the interconnecting loops [1–3].

Compression sportswear is a tight-fitting, compressive form of clothing utilizing the material's elasticity. Professional athletes wear compression suits to improve their athletic performance and speedy recovery from injury. Compression garments are used in high-performance sports such as running, skiing, swimming, and cycling [33]. It has been reported that compression garments improve the perception of muscle damage and increase performance in endurance tests [34]. Compression pants help improve athletic performance and reduce injuries by reducing muscle oscillations [35]. The use of compression stockings minimizes the risk of injury from the overall impact of physical exertion [34].

This case study aims to analyze whether the compression of the tight-fitting sportswear affects the clothing physiology comfort of the athlete and their motion parameters. In our literature search, we did not find any source that investigated the relationship between the compression of sportswear and the clothing physiology of an athlete. Therefore, we believe that the idea that this is worth exploring is novel.

2. Materials and Methods

We tested three tight-fitting sportswear with different compression. In the study, four subjects wore these tight-fitting sports garments while running with increasing intensity on a treadmill.

2.1. The Test Persons

We included four girls (TP1, TP2, TP3, and TP4) of similar age and body type in the study. The age, body mass, and main body measurements of the test subjects are detailed in Table 1.

Table 1. The age, body mass, and main body measurements of the test persons.

Designation	Test Persons			
	TP1	TP2	TP3	TP4
Age (years)	23	23	18	24
Body mass (kg)	59.32	66.88	65.25	70.60
Body height (cm)	166	169	171	171
Chest girth (cm)	96	95	92	94
Waist girth (cm)	73	70	71	77
Hip girth (cm)	97	104	99	111
Thigh girth (cm)	55	58	57	64
Lower leg/calf/girth (cm)	35.5	39	38.5	40.5
Inside leg length (cm)	78	76.5	77	79
Dress size upper	S	S	S	M
Dress size pants	S	M	M	M

The fitness levels of the girls are comparable. Currently, they do sports as a hobby, but as children and teenagers, they were active athletes. They exercise regularly every week, so the running intensity and interval in the tests matched their fitness level.

2.2. Materials

For our purpose, three tight-fitting sportswear were used: one ready-made sportswear made of polyester/elastane knitted fabric and two made-to-measure sportswear sets made of polyamide/elastane knitted fabric. Table 2 gives their designation and material composition.

Table 2. The examined sportswear.

Designation	Description	Composition of the Weft-Knitted Fabrics			
		Long-Sleeved T-Shirt		Pants	
Ready-made Sportswear	Ready-made sportswear	KF1	80% Polyester 20% Elastane	KF2	74% Polyester 26% Elastane
Made-to-measure Sportswear 1	Made-to-measure sportswear with 1% body size reduced	KF3	74% Polyamide 26% Elastane	KF3	74% Polyamide 26% Elastane
Made-to-measure Sportswear 2	Made-to-measure sportswear with 5% body size reduced	KF3	74% Polyamide 26% Elastane	KF3	74% Polyamide 26% Elastane

All three materials are a single weft-knitted fabric and contain a high percentage (20–26%) of elastane fibers. The structure of the knitted fabrics used is shown in Figure 1. The knitted structure with integrated elastane yarn ensures large-scale, multiaxial elastic deformation for the fabrics. In addition, the polyester (PES) and polyamide (PA) fibers provide strength and abrasion resistance and quickly wick sweat away from the body and allow it to evaporate, as they can retain very little moisture.
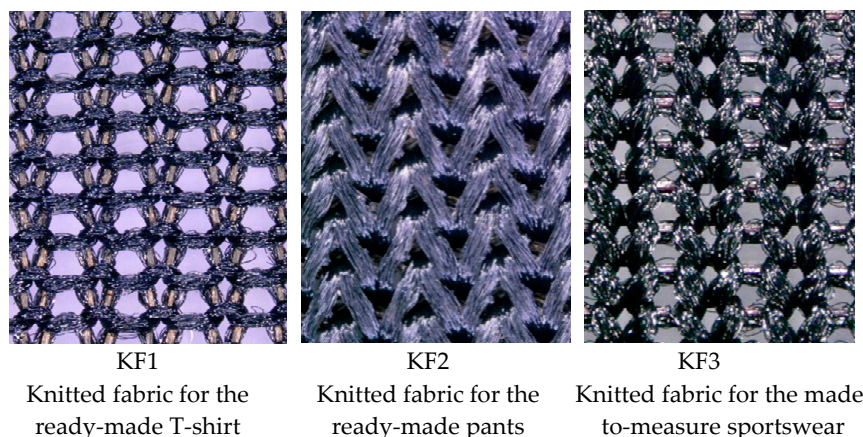

KF1
Knitted fabric for the ready-made T-shirt

KF2
Knitted fabric for the ready-made pants

KF3
Knitted fabric for the made-to-measure sportswear

Figure 1. The structure of the knitted fabrics used (microscopic images at $100\times$ magnification).

Although the composition of the studied knitted fabrics is different, they can be used for our research purpose. This is because, although the properties of PA and PES fibers are not the same, the pressure exerted by sportswear made from these knitted fabrics is determined by the elastane fibers, which are present in a high proportion (20–26%) in the knitted fabrics in addition to PA and PES fibers.

The Ready-made Sportswear was bought in sizes S and M, corresponding to the size of the test persons and contains a long-sleeved T-shirt made from knitted fabric KF1 and pants made from knitted fabric KF2. The two made-to-measure sports suits (a long-sleeved T-shirt and pants) were constructed and made by us according to the cut of Ready-made Sportswear from the knitted fabric, KF3. They differ only in ease allowance (Table 2).

The Made-to-measure Sportswear 1 and 2 are made based on the test persons' body measurements. To ensure comparability, we constructed the patterns of the Made-to-measure Sportswear 1 and 2 to be similar to the bought Ready-made Sportswear. To

achieve a compression effect of the sportswear, we have constructed the pattern for the tailored sportswear with negative ease allowance. This negative ease allowance was 1% in the case of the Made-to-measure Sportswear 1 and 5% for the Made-to-measure Sportswear 2, reducing the pattern size by 1% and 5% to under body size, respectively.

Table 3 summarizes the most important properties of the knitted fabrics used. The tests were performed in the Research and Innovation Centre for Design and Clothing Science at Faculty of Mechanical Engineering, University of Maribor, by standard conditions, according to ISO 139 (a temperature of 20 °C and a relative humidity of 65%). The following instruments were used: a Hildebrand thickness gauge, an Akustron Air-Permeability Measuring Instrument, an HC103/01 Moisture Analyzer, a KES-F7 Thermo Labo II for thermal properties, and a Zwick 005 universal testing machine for tensile tests (Zwick Roell GmbH, Ulm, Germany). The static immersion water absorption of the knitted fabrics used was determined according to the ASTM D 583-63 standard.

Table 3. Properties of the knitted fabrics of the examined sportswear.

Code of Knitted Fabric	Mass (g/m²)	Thickness (mm)	Course Density (Piece/ 10 mm)	Wale Density (Piece/ 10 mm)	Air Permeability (L/m²·s)	Moisture Content (%)	Immersion Water Absorption (%)	Dry Heat Flow (W)	Thermal Resistance R_{ct} (m·²K/W)	Force at 5% Elongation * (N/m)
KF1	194.1 ± 1.5	0.397 ± 0.005	30	22	388.6 ± 7.2	3.15 ± 0.27	69.0 ± 2.38	2.07 ± 0.09	0.0719	7.44 ± 0.14
KF2	279.1 ± 5.3	0.497 ± 0.012	25	22	427.2 ± 25.9	1.35 ± 0.02	45.6 ± 0.85	2.01 ± 0.04	0.0636	10.36 ± 0.39
KF3	206.2 ± 0.3	0.356 ± 0.003	28	24	133.0 ± 5.3	2.93 ± 0.15	82.2 ± 1.64	2.13 ± 0.12	0.0721	12.35 ± 0.21

* In course direction.

2.3. Test Protocol

The four selected healthy girls participated in the experiment, where we studied the compression effect of clothing on the physiological response of the test subjects. They were selected to be approximately the same age (their average age is 21.0 ± 2.2 years), roughly the same size (body mass 63.3 ± 2.1 kg, height 170.5 ± 2.5 cm), and a similar level of fitness. This way, despite the relatively low number of test persons, we can draw sufficiently well-founded conclusions about the given population.

The wear trial tests were performed under the following ambient conditions: an ambient temperature of 24 °C and relative humidity of 40%.

The test persons wore the previously presented sportswear and ran on a treadmill at increasing intensity. The tests were carried out in the Motion Laboratory of the Department of Mechatronics, Optics and Mechanical Engineering Informatics, and the Biomechanical Research Centre of the Faculty of Mechanical Engineering of the Budapest University of Technology and Economics. The Motion Laboratory also allowed the biomechanical examination of the motion characteristics of the test persons. These results are presented in a separate paper [36].

The test subject performed the same physical activities in each test; a 15-min run, in which running speed was increased every 3 min in the following order:

− 3 min: Load I (running speed of 4 km/h);
− 3 min: Load II (running speed of 7 km/h);
− 3 min: Load III (running speed of 8 km/h);
− 3 min: Load IV (running speed of 10 km/h);
− 3 min: Load V (running speed of 11 km/h).

We performed the tests every morning at the same time. The test girls ran on the treadmill wearing another sports suit once each day. Figure 2 shows one of the test subjects in the Ready-made Sportswear while running on the treadmill, with the markers necessary for the movement tests.
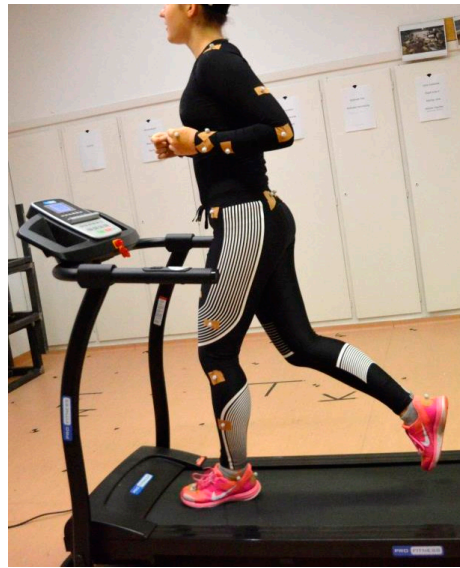
Figure 2. A test person on the treadmill in the Ready-made Sportswear, with the markers for motion tests.

According to the study protocol, we determined the compression effect of the suit on the test subjects' bodies, the temperature distribution of the subjects, and the intensity of their sweating during running. For this purpose, the following measurements were carried out for each test subject while they were wearing their sportswear:

—   The compression effect of sportswear on the body (measuring the pressure exerted by the sportswear on the body of the test person);
—   Body mass loss due to sweat;
—   Thermal imaging during running.

2.3.1. Determination of Pressure Distribution

We measured the compression of sportswear on the test person's body with the PicoPress tester at 17 points on the body (Figure 3).

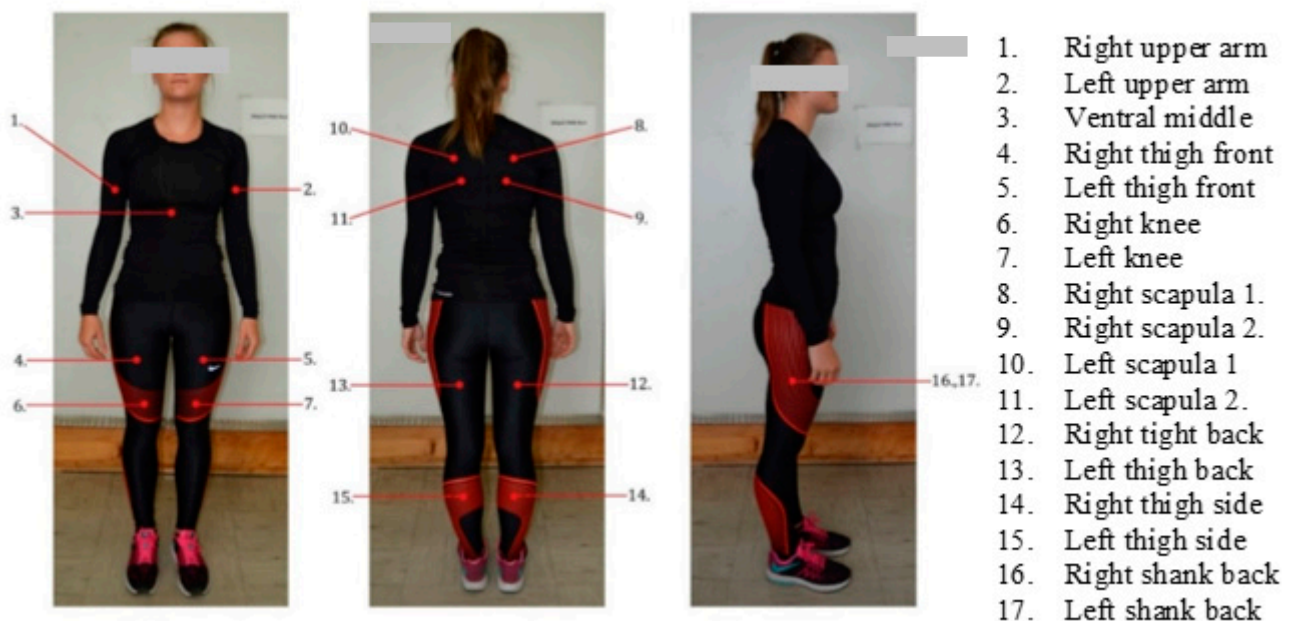|	
1.	Right upper arm
2.	Left upper arm
3.	Ventral middle
4.	Right thigh front
5.	Left thigh front
6.	Right knee
7.	Left knee
8.	Right scapula 1.
9.	Right scapula 2.
10.	Left scapula 1
11.	Left scapula 2.
12.	Right tight back
13.	Left thigh back
14.	Right thigh side
15.	Left thigh side
16.	Right shank back
17.	Left shank back

Figure 3. Pressure measurement points.

Compression was measured on all test persons before the subjects started running. The measurement results are given as mean values of pressure on the upper body (Figure 3, pressure measurement points: 1–3, 8–11) and on the lower body (Figure 3, pressure measurement points: 4–7, 12–17).

2.3.2. Determination of Excreted and Absorbed Sweat

The amount of evaporated sweat was determined based on body mass loss, as the difference in the test subject's body mass without any clothing, before and after the study. The amount of sweat absorbed in clothing was determined based on the mass of clothing that a test subject was supposed to wear during the test. Test subjects were measured upon completing the study: first dressed, and then the clothing, piece by piece.

The mass of the clothing was measured with an AA Labor MT -XY 6000 (Midwest Microwave Solutions, Hiawatha, IA, USA) balance, which has an accuracy of 0.1 g, while body mass was measured with a Sartorius IS300IGG (Minebea Intec, Hamburg, Germany) balance with an accuracy of 2 g.

2.3.3. Thermal Imaging Analysis

From the clothing physiology point of view, the critical parameter is the thermal load on the subject during running. For this purpose, the body surface temperature was recorded with a FLIR A325sc thermal imaging camera (FLIR Systems, Wilsonville, OR, USA) (Figure 4).
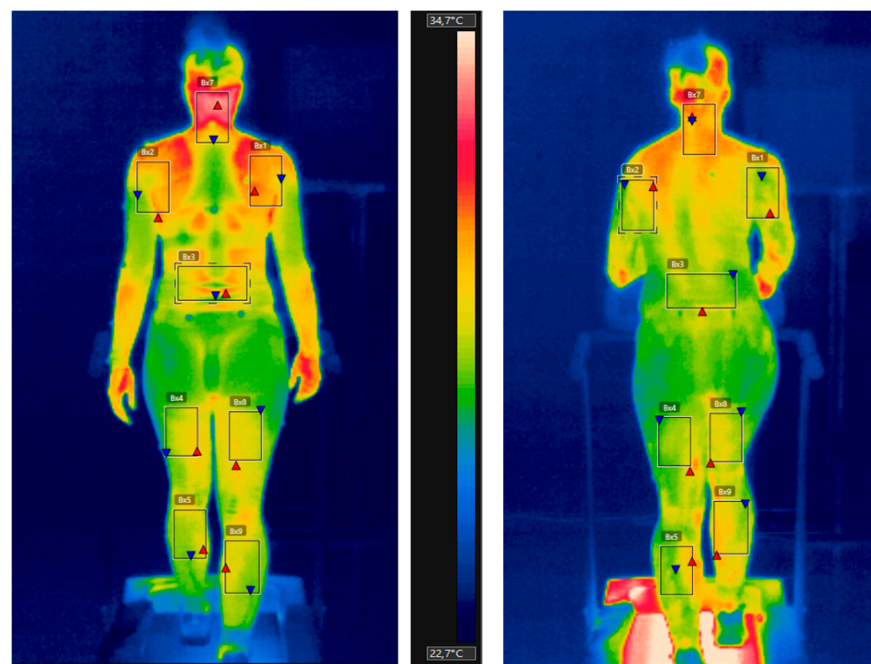

Figure 4. Thermal images at 0.0 min (**left**) and 15.0 min (**right**) with the marked reference areas.

For analysis, we selected eight areas on the body and determined their temperature values based on the thermal images when running speed was changed.

The selected areas were: neck-nape, right and left upper arm, back, right and left thigh, right and left calf. The times of evaluation were: 0 min, 3.0 min, 6.0 min, 9.0 min, 12.0 min, and 15.0 min.

Figure 4 shows the thermal image with the marked selected areas of one test person at 0.0 min and 15.0 min. Except for the neck, all selected areas are covered by sportswear.

3. Results and Discussion

Table 4 contains the average pressure values of each sportswear on each test person. (The detailed pressure values for each test person and sportswear at each measurement point are provided in the Appendix A, Table A1). The average pressure values show that the compression of Made-to-measure Sportswear 2 is higher for each test person than in the case of Made-to-measure Sportswear 1 and that the compression of garments constructed with the same amount of reduction in body size is about the same in the case of each test person. In addition, the Ready-made Sportswear has the highest compression, except for Test Person 2, in whose case the compression of the Ready-made Sportswear is between that of the two other, made-to-measure sports suits. It can also be observed that the standard deviation of the measured compression values for the Ready-made Sportswear is greater than that of the two made-to-measure sports suits. This is probably because the Ready-made Sportswear was not made for the size of the test persons; the persons had to choose from the sizes available. For this reason, the compression of the Ready-made Sportswear shows a higher difference between the test persons than that of made-to-measure sportswear.

Table 4. Average pressure values for each test person and sports suit.

Examined Sportswear	Body Part	Average Pressure (mmHg)			
		TP 1	TP 2	TP 3	TP 4
Ready-made Sportswear	upper	03.43 ± 1.72	2.57 ± 0.79	3.14 ± 1.21	03.72 ± 2.14
	lower	12.08 ± 6.13	7.92 ± 4.76	9.75 ± 5.67	10.75 ± 4.86
Made-to-measure Sportswear 1	upper	1.72 ± 1.70	1.86 ± 0.69	2.00 ± 1.00	2.00 ± 1.41
	lower	6.17 ± 3.27	5.83 ± 2.12	6.25 ± 2.60	6.83 ± 2.52
Made-to-measure Sportswear 2	upper	3.43 ± 1.99	3.57 ± 0.98	3.14 ± 1.21	3.43 ± 1.90
	lower	7.25 ± 2.63	8.25 ± 2.99	8.25 ± 2.86	7.67 ± 2.84

We analyzed the amount of sweat the test persons produced. Figure 5 shows the difference in body mass without clothing, that is, the mass loss of the test persons. Figure 6 shows the amount of sweat absorbed by the sportswear for each test person and suit.

On average, the test persons lost 100–200 g from their body mass during running (Figure 5). Some of it remained in the sportswear as sweat, and the rest evaporated, cooling the body.
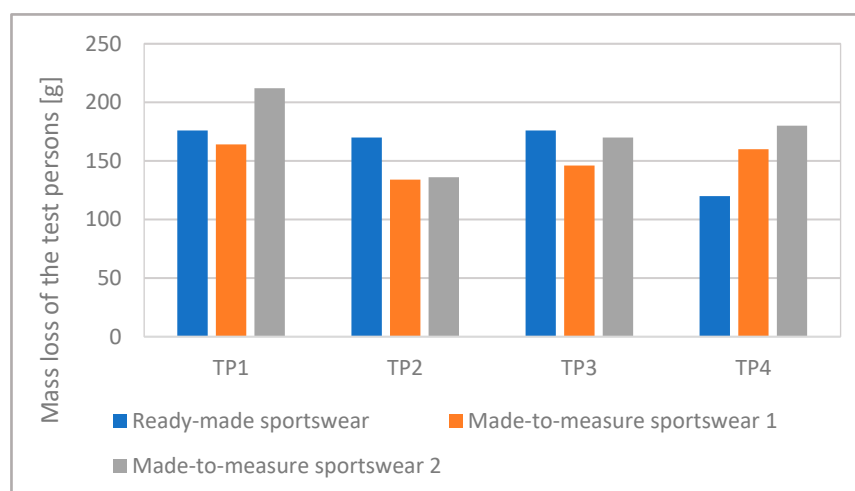

Figure 5. The mass loss of the test persons in the different compression sports suits.

The moisture absorbed by Made-to-measure Sportswear 1 and 2 can be compared well because they were made of the same fabric and the only difference between them

is in compression (Figure 6). The higher compression Made-to-measure Sportswear 2 absorbed far more moisture than the lower compression Made-to-measure Sportswear 1 in the case of three test persons (TP2, TP3, and TP4), while in the case of Test Person 1, the two values were nearly identical. The higher compression Made-to-measure Sportswear 2 caused a higher reduction in body mass than the lower compression suit in the case of three test persons (TP1, TP3, and TP4), while with Test Person 2, both sports suits resulted in nearly identical body mass loss (Figure 5). These results indicate that higher compression generated more sweating.
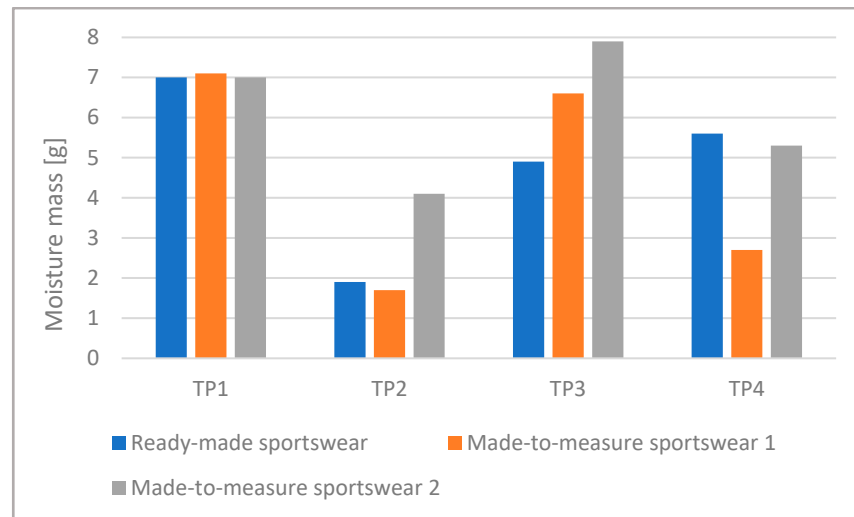

Figure 6. The amount of moisture remaining in the sportswear for each test person and suit.

Figure 7a–d shows the average body surface temperatures as a function of time for each test person and sports suit. As time passes, the average temperature decreases, due to the more intensive sweating, as the evaporating sweat and the moving air caused by running take heat away. The test persons stopped after 15 min.
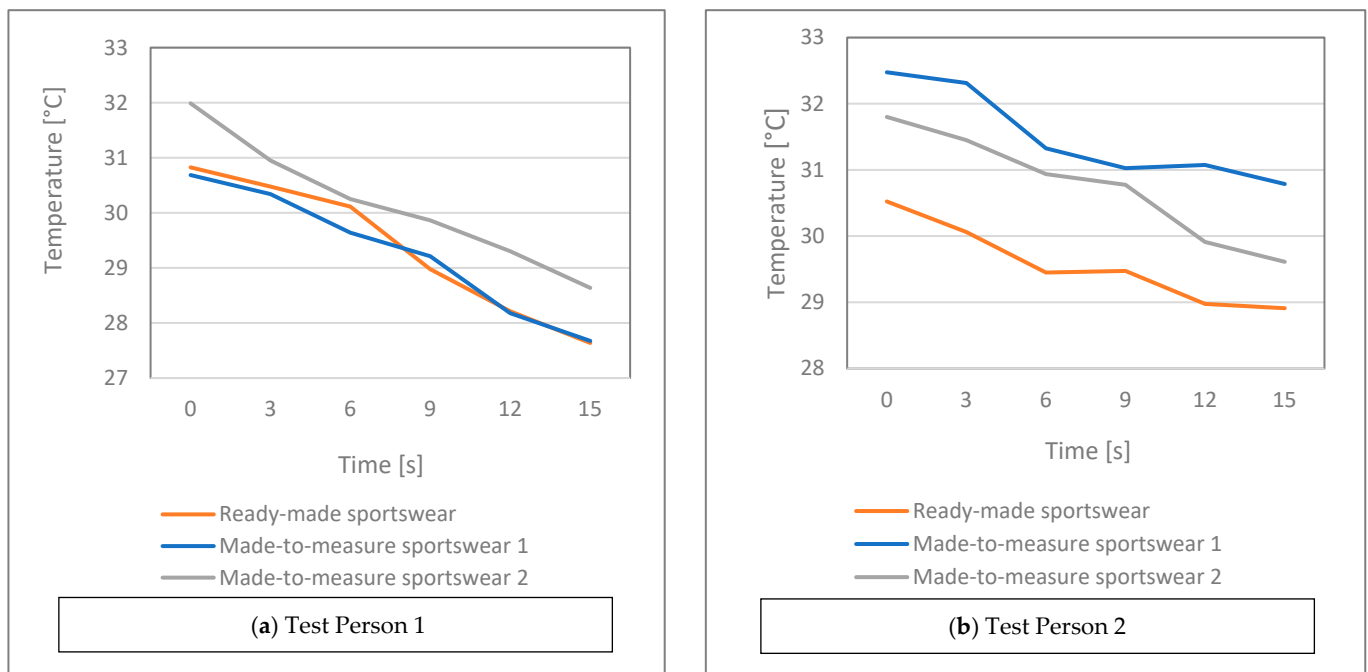

(**a**) Test Person 1

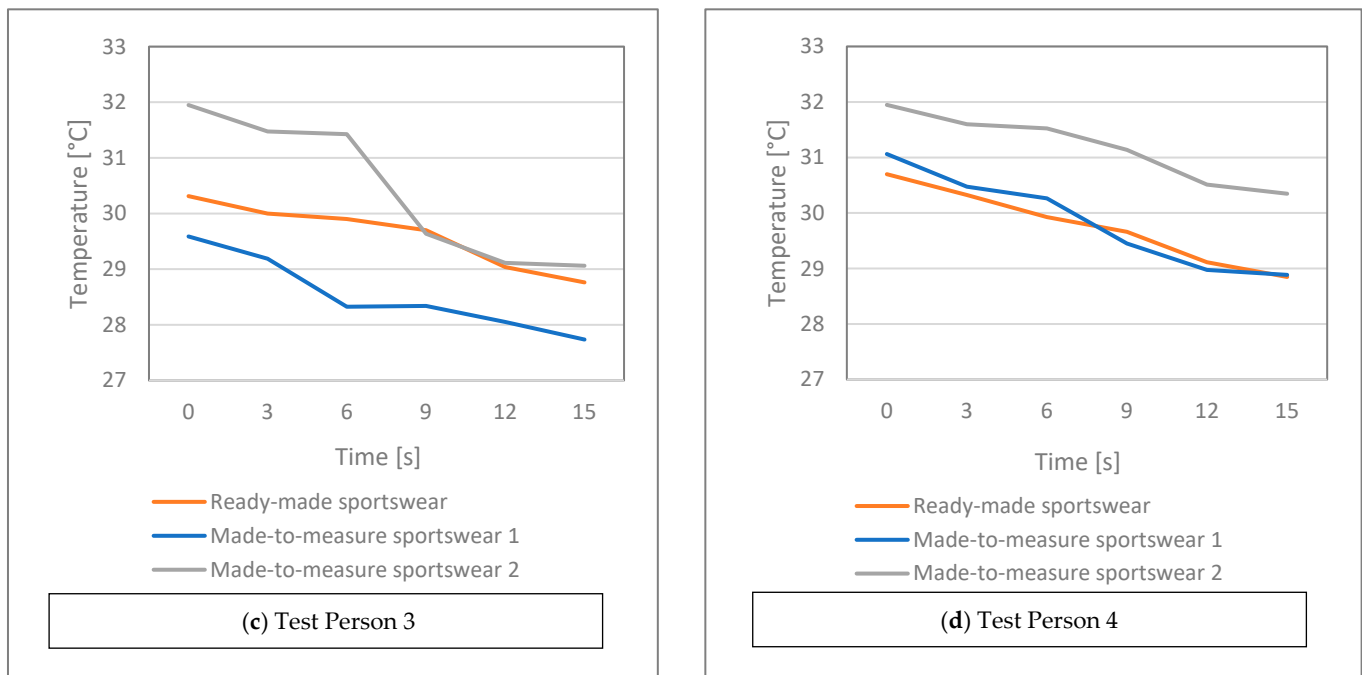(**b**) Test Person 2

Figure 7. *Cont.*

Figure 7. Average body surface temperature as a function of characteristic time points during running for each test person and sports suit.

The results obtained for Made-to-measure Sportswear 1 and 2 can be compared well in the case of thermal imaging as well since they were made from the same fabric; the only difference between them is in compression.

For better comparison, Figure 8 shows the average body surface temperature calculated for the whole running period. While wearing the higher compression Made-to-measure Sportswear 2, three test persons (TP1, TP3, and TP4) had a higher body surface temperature during running than in the case of the lower compression Made-to-measure Sportswear 1. In the case of Test Person 2, the opposite was true. These results indicate that higher compression generated higher body surface temperature.
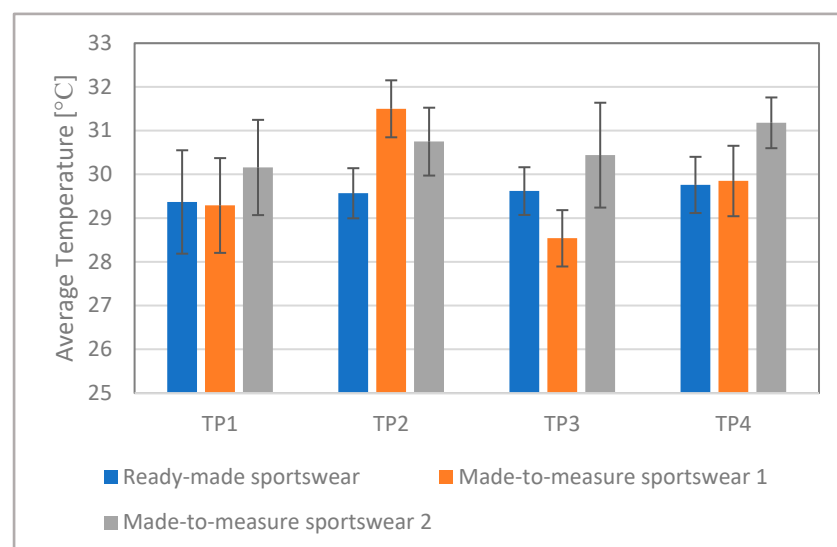

Figure 8. Average body surface temperature calculated for the whole period of running.

4. Conclusions

Our goal was to analyze whether the compression of sportswear on the athlete's body influences the clothing physiology comfort of the athlete. We included four test persons and used three different types of compression sportswear. We measured the compression of sportswear on the test persons, their body surface temperature, and the intensity of their sweating during running at increasing speed.

Our results indicate that the test persons sweated more in the higher compression Made-to-measure Sportswear 2. Their body surface temperature was higher than in the lower compression Made-to-measure Sportswear 1. We plan to conduct more extensive tests with more test persons to reveal more accurate relationships. Furthermore, we wish to supplement our research with measurements with zero compression sportswear.

However, our initial results strongly indicate that in high-tech sports clothing, the compression applied to increase performance has a considerable effect on the clothing physiology comfort of the athlete. This fact cannot be ignored when sports clothing is designed and fitted.

Appendix A

Table A1. Detailed pressure values for each test person and sportswear at each measurement point.

Person		TP1				TP2		
Number of Points	Name of Points	Pressure (mmHg)			Name of Points	Pressure (mmHg)		
		Ready-made	Made-to-Measure 1	Made-to-Measure 2		Ready-made	Made-to-Measure 1	Made-to-Measure 2
1.	Right upper arm	3	2	2	Right upper arm	2	2	3
2.	Left upper arm	4	2	3	Left upper arm	2	2	4
3.	Ventral middle	1	0	1	Ventral middle	2	1	2
4.	Right thigh front	7	5	7	Right thigh front	4	5	7
5.	Left thigh front	6	5	7	Left thigh front	4	4	6
6.	Right knee	7	5	7	Right knee	5	6	6
7.	Left knee	8	6	5	Left knee	5	5	7
8.	Right Scapula 1	2	1	3	Right Scapula 1	3	2	3

Table A1. *Cont.*

Person		TP1				TP2		
Number of Points	Name of Points	Pressure (mmHg)			Name of Points	Pressure (mmHg)		
		Ready-made	Made-to-Measure 1	Made-to-Measure 2		Ready-made	Made-to-Measure 1	Made-to-Measure 2
9.	Right Scapula 2	5	2	5	Right Scapula 2	3	3	4
10.	Left Scapula 1	3	0	3	Left Scapula 1	2	1	4
11.	Left Scapula 2	6	5	7	Left Scapula 2	4	2	5
12.	Right tight back	14	11	6	Right tight back	5	5	7
13.	Left thigh back	16	11	6	Left thigh back	6	4	8
14.	Right thigh side	6	5	4	Right thigh side	5	4	5
15.	Left thigh side	5	5	4	Left thigh side	4	3	5
16.	Right shank back	18	5	9	Right shank back	16	9	13
17.	Left shank back	17	4	9	Left shank back	14	8	13
18.	Right waist	20	13	10	Right waist	14	8	12
19.	Left waist	21	11	13	Left waist	13	9	10
Average [mmHg]:		8.89	5.16	5.84		5.95	4.37	6.53
Stand. dev. [mmHg]:		6.51	3.85	3.02		4.59	2.61	3.34
Person		TP3				TP4		
Number of Points	Name of Points	Pressure (mmHg)			Name of Points	Pressure (mmHg)		
		Ready-made	Made-to-Measure 1	Made-to-Measure 2		Ready-made	Made-to-Measure 1	Made-to-Measure 2
1.	Right upper arm	4	2	2	Right upper arm	3	1	3
2.	Left upper arm	4	2	4	Left upper arm	3	2	7
3.	Ventral middle	2	2	2	Ventral middle	1	1	1
4.	Right thigh front	5	5	6	Right thigh front	7	5	5
5.	Left thigh front	6	6	6	Left thigh front	7	5	5
6.	Right knee	7	5	8	Right knee	11	5	6
7.	Left knee	7	5	9	Left knee	8	5	6
8.	Right Scapula 1	3	2	2	Right Scapula 1	6	2	2
9.	Right Scapula 2	2	1	5	Right Scapula 2	4	1	4
10.	Left Scapula 1	2	1	3	Left Scapula 1	2	2	3
11.	Left Scapula 2	5	4	4	Left Scapula 2	7	5	4
12.	Right tight back	7	7	6	Right tight back	7	6	6
13.	Left thigh back	10	9	7	Left thigh back	8	9	5
14.	Right thigh side	4	2	5	Right thigh side	7	4	4
15.	Left thigh side	3	2	5	Left thigh side	7	4	3
16.	Right shank back	18	10	11	Right shank back	14	10	10
17.	Left shank back	17	8	12	Left shank back	14	10	13
18.	Right waist	15	7	13	Right waist	19	10	8
19.	Left waist	18	9	11	Left waist	20	9	9
Average [mmHg]:		7.32	4.68	6.37		8.16	5.05	5.47
Stand. dev. [mmHg]:		5.56	2.98	3.45		5.30	3.21	2.95

References

1. Shishoo, R. *Textiles in Sports*; The Textile Institute, Woodhead Publishing: Cambridge, UK, 2005.
2. Shishoo, R. *Textiles for Sportswear*; The Textile Institute, Woodhead Publishing: Cambridge, UK, 2015.
3. Hayes, S.G.; Venkatraman, P. *Materials and Technology for Sportswear and Performance Apparel*; CRC Press, Taylor & Francis Group: Boca Raton, FL, USA, 2016.

4. Rödel, H.; Schenk, A.; Herzberg, C.; Krzywinski, S. Links between design, pattern development and fabric behaviours for clothes and technical textiles. *Int. J. Cloth. Sci. Technol.* **2001**, *13*, 217–227. [CrossRef]

5. Venkatraman, P. Compression garments in sportswear: Case studies to explore the effect of body type, tactile sensation and seam position in garments. In *Proceedings of the Indo-Czech International Conference on the Advancements in Speciality Textiles and their Applications in Material Engineering and Medical Sciences, Coimbatore, India, 29–30 April 2014*; Kumaraguru College of Technology: Coimbatore, India, 2014; pp. 1–4. [CrossRef]

6. Jariyapunya, N.; Musilová, B.; Geršak, J.; Baheti, S. The influence of stretch fabric mechanical properties on clothing pressure. *Fibres Text.* **2017**, *24*, 43–48.

7. Kraemer, W.J.; Bush, J.A.; Newton, R.U.; Duncan, N.D.; Volek, J.S.; Denegar, C.R.; Canavan, P.; Johnston, J.; Putukian, M.; Sebastianelli, W.J. Influence of a Compression Garment on Repetitive Power Output Production Before and After Different Types of Muscle Fatigue. *Res. Sports Med.* **1998**, *8*, 163–184. [CrossRef]

8. Doan, B.K.; Kwon, Y.-H.; Newton, R.U.; Shim, J.; Popper, J.E.; Rogers, R.; Bolt, L.; Robertson, M.; Kraemer, W.J. Evaluation of a Lower-Body Compression Garment. *J. Sports Sci.* **2003**, *21*, 601–610. [CrossRef]

9. Ali, A.; Caine, M.P.; Snow, B.G. Graduated Compression Stockings: Physiological and Perceptual Responses During and After Exercise. *J. Sports Sci.* **2007**, *25*, 413–419. [CrossRef]

10. Duffild, R.; Portus, M. Comparison of Three Types of Full-Body Compression Garments on Throwing and Repeat Sprint Performance in Cricket Players. *Br. J. Sport Med.* **2007**, *41*, 409–414. [CrossRef]

11. Tanaka, S.; Midorikawa, T.; Tokura, H. Effects of pressure exerted on the skin by elastic cord on the core temperature, body weight loss and salivary secretion rate at 35 °C. *Eur. J. Appl. Physiol.* **2006**, *96*, 471–476. [CrossRef]

12. Jin, Z.-M.; Yan, Y.-X.; Luo, X.-J.; Tao, J.-W. A Study on the Dynamic Pressure Comfort of Tight Seamless Sportswear. *J. Fiber Bioeng. Inform.* **2008**, *1*, 217–224. [CrossRef]

13. MacRae, B.A.; Cotter, J.D.; Laing, R.M. Compression garments and exercise: Garment considerations, physiology and performance. *Sports Med.* **2011**, *41*, 815–843. [CrossRef]

14. Ashayeri, E. An Investigation into Pressure Delivery by Sport Compression Garments and Their Physiological Comfort Properties. Master's Thesis, RMIT University, Melbourne, Australia, 2012. Available online: https://researchbank.rmit.edu.au/eserv/rmit:161394/Ashayeri.pdf (accessed on 6 July 2018).

15. Senthilkumar, M.; Kumar, L.A.; Anbumani, N. Design and Development of a Pressure Sensing Device for Analysing the Pressure Comfort of Elastic Garments. *Fibres Text. East. Eur.* **2012**, *20*, 64–69. Available online: http://www.fibtex.lodz.pl/article645.html (accessed on 20 November 2020).

16. Beliard, S.; Chauveau, M.; Moscatiello, T.; Cros, F.; Ecarnot, F.; Becker, F. Compression Garments and Exercise: No Influence of Pressure Applied. *J. Sports Sci. Med.* **2015**, *14*, 75–83. Available online: https://www.ncbi.nlm.nih.gov/pmc/articles/PMC4306786/ (accessed on 20 November 2020).

17. Umar, J.; Hussain, T.; Ali, Z.; Maqsood, M. Prediction Modeling of Compression Properties of a Knitted Sportswear Fabric Using Response Surface Method. *Int. J. Mater. Metall. Eng.* **2016**, *10*, 2019–2027. [CrossRef]

18. Xiong, Y.; Tao, X. Compression Garments for Medical Therapy and Sports. *Polymers* **2018**, *10*, 663. [CrossRef]

19. Cunnington, P.; Mansfield, A. *English Costume for Sports and Outdoor Recreation—From the Sixteenth to the Nineteenth Centuries*; Adam & Charles Black: London, UK, 1969.

20. Tyler, M. *The History of the Olympics*; Marshall Cavendish: London, UK, 1975.

21. Riordan, J.; Krüger, A. *European Cultures in Sport*; Intellect: Bristol, UK, 2003.

22. Vadhera, N. Historical sketch of women's participation in sports: An overview. *Int. J. Yogic Hum. Mov. Sports Sci.* **2018**, *3*, 417–422. Available online: http://www.theyogicjournal.com/pdf/2018/vol3issue2/PartG/3-2-70-822.pdf (accessed on 20 November 2020).

23. Fanger, P.O. *Thermal Comfort*; Danish Technical Press: Copenhagen, Denmark, 1970.

24. Mecheels, J. *Körper—Klima—Kleidung*; Schiele & Schön: Berlin, Germany, 1998.

25. Tochihara, Y.; Ohnaka, T. *Environmental Ergonomics—The Ergonomics of Human Comfort, Health, and Performance in the Thermal Environment*; Elsevier: Amsterdam, The Netherlands, 2005.

26. Magyar, Z. Possibilities of Application of Thermal Manikin in Thermal Comfort Tests. Ph.D. Thesis, Szent István University, Gödöllő, Hungary, 2011.

27. Liu, Y.; Hu, H. Compression property and air permeability of weft-knitted spacer fabrics. *J. Text. Inst.* **2011**, *102*, 366–372. [CrossRef]

28. Ramesh, B.V.; Ramakrishnan, G.; Subramanian, V.S.; Kantha, L. Analysis of Fabrics Structure on the Character of Wicking. *J. Eng. Fibers Fabr.* **2012**, *7*, 28–33. [CrossRef]

29. Nagyné Szabó, O. Wear Comfort Improvement of Medical Aids Used for Spine Deformity Treatment. Ph.D. Thesis, University of West Hungary, Sopron, Hungary, 2014. Available online: http://doktori.nyme.hu/484/3/nagyne_szabo_orsolya_angoltezis.pdf (accessed on 20 November 2020).

30. Fangueiro, R.; Filgueiras, A.; Soutinho, F.; Meidi, X. Wicking Behavior and Drying Capability of Functional Knitted Fabrics. *Text. Res. J.* **2010**, *80*, 1522–1530. [CrossRef]

31. Chowdhury, P.; Samanta, K.K.; Basak, S. Recent Development in Textile for Sportswear Application. *Int. J. Eng. Res. Technol.* **2014**, *3*, 1905–1910.

32. Stojanović, S.; Geršak, J. Textile materials intended for sportswear. *Tekstil* **2019**, *68*, 72–88. Available online: https://hrcak.srce.hr/250867 (accessed on 20 November 2020).
33. Engel, F.; Stockinger, C.; Wall, A.; Sperlich, B. Effects of Compression Garments on Performance and Recovery in Endurance Athletes. In *Compression Garments in Sports: Athletic Performance and Recovery*, 1st ed.; Engel, F., Sperlich, B., Eds.; Springer: Cham, Switzerland, 2016; pp. 33–61. [CrossRef]
34. Pérez-Soriano, P.; García-Roig, Á.; Sanchis-Sanchis, R.; Aparicio, I. Influence of compression sportswear on recovery and performance: A systematic review. *J. Ind. Text.* **2019**, *48*, 1505–1524. [CrossRef]
35. Lovell, D.I.; Mason, D.G.; Delphinus, E.M.; McLellan, C.P. Do Compression Garments Enhance the Active Recovery Process after High-Intensity Running? *J. Strength Cond. Res.* **2011**, *25*, 3264–3268. [CrossRef]
36. Pálya, Z.; Kiss, R.M. Biomechanical analysis of the effect of compression sportswear on running. *Mater. Today-Proc.* **2020**, *32*, 133–138. [CrossRef]

Sylvie® 3D Drape Tester – New system for measuring fabric drape

Dr. eng. **Péter Tamás**[1]
Prof. dr.sc. **Jelka Geršak**[2]
Prof. dr. **Marianna Halász**[3]
[1] Budapest University of Technology and Economic
   Faculty of Mechanical Engineering, Department of Information Engineering
   Budapest, Hungary
[2] Univerza v Mariboru
   Faculty of Mechanical Engineering
   Department of Textile Materials and Design, Maribor, Slovenia
[3] Budapest University of Technology and Economic
   Faculty of Mechanical Engineering, Department of Polymer Engineering
   Budapest, Hungary

Newly developed measuring system Sylvie® 3D Drape Tester, used to determine static fabric drape, is presented. As opposed to the conventional Cusick drapameter, the measuring system described is based on storing the 3D geometrical properties of the draped sample form, using photographs in the process. The photos and their processing are employed to reconstruct mathematically the geometrical shape, while the drape coefficient evaluation is based on the geometrical model, using two methods.

1. Introduction

The aims of modelling textile materials and woven structures, for the purposes of garment industry and computer graphics, are quite different. If you, for example come to a real or virtual tailor, select the fabric you wish and, prior to making the final decision, wish to see how the suit or skirt would fit, it is preferable that you could see the precisely modelled article of clothing on the computer screen. When such applications are concerned, the aim is to create the simplest model to offer a real result or one acceptable to an average observer [1].

The purpose of creating a physically precise and predictable model is minimal, if any. The main aim is to create computer-generated pictures and animations for the so-called proper appearance of the clothing. Garment constructor should be able not only to measure the body (take the measures) and create a personal virtual model, but to define some characteristics of the real fabrics necessary for the 3D visualisation as well.

In practice, fabrics are exposed to numerous complex deformations, such as draping, folding or bending. In order for the designer to be able to reach the optimal level of a rational engineering design, it is necessary to know and understand complex fabric deformations.

It is much more convenient, in some cases, to determine the parameters of the simulation system by using the conventional equipment, such as a photo/video equipment used for data acquisition and storage. This is why the new measuring system Sylvie® 3D Drape Tester has been developed. The system used conventional equipment and offers computer-generated simulation of the draped fabric geometry. The parameters of the fabric simulation model, based on the so called parameterised system of particle elements, have been adapted so as to match the geometry of the real fabric in a static state, draped over a round surface (Drapemeter), evaluating the parameters according to the photograph of the fabric.

2. Sylvie® 3D Drape Tester – system for measuring textile fabric drape

A round fabric sample, with the diameter of 30 cm is used with the Sylvie® 3D Drape Tester measuring system, the same as with the conventional Cusick Drapemetre. The diameter of the round table in the equipment is 18 cm. The sample draped exhibits conventional mechanical deformations.

To determine the sample geometry, defined using for laser beams used to illuminate the sample through mirrors, special 3D scanner is used. Laser beam lines on the draped sample, which determine the cross-sections of the curve, are recorded as digital photographs. Based on the recordings of the cross-section curves of the draped samples, an analytical characterisation of the curve cross-section geometry is done, employing the regression Fourier series. The interpolation of the positioned draped sample cross-section curve is done using a special type of the cube B-spline method [2]. The surface interpolated is used to reconstruct the original 3D-sample geometry.

2.1 Equipment used

The computer-controlled equipment is mounted in a black box, Fig. 1a. The computer moves the centrally positioned round table, ensuring thus a natural fabric folding and drape, necessary for the testing. The central part of the equipment is a computer-controlled frame,

with laser beams used to illuminate the sample through the mirrors and four cameras used to record the laser beams, i.e. the cross-sections of the curves at the various levels of the draped sample, Fig. 1b.
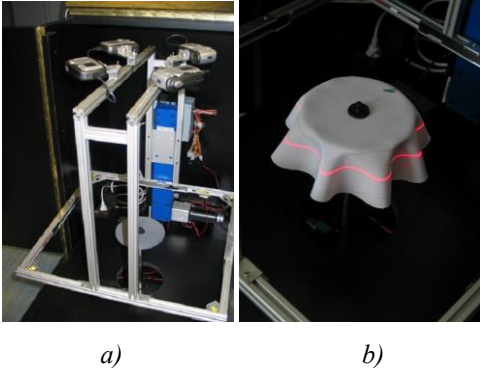

a)   *b)*

Fig. 1. Sylvie 3D Drape Tester: a) Computer-controlled equipment mounted in a black box,
b) Laser beams lines on a draped sample

2.2   Measuring procedure

The new system offers storing and recording the sample form at various levels of the draped sample, enabled by the computer-controlled frame, with the lasers and the system of 4 digital cameras on it. Although this procedure yields numerous curves to determine the drape coefficient, only the curve of the lower edge of the draped sample is used, the lower edge being the last point of the outer fold, Fig. 1b.

Prior to determining the curves recorded by the four cameras, it is necessary to calibrate the measuring system. This is done by interpolating the curves based on the calibration pictures. Calibration is done in order to define the dimensions of the curves of the sample draped form ground-plan cross-section. Based on the recordings of the etalone, recorded by the equipment described, the computer software calculates and stores the distortion and the necessary rotation of the four fourths. One fourth of calibration etalon can be seen in Fig. 2.
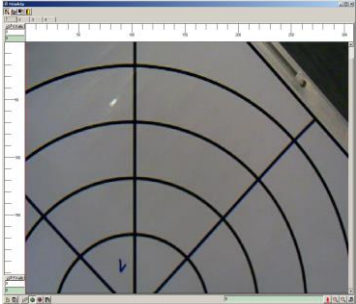

Fig. 2. A fourth of calibration etalon

2.2.1 Processing the images

The four images, making the cross-section curves, are stored by the newly developed computer software, Fig. 3. The curve points are defined using the methods of image processing. Taking into account the distortion and rotation of the individual curve segments, they are positioned into a single image, Fig. 4.
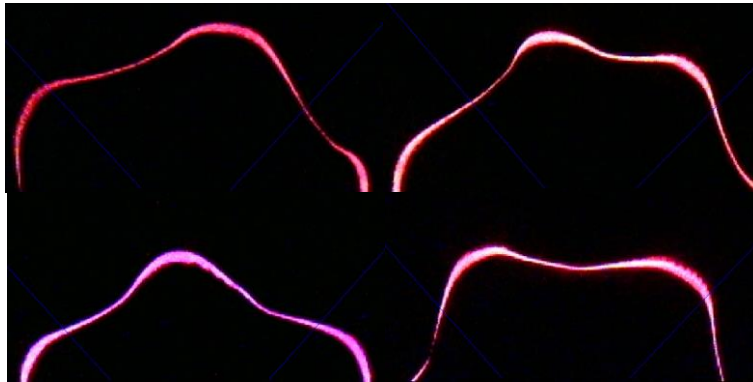

Fig. 3. Four images of curve cross section

Fig. 4. Reconstructed curve cross section

The cross-section curves are approximated by the members of the Fourier series, in a polar co-ordinate system (1). Most of the members (*n*) can be defined by the computer software in question.

$$R(\varphi) = \frac{1}{2}a_0 + \sum_{i=1}^{n} a_i \, cos(i\varphi) + \sum_{i=1}^{n} b_i \, sin(i\varphi) \qquad (1)$$

The Fourier's coefficients are defined by the minimal square method. If the N number of the cross-section points measured are at the actual level (R_k, φ_k), then the a_i, b_i are the coefficients defined by the minimum of the function (2).

$$\sum_{k=1}^{N}\left\{ R_k - \left[\frac{1}{2}a_0 + \sum_{i=1}^{n} a_i \, cos(i\varphi_k) + \sum_{i=1}^{n} b_i \, sin(i\varphi_k) \right] \right\}^2 = min\,imum \qquad (2)$$

2.2.2 3D reconstruction

The geometry of the sample draped form is modelled by the Bezier's surface patches. The shape of the surface patches is defined by the $P_{i,j}$ vertices, Fig. 5.
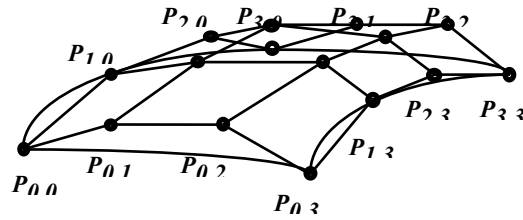

Fig. 5. Bezier's surface patches

The surfaces patches are continually linked with each other, based on the interpolation by the Catmull-Romm spline method. The slopes of the edges of the surfaces patches are also defined by the vertices of the actual element.

The values in the vertices of the 3D geometry are defined by the approximating curves (1) at various levels [3].

3D reconstruction, Fig. 6, is appropriate to calculate the drape coefficient K_D, defined according to the following equation:

$$K_D = \frac{A - \pi R_1^2}{\pi \left(R_2^2 - R_1^2 \right)} \cdot 100 \qquad (3)$$

where R_1 is the radius of the fabric supporting disc, R_2 is the radius of the fabric sample, and A is the projected shadow of the draped fabric.
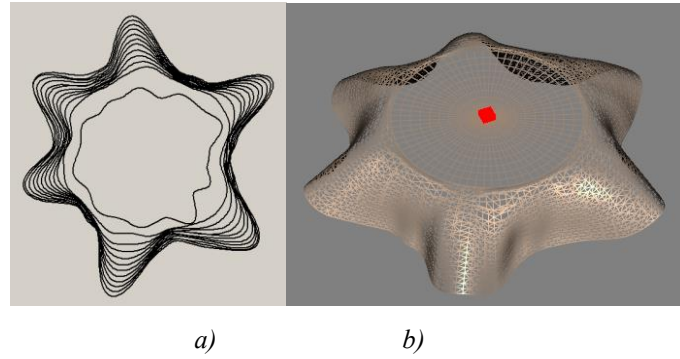
Fig. 6. 3D Reconstruction of the sample draped shape: a) Approximating curves of the 3D draped sample geometry, b) Simulation of the draped sample appearance

2.3. Measuring the drape coefficient

The measuring system described offers two ways of determining drape coefficients. The first is based on the four original photographs of the curve cross sections, Fig. 3. The software determines the curves of covering the outer points of the laser beams on the draped sample. The surface enclosed by the points can easily be measured. The drape coefficient K_D is determined numerically, using integers according to the equation (3). This method of determining drape coefficient is analogous to the conventional method of the Cusick drapemeter.

Although numerical integration is used with the other method of determining drape coefficients as well, the surface used in the calculation is a horizontal projection of the 3D draped samples created by the simulation [4].

3. Experimental

Based on the *Sylvie*® *3D Drape Tester* measuring system presented and the methods of determining drape coefficients described, we have compared the results of determining drape coefficient obtained by the measuring system presented and the ones obtained by the conventional Cusick drapemeter.

15 fabrics have been used in the experiments, differing by the raw material content, surface area mass, construction, thickness and mechanical properties. Some properties of the fabrics used can be seen in Tab. 1.

Table 1 Characteristics of the fabrics tested

Desig-nation	Raw material content	Weave	Surface mass W/gm^{-2}	Fabric* thickness h/mm	Elongation** ε_{-1} / %	Deformation work WT_{-1}/cN cm	Bending rigidity B_{-1}/cN cm^2	Shear rigidity G_{-1}/cN(st)$^{-1}$
01	100% Cotton	Plain	191.06	0.61	7.05	13.23	0.1059	2.84
02	100% Cotton	Plain	191.47	0.61	7.69	14.11	0.0933	2.84
03	100% Cotton	Plain	188.55	0.62	6.51	12.15	0.1117	3.07
04	100% Cotton	Twill	197.07	0.77	10.00	16.17	0.1212	1.52
05	100% Cotton	Twill	191.65	0.92	8.17	11.56	0.0964	0.64
06	100% Cotton	Satin	194.03	0.81	6.54	9.90	0.0854	0.60
07	100% Cotton	Panama	187.70	0.86	8.81	12.45	0.0789	0.53
08	100% Cotton	Rips	186.90	0.85	8.00	11.66	0.0839	0.43
09	67% CV; 33% flax	Plain	206.89	0.61	6.86	12.54	0.1021	3.03
10	50% PES; 50% Cotton	Plain	204.09	0.62	7.42	14.50	0.1241	4.05
11	100% PES	Plain	202.03	0.59	7.76	14.31	0.1263	3.55
12	100% Cotton	Plain	167.12	0.57	6.98	12.64	0.0899	2.16
13	100% Cotton	Plain	148.08	0.56	6.22	10.98	0.0760	1.43
14	100% Cotton	Plain	185.37	0.68	8.91	15.09	0.0923	1.91
15	100% Cotton	Plain	169.62	0.69	8.42	13.13	0.0727	0.71

* h – fabric thickness at the load of 0.49 cN cm^{-2}

** ε – elongation at the load of 490.35 cN cm^{-1}

index $_{-1}$ – measuring values warp wise

3.1. Testing methods

Determining drape coefficients using the Sylvie$^{®}$ 3D Drape Tester-a has been done based on the investigations of the 3D geometrical shape of the draped sample surface, employing the described manners of determining the drape coefficients. Contrary to this, the experimental method of measuring drape coefficients using the conventional Cusick drapemeter, equipped with a video camera and a Drape Analyzer software package, is based on the projection (shadow) of the draped surface of the sample, obtained by light reflection (light beam) from a parabolic mirror, Fig. 7. The drape coefficient K_D is defined as a

ration of the surface of the rectangular projection of the draped fabric and the surface of the unreformed fabric sample, equation (3) [5-7].
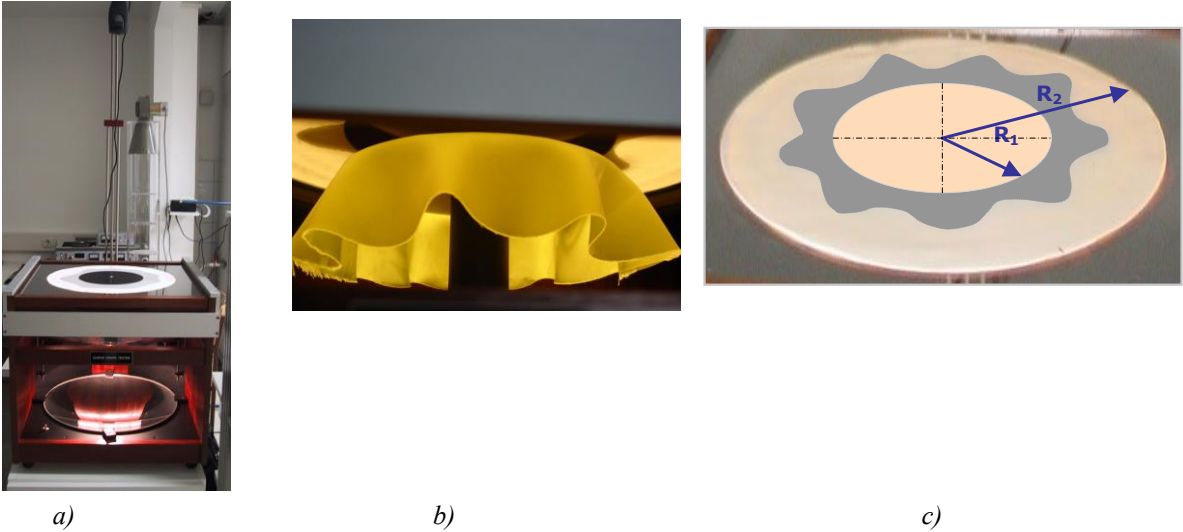

a)   b)   c)

Fig. 7:   Draping the fabric on the Cusick drapemeter
            a) Cusick Drapemeter with a video camera
            b) The shape of the draped fabric
            c) Projected shadow of the draped fabric

The investigation has been divided into two parts. The first one included the analysis of the draping result reproducibility, while the second involved a comparative analysis of the drape coefficient calculated values, obtained by the Sylvie® 3D Drape Tester presented and the conventional Cusack drapameter respectively.

4.   Results and discussion

The results of the reproducibility of measuring drape coefficients, determined by the proposed *Sylvie® 3D Drape Tester-a*, for both methods of determining drape coefficients, are shown in Tab 2. The Tab. 2 shows the average value, standard deviation and variation coefficient of the draping for ten parallel measurements of a single fabric sample.

Analysis of the reproducibility results for the fabrics processed by the Sylvie® 3D Drape Tester shows that the method developed ensures good measuring results reproducibility, since the variation coefficient of the drape coefficient obtained by the first method is 0.135 %, while for the second method it is 0.211 %.

*Table 2 Repeatability results for the drape coefficient values calculated for ten
parallel measurements on the Sylvie 3D Drape Tester*

Number of measurements	Drape coefficient K_D / %	
	Manner of evaluating K_D	
	I	**II**
1	60.5	56.1
2	60.9	56.1
3	60.9	56.3
4	60.9	56.3
5	60.9	56.5
6	60.9	56.3
7	60.9	56.3
8	61.0	56.7
9	60.8	56.4
10	60.8	56.7
Average value	60.85	56.37
Standard deviation with	0.135	0.211
Variation coefficient CV / %	0.223	0.375

The values of the drape coefficient obtained by the Sylvie$^{®}$ 3D Drape Tester and the
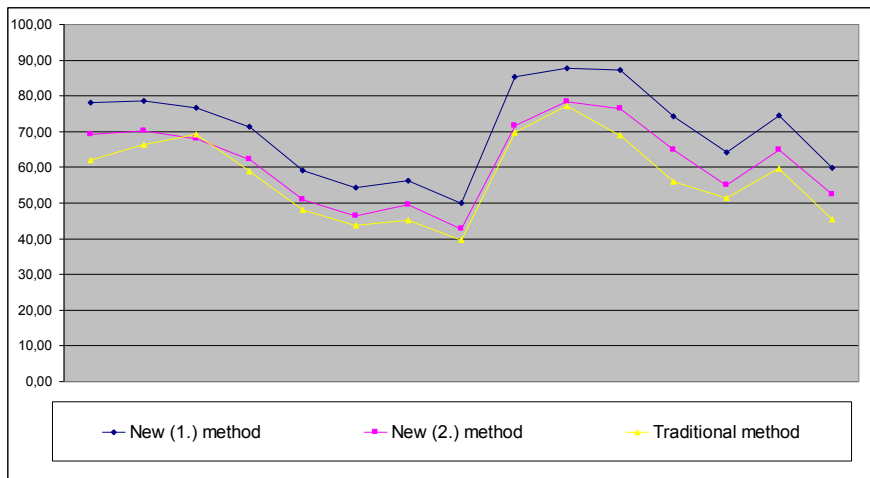Cusick drapemeter, for 15 different fabric samples (Table 1), are shown in Fig. 8.

*Fig. 8. Comparison of the drape coefficient values (Table 1), obtained by different methods and with different
manners of evaluation*

Comparing the values of the drape coefficient K_D shows that it is defined by processing the
image of the draped sample curve shape, as well as by the projection twisting final curve
3D of the reconstructed fabric sample draped shape, which exhibits higher values than the
drape coefficient determined by the conventional method, employing the Cusick
drapemeter. The differences in drape coefficient values can be attributed to the differences

in defining the draped shape of the sample, both between the two methods (Sylvie® 3D Drape Tester - Cusick drapemeter), and between the two manner of evaluating drape coefficients according to the Sylvie® 3D Drape Tester. Since the first one involves evaluating drape coefficients according to the computer-processed images of the curve cross-sections (curves covering the outer points of the laser beams on the draped sample), while the second determines drape coefficients by projecting the twisting final curve of the 3D reconstructed (simulated) geometry of the draped sample modelled by the Bazier's surfaces, we can rightfully conclude that the surfaces of the draped sample projection obtained thus are bigger than the real rectangular projection of the draped sample. It is also confirmed by the analysis of drape coefficient values, Fig. 8, since drape coefficient values, obtained by projecting the twisted final curve of the 3D simulated geometry of the draped sample, come close to the values of drape coefficients determined by the conventional Cusick drapemeter.

A detailed analysis of the evaluation of drape coefficients leads to an interesting fact that both methods of evaluation, as well as all the three manners of determining drape coefficients have certain disadvantages.

The conventional method with the Cusick drapemeter leads to problems when, due to high deformability of the fabric, the depth of the folds exceeds the width of the area $\Pi(R_2^2 - R_1^2)$, which means that the geometry of the fold is partially below the projection of the horizontal plate surface, with the diameter R_1, and the existing measuring technique cannot recognise it.

When the draping parameters are determined by the measuring system Sylvie® 3D Drape Tester, where the geometrical shape of the draped surface is defined on the basis of processed images of the curve cross-sections, while the software seeks the curves of covering the laser beams on the draped sample, the problem arises of objective recording of the draped sample shape geometry. Because of the folds formed, the lower edge of the outer and inner side of the fold are not in the same plane, and laser beams can recognise only the depth of the fold as a rectangular projection of the lowest position of the fold inner part indentation and not the whole of the fold geometry, i.e. the outer part of the fold.

The measuring system presented offers, besides determining draping properties of static textile fabrics, a representation of the fabric simulation model as well, based on the so called parameterised system of particle elements. Since the parameters of the fabric

10

simulation model are adapted so as to match the real fabric geometry in a static state, the measuring system developed also offers a simulation of the draped fabric related to the visualisation of the fabric incorporated in an article of clothing, as can be seen in Fig. 9 [8-9].

Fig. 9. Virtual Fitting On

5. Conclusions

The measuring system Sylvie® 3D Drape Tester, developed in order to evaluate the characteristics of draped textile fabrics, is a new and original way of evaluating the geometry of a draped shape of a fabric. Apart from the computer-aided simulation of the draped shape geometry, it also offers the possibility of calculating drape coefficients. The results obtained for the drape coefficients calculated exhibit high correlation to the ones obtained by conventional methods.

The method presented is highly acceptable for the purpose of measuring textile fabric draping parameters, as well as for virtual presentation of garment fit.

Reference

[1]   D. H. House; D. E. Breen: Cloth Modelling and Animation, Publisher: A. K. Peters Ltd., Wellesley, USA, 2000, 19-107; 197-214.

[2]   P. Tamás; M. Halász: 3D body modelling in clothing design, IMCEP 2003, 4th International Conference, Maribor, Slovenia, 9-11. October 2003, ISBN 86-435-0575-7, 64-68

[3]   T. McReynolds; D. Blythe: Advanced Graphics Programming Using OpenGL, Series in Computer Graphics and Geometric Modelling, Morgan Kaufmann Publishers, San Francisco, USA, 2002

[4]   J. Kuzmina; P. Tamás; B. Tóth: Programozzunk Delphi 7 rendszerben!, Publisher: Computer Books Ltd., Budapest, 2003

[5]   Cusick, G. E.: The Dependence of Fabric Drape on Bending and Shear Stiffness, Journal of Textile Institute, **56** (1965), 11, 596-606

[6]   Cusick, G. E.: The Measurement of Fabric Drape, Journal of Textile Institute, **59** (1968), 253-260

[7]   Geršak, J.: Mehanske in fizikalne lastnosti tekstilnih materialov, Univerza v Mariboru, Fakulteta za strojništvo, Maribor, 2006, ISBN 86-435-0754-7

[8]   J. Gräff; J. Kuzmina: Cloth Simulation using Mass and Spring Model, GÉPÉSZET '2004, 4th Conference on Mechanical Engineering, BUTE, Budapest, 27-28. May 2004, ISBN 963 214 748 0, 443-447

[9]   P. Tamás; M. Halász; J. Gräff: 3D dress design, AUTEX 2005, 5th World Textile Conference, Portorož, Slovenia, 27-29. June 2005, ISBN 86-435-0709-1, 436-441